Aspects of Geometry and Topology in Liquid Crystalline Phases

Thomas John Machon

Submitted for the degree

of

Doctor of Philosophy

University of Warwick

March 2016

Contents

FIGURES

TABLES

There is only one name on this thesis, but it is the work of many people. My supervisor, Gareth Alexander, has gone far beyond any reasonable expectation one might have of their supervisor. His patience, wisdom and insight never ran dry; my debt to him can be done no justice here. I would like to acknowledge my second supervisor, Miha Ravnik, and also Randall Kamien for their generosity and for many helpful conversations and both Bryan Chen and Simon Čopar, whose work has influenced mine greatly.

The soft matter group at Warwick have been excellent and stimulating place to spend the last three years. In particular I would like to mention Davide Michieletto, Dario Papavassiliou, Alex Rautu and Diana Khoromskaia for their good advice and good company.

I shared many great times with my fellow students in the 2011 complexity cohort: Peter Dawson, Dominic Kerr, Yuri Lifanov, Michael Maitland, Arran Tamsett, Ellen Webborn and Rachel Wilkerson, my officemates in D2.14: Matt Graham and Joel Nicholls and also Ben Collyer, Matthew Dale and Felicity Kendrick.

I would like to thank my family, my mother Barbara, my father Paul and my brother George for their love and support.

Finally, for the rest and for everything, I thank Elena.

Declaration

This thesis is submitted to the University of Warwick in support of my application for the degree of Doctor of Philosophy. It has been composed by myself and has not been submitted in any previous application for any degree. Part of the material in this thesis has been published in the following papers:

Material from Chapter 5 has been published in:

T. Machon and G.P. Alexander, *Knots and non-orientable surfaces in chiral nematics*, Proc. Natl. Acad. Sci. USA **110**, 14174 (2013).

A summary of some material in Chapter 2 has been published in:

T. Machon and G.P. Alexander, *Knotted Defects in Nematic Liquid Crystals*, Phys. Rev. Lett. **113**, 027801 (2014).

The arguments in §4.2-3 formed a small part of the publication:

D.A. Beller, T. Machon, S. Čopar, D.M. Sussman, G.P. Alexander, R.D. Kamien and R.A. Mosna, *Geometry of the Cholesteric Phase*, Phys. Rev. X **4**, 031050 (2014).

The material in Chapter 3 has been accepted for publication as:

T. Machon and G.P. Alexander, *Umbilic Lines in Orientational Order*, Phys. Rev. X, *accepted* (2016).

Material from Chapters 2,4 and 6 is currently being prepared for publication.

Abstract

Liquid crystals exhibit a rich set of phenomena with a geometric and topological flavour. In this thesis the study nematic and cholesteric phases of liquid crystals from the perspective of geometry and topology. We show that a global extension of the homotopy theory of defects in three dimensional nematics allows one to associate a topological 'internal state' to knotted and linked defects lines, such as those made experimentally. This internal state reflects the way in which the liquid crystal 'wraps around' the defects in the system and can be associated to baby Skyrmion tubes and relative orientations. Moving on from this we give a geometric analysis of orientational order, showing that there are a natural set of lines, realised as geometric singularities, the generalisation of the umbilical points of a surface. These lines can be identified with a number of structures seen experimentally in chiral systems such as double twist cylinders, the centres of Skyrmions and λ lines. We describe the theoretical properties of these lines, in particular how they reflect the topology of the underlying orientation by furnishing a representation of (four times) the Euler class of the orthogonal 2-plane bundle. We then combine these two theoretical structures to give a description of the cholesteric phase. In particular, our description allows all structures to be derived from the orientational order, and we show how previous theories and interesting structures such as τ lines fit into this scheme. We extend this theory by making the connection between cholesteric liquid crystals and contact structures, where we show that one can obtain additional topological distinctions between field configurations. We discuss topological aspects of colloidal inclusions and show that non-orientable colloids can precipitate the creation of knotted defect lines *in silico*. Finally, we show how one can use Milnor fibrations to give explicit formulae for director fields that contain knotted defect lines.

"We shall not cease from exploration, and the end of all our exploring will be to arrive where we started and know the place for the first time."

T.S. Eliot, *Little Gidding*

Chapter 1

Liquid Crystals, Defects and Topology

Liquid crystals are phases of matter lying between liquid and crystalline order. They are typically composed of long, thin molecules such as MBBA (N-(4-Methoxybenzylidene)-4-butylaniline), shown in Figure 1.1, they flow as a liquid but experience the long-range orientational correlations and elastic distortions of a solid [1]. There are several different liquid crystalline mesophases, the most basic being the nematic phase, but others such as cholesteric (chiral) and smectic (layered) liquid crystals also exist, along with their own set of complex phenomena. The nematic phase is typically obtained by cooling from the isotropic (liquid) phase through a first order phase transition [2], known as a thermotropic nematic. As well as thermotropic phases, there are others such as lyotropics whose transition depends on the concentration of liquid crystal molecules in a solvent. Common to all these liquid crystalline phases, is the creation of orientational order due to a non-zero average local molecular alignment. In theoretical descriptions of liquid crystals this is typically coarse-grained to produce a unit magnitude orientation field, known as the director [3]. One of the key aspects of liquid crystalline order that this orientation is apolar, it picks out only an unoriented direction in space, rather than the oriented direction given by a vector. One should observe, however, that the molecule in Figure 1.1 is not head-tail symmetric. Indeed, in general it is possible to obtain nematic ordering with polar molecules, the apolar nature is a property of the phase, not the

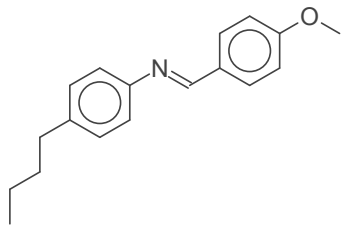

Figure 1.1: Molecular structure of MBBA, a material that forms a nematic phase at room temperature.

molecules themselves. In general, however, it is possible to change the phase through alterations of the molecular symmetry properties, for example to a chiral phase or one with a ferroelectric response [4].

From a theoretical perspective, while the order is apolar, it is traditional in the literature to represent it as a unit vector, $\mathbf{n}$. Locally there is no issue with this as one can always locally orient a director field. Globally, however, this orienting is not always possible. As a consequence of this apolarity, liquid crystalline systems exhibit a huge variety of interesting phenomena that very often have a geometric or topological flavour. Of particular note are the line-like structures one observes: disclinations, dislocations and others. Recent experimental work has give extremely fine control of these line structures, with the resulting creation of knotted defects lines [5–7], and a variety of other solitons [8–10]. These elaborate objects strengthen the connection between the physics of liquid crystals and the fields of geometry and topology, and provide a beautiful set of motivating examples for much of this thesis.

1.1 Free Energies for Liquid Crystals

The most elementary liquid crystal phase is the nematic, in which the system prefers a uniform molecular alignment with no positional order. As such, in the nematic phase distortions from uniform alignment are energetically costly. Static configurations of nematics can therefore be understood by constructing an appropriate elastic free energy in terms of distortions in

$\mathbf{n}$ [1,2]. The first point to note, and this will be stressed throughout this thesis, is that $\mathbf{n}$ represents a genuine direction in space, rather than an internal state. To construct an elastic free energy we should therefore look for symmetry protected quantities in $\nabla\mathbf{n}$, that is scalars that are left invariant under global rotations. This is a classical calculation, reformulated in Chapter 3 in terms of vector bundles, where it is shown that one can decompose the gradient tensor as

$$\nabla\mathbf{n} = \frac{\nabla\cdot\mathbf{n}}{2}\big(\mathbb{I}-\mathbf{n}\otimes\mathbf{n}\big) - \frac{\mathbf{n}\cdot\nabla\times\mathbf{n}}{2}J + \mathbf{n}\otimes(\mathbf{n}\cdot\nabla)\mathbf{n} + \Delta, \tag{1.1}$$

where $J_{ij} = \epsilon_{ijk}n_k$ and Δ corresponds to the anisotropic orthogonal gradients, which are dealt with extensively in Chapter 3. Each of these pieces is orthogonal with respect to the inner product $\langle A,B\rangle = A_{ij}B_{ij}/2$ and the pieces transform among themselves under rotations. As such the symmetry protected quantities we can extract from $\nabla\mathbf{n}$ are precisely the magnitudes of each of these components. These scalars are

$$\frac{\nabla\cdot\mathbf{n}}{2}, \tag{1.2}$$

$$\frac{\mathbf{n}\cdot\nabla\times\mathbf{n}}{2}, \tag{1.3}$$

$$\big((\mathbf{n}\cdot\nabla)\mathbf{n}\big)^2, \tag{1.4}$$

$$|\Delta|^2 = \left(\frac{\nabla\cdot\mathbf{n}}{2}\right)^2 + \left(\frac{\mathbf{n}\cdot\nabla\times\mathbf{n}}{2}\right)^2 - \frac{1}{2}\nabla\cdot\left((\nabla\cdot\mathbf{n})\mathbf{n} - (\mathbf{n}\cdot\nabla)\mathbf{n}\right). \tag{1.5}$$

The first three of these are known as splay, twist and bend. The final one is related to a quantity known as saddle-splay. The first two, splay and twist can take both positive and negative values, whereas bend and $|\Delta|^2$ are non-negative. Technically this is because splay and twist correspond to sections of line bundles, which are one dimensional. Note that $\nabla\cdot\mathbf{n}$ is not invariant under $\mathbf{n}\to-\mathbf{n}$, so we can only look at $(\nabla\cdot\mathbf{n})^2$. This slight complication comes from the deficiency of the description in terms of $\mathbf{n}$, really one should use a tensor, such as $\mathbf{n}\otimes\mathbf{n}$, and examine irreducible representations of $\nabla(\mathbf{n}\otimes$

$\mathbf{n}$), at which point one would only find $(\nabla \cdot \mathbf{n})^2$ as an allowed scalar. With these quantities we can construct an elastic free energy as a weighted sum of these allowed scalars

$$F = \int A(\nabla \cdot \mathbf{n})^2 + B\mathbf{n} \cdot \nabla \times \mathbf{n} + C\big(\mathbf{n} \cdot \nabla \times \mathbf{n}\big)^2 + D\big((\mathbf{n} \cdot \nabla)\mathbf{n}\big)^2 + E\left(\left(\frac{\nabla \cdot \mathbf{n}}{2}\right)^2 + \left(\frac{\mathbf{n} \cdot \nabla \times \mathbf{n}}{2}\right)^2 - \frac{1}{2}\nabla \cdot ((\nabla \cdot \mathbf{n})\mathbf{n} - (\mathbf{n} \cdot \nabla)\mathbf{n})\right) dV. \quad (1.6)$$

These terms are typically combined to form the Frank free energy [1]

$$F = \int \frac{K_1}{2}\big(\nabla \cdot \mathbf{n}\big)^2 + \frac{K_2}{2}\big(q_0 + \mathbf{n} \cdot \nabla \times \mathbf{n}\big)^2 + \frac{K_3}{2}\big((\mathbf{n} \cdot \nabla)\mathbf{n}\big)^2 - \frac{K_{24}}{2}\nabla \cdot ((\nabla \cdot \mathbf{n})\mathbf{n} - (\mathbf{n} \cdot \nabla)\mathbf{n})\,\big)dV \quad (1.7)$$

where the fourth term is now saddle-splay proper. There are a few points we will make about this equation. The first is that if $q_0 \neq 0$ then the free energy is chiral, and corresponds to a type of liquid crystal known as cholesteric that exhibits a particularly rich set of phenomena [11,12], which will be explored in Chapter 4. The second point is that the saddle-splay term is a total divergence. This is because it corresponds to the 'Gaussian curvature' of the vector field, by which we mean that if $\mathbf{n}$ defines a foliation, *i.e.* a system of layers, then the saddle-splay is the Gaussian curvature of the layers. As such it is subject to a variant of the Gauss-Bonnet formula and can be reduced to boundary information, something that will again be explored in Chapter 3. The final point we will make is that, as a consequence of (1.1), if one sets $A = C = D = E$ and $B = 0$ in (1.6), then the free energy density is proportional to $|\nabla \mathbf{n}|^2 = (\partial_i n_j)(\partial_i n_j)$; this is known as the one elastic constant approximation [13].

As a unit magnitude director, the Frank free energy is not capable of acting as an order parameter [14]. This is not only an issue in understanding phase transitions, but also in the study of defects, where the elastic energy diverges in many situations. To solve these issues one turns to the Q-tensor

theory, commonly known as Landau-de Gennes theory [1]. Briefly, in this theory the order parameter is a traceless symmetric rank 2 tensor Q. This tensor has two independent invariants, $\mathrm{Tr}(Q^2)$ and $\mathrm{Tr}(Q^3)$, and a Landau theory can then be constructed as

$$F_{bulk} = A\mathrm{Tr}(Q^2) + B\mathrm{Tr}(Q^3) + C(\mathrm{Tr}(Q^2))^2, \tag{1.8}$$

which indicates a first order transition to an ordered phase. An elastic energy density can also be given as

$$F_{el} = \frac{L_1}{2}(\partial_a Q_{ab})^2 + \frac{L_2}{2}(\epsilon_{abc}\partial_b Q_c)^2. \tag{1.9}$$

This free energy has been shown to be remarkably effective when used as a basis for computer simulations, with a number of exotic structures correctly predicted *in silico* before later being realised experimentally [15–17]. Many of the simulation results shown in this thesis were achieved using a finite difference code using this free-energy.

Finally, of some relevance to this thesis is the correspondence between the Q tensor and director field descriptions. A generic Q tensor has three distinct eigenvectors, and so picks out a triad of directions (a so-called biaxial liquid crystal). However, typically, the free energy favours a uniaxial form with only one non-degenerate eigenvector. Indeed, experimentally uniaxial liquid crystals are observed and, in particular, the topology is that of uniaxial liquid crystals; the predicted distinctive topology of biaxial nematics has not been observed experimentally. This uniaxial Q tensor can be related to a director field as

$$Q_{ij} = s_1(n_i n_j - \frac{1}{3}\delta_{ij}). \tag{1.10}$$

As such, we will focus our efforts on understanding uniaxial liquid crystals, though those for which the Q tensor is not uniaxial will play an important role.

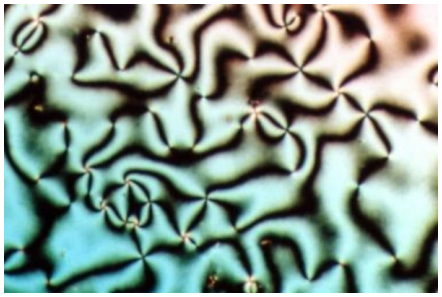

Figure 1.2: Schlieren texture obtained from a thin sample of nematic liquid crystal between cross-polarisers. The dark regions are where the local orientation of the nematic is aligned with either of the polarisers. The lightest regions are where the molecular orientation is at an angle of (approximately) $\pi/4$ to both polarisers. Reproduced from [19].

1.2 Topological Defects

Take a sample of nematic and place it between two cross-polarisers. Under an optical microscope you will observe a Schlieren texture, a beautiful pattern of light and dark brushes meeting at points [18]. An example is given in Figure 1.2. Remarkably for a macroscopic image, Figure 1.2 can be used to infer microscopic information about the local orientation of the nematic at each point in the sample [9, 20, 21]. Because the nematic is between cross-polarisers, no light will pass if it is aligned with either of the polarisers – these are the dark brushes. If, however, the nematic is oriented at an angle of approximately $\pi/4$ to either (and hence both) of the cross-polarisers, light will pass – these are the light brushes. What of the points where the brushes meet? At these points the transition from light to dark and back again is extremely fast, this indicates that the gradients of $\mathbf{n}$ diverge and we find a singularity in the order, a topological defect. Of course, in reality $\nabla\mathbf{n}$ does not diverge, at the defect core the liquid crystal locally melts into the isotropic phase [1].

We can understand the nature of the defects purely by counting the brushes. There are two types of defects, those with two dark brushes and those with four. Since the nematic is thin, we can treat it as a two dimensional system with $\mathbf{n}$ lying tangent to the plane. In the vicinity of a defect with two dark

brushes, we must have that the director is vertical and horizontal (supposing that these are the two orientations of the polarisers) only once each and so the director must wind by π around the defect, whereas for the defects with four brushes the director must be vertical and horizontal twice, and so the director must wind by 2π around the defect. We can make this more formal as follows. Firstly, in the vicinity of the of a half strength defect a description in terms of a vector, $\mathbf{n} = (n_1, n_2)$, is no longer sufficient, and we must use an orientationless description. The simplest is the tensor $\mathbf{n} \otimes \mathbf{n}$ given (locally) by

$$\mathbf{n} \otimes \mathbf{n} = \begin{pmatrix} n_1^2 & n_1 n_2 \\ n_1 n_2 & n_2^2 \end{pmatrix}, \tag{1.11}$$

which has $\mathbf{n}$ as its only eigenvector with non-zero eigenvalue. Removing the isotropic part (corresponding to $(\mathrm{Tr}(\mathbf{n} \otimes \mathbf{n})/2)\mathbb{I} = (1/2)\mathbb{I}$, since $n_1^2 + n_2^2 = 1$) we obtain the Q tensor

$$Q = \frac{1}{2} \begin{pmatrix} n_1^2 - n_2^2 & 2n_1 n_2 \\ 2n_1 n_2 & n_2^2 - n_1^2 \end{pmatrix}. \tag{1.12}$$

Since $(n_1^2 + n_2^2)^2 = (n_1^2 - n_2^2)^2 + (2n_1 n_2)^2 = 1$, we can rewrite this as

$$Q = \frac{1}{2} \begin{pmatrix} \cos\theta & \sin\theta \\ \sin\theta & -\cos\theta \end{pmatrix}, \tag{1.13}$$

where now $\mathbf{n} = (\cos\theta/2, \sin\theta/2)$. In this way we can describe the local orientation with the angle θ which is well-defined everywhere. Suppose one has a defect in a Schlieren texture then, in order to be well-defined, around that defect that angle θ must wind by $q2\pi$, $q \in \mathbb{Z}$, corresponding to the director field winding by an angle of $q\pi$. This integer q labels the charge of the defect, and example profiles are illustrated in Figure 1.3. Note that if q is odd then the director is non-orientable around the defect line. The existence of these non-orientable defects is a direct consequence of the non-orientability of

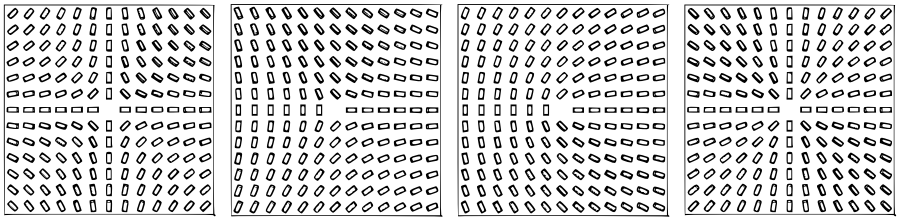

Figure 1.3: Defect profiles in two-dimensional nematics with $|q/2| \leq 1$. Note that if q is odd, then the defect is non-orientable.

the nematic order.

What happens if we bring together two defects of charge p and q? Consider the function $f_\epsilon(z) = (z-\epsilon)^p(z+\epsilon)^q$, where $z = x + iy$ is the standard complex coordinate in the plane. We can then construct an associated Q by writing $\theta_\epsilon = \mathrm{Arg}(f_\epsilon)$. For any non-zero value of ϵ, θ_ϵ has two singularities, one at $(\epsilon, 0)$ and one at $(-\epsilon, 0)$. From the form of f_ϵ one can see that the singularity at $(\epsilon, 0)$ will have winding p and the other winding q. In the limit $\epsilon \to 0$ the two singularities are brought together and we are left with $f_0 = z^{p+q}$, which contains a single singularity of winding $p+q$; bringing defects together adds their charges.

While the two dimensional case is instructive the most interesting phenomena are found in one dimension higher. In three dimensions the defects that were points in two dimensions become line defects, or disclinations (one can think of them as being extruded along the third axis). It is arguable that from a theoretical perspective these characteristic disclinations are the most interesting aspect of liquid crystalline order; indeed the term nematic comes from the Greek $\nu\epsilon\mu\alpha$, meaning thread, referring to the thread-like disclination lines observed in a three dimensional sample.

This move to three dimensions has profound consequences for the topological properties of the defects in the system. Singularities corresponding to an integer winding of $\mathbf{n}$ in two dimensions become removable in three dimensions. Perhaps the most famous example of this is the so-called 'escape

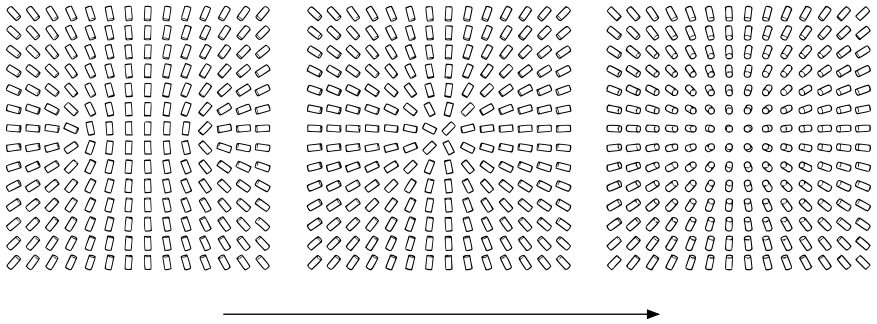

Figure 1.4: Escape in the third dimension. Two half strength defects are brought together, if the system is in two dimensions this is still a topological defect with winding $+1$. In three dimensions, however, the singularity can be removed by rotating the director to the vertical, as shown in the far right image. This process is an illustration of the fact that $\pi_1(\mathbb{RP}^2) \cong \mathbb{Z}_2$ and that $1 + 1 \equiv 0 \bmod 2$.

in the third dimension' [22–24], illustrated in Figure 1.4, where a $+1$ winding profile is removed by rotating the director field towards the vertical as one approaches the singularity. Because a singularity with winding p can be split into two singularities with winding $q + r = p$ and since every half-integer is equal to $q + 1/2$, $q \in \mathbb{Z}$, this immediately means that not only are integer windings removable in three dimensions, but that all half-integer windings can be made equivalent. Not only this, but if we have two disclination lines, then they will each have half-integer profiles, which combine to create a removable integer profile, so disclination lines can self-annihilate. As well as disclination lines, three-dimensional nematic order also contains point defects. The most common of these is the so-called 'hedgehog', given by the radial texture $\mathbf{n} = \mathbf{e}_r$, found, for example, in nematic droplets [25].

1.3 The Homotopy Theory of Defects

While the two-dimensional case is simple enough to understand on an intuitive basis, the more complex phenomena arising in three dimensions necessitate the development of a theoretical framework to give a precise description. Traditionally this has been supplied by the homotopy theory of defects [21, 26]. This theory studies configurations of an ordered material

up to an equivalence relation of homotopy, that is $\mathbf{n}_0$ and $\mathbf{n}_1$ are held to be topologically equivalent if there is a one-parameter family of directors $\mathbf{n}_t$ interpolating between them. The study of an individual defect in this scheme is done locally – defects are classified according to the topology of the director on an appropriate subset of the sample that either surrounds or encircles the defect. It is important to note that the homotopy theory of defects incorporates no information about the energetics. It is often the case that two topologically equivalent configurations are separated by a large energy barrier and so may be considered as inequivalent configurations from an experimental perspective. Nevertheless, if the topological theory indicates a distinction between configurations, then the distinction is robust.

To give a flavour of the theory, we can study the two-dimensional case. Suppose one has a defect in a nematic at a point $p \in \mathbb{R}^2$. Consider an open neighbourhood $N(p)$, given by the set of points $\{x \in \mathbb{R}^2 \ : \ |x-p| < \epsilon\}$ for $\epsilon > 0$. Then locally we can treat $\mathbf{n}$ as a director field defined on the set $D = N(p) - p$. If we give a local basis for tangent vectors, $\{\mathbf{e}_1, \mathbf{e}_2\}$, then at a point $a \in D$, $\mathbf{n}$ describes an unoriented direction. The space of unoriented directions in two dimensions is the real projective line $\mathbb{RP}^1$, given by identifying antipodal points on the circle. We can then extend $\{\mathbf{e}_1, \mathbf{e}_2\}$ to a basis over the entirety of D and regard $\mathbf{n}$ as a map, $\mathbf{n} : D \to \mathbb{RP}^1$. The homotopy theory of defects then states that we should consider classes of maps up to the relation of homotopy, which we denote $[D, \mathbb{RP}^1]$. Now our domain is an open annulus, $D \cong S^1 \times (0,1)$ and is homotopy equivalent to the circle S^1, an operation which can be visualised by making the annulus progressively thinner. As such $[D, \mathbb{RP}^1] \cong [S^1, \mathbb{RP}^1]$.

From the previous discussion we already know the answer to this problem, $[S^1, \mathbb{RP}^1] \cong \mathbb{Z}$, the winding number. To calculate this from a homotopy theoretic perspective we first consider a restricted set of maps, where we fix the value of $\mathbf{n}$ at a given point, known as the basepoint. The set of all maps from S^1 to any space X with a fixed basepoint has the structure of a group

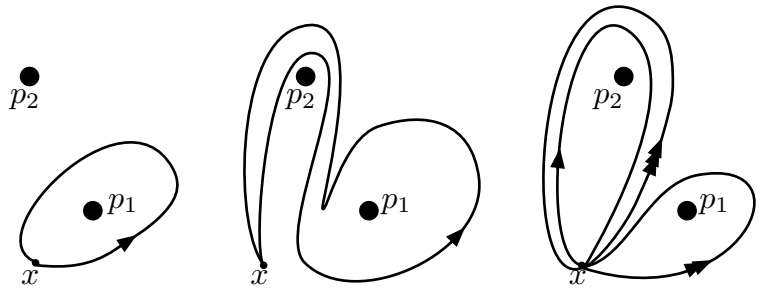

Figure 1.5: Changing the basepoint. Suppose the defects at p_1 and p_2 correspond to elements a and b respectively in $\pi_1(X)$, for an order parameter space X. By dragging the basepoint, x around p_2 a map corresponding to a is freely homotopic to bab^{-1}, for any $b \in \pi_1(X)$.

(the group operation is composition of maps), and is known as the fundamental or first homotopy group $\pi_1(X)$ [27]. The first step in the homotopy classification is therefore computing the fundamental group of X. In our case it is a standard result that $\pi_1(\mathbb{RP}^1) \cong \mathbb{Z}$. The final step is allowing the basepoint, previously held fixed, to vary. Doing this gives an equivalence between $a \in \pi_1(X)$ and bab^{-1} for any $b \in \pi_1(X)$, as indicated in Figure 1.5. In our case $\mathbb{Z}$ is abelian so $bab^{-1} = a$, and we find that homotopy classes of point defects in two-dimensional nematics are given by the integers.

Now we need to generalise the procedure to other dimensions and systems. First we identify the order parameter space, X, for our system. We then examine homotopy classes of maps from the neighbourhood of a singularity into our order parameter space. In two dimensions the circle, S^1, surrounded a point defect but in three dimensions it surrounds a line defect. By identical reasoning, point defects in three dimensions are given by studying maps from S^2 into the order parameter space. To do this we need to generalise the fundamental group to $\pi_n(X)$, denoting the group of homotopy classes of basepoint preserving maps from S^n to X. The topological type of point defects are then given by elements in $\pi_2(X)$, modulo an equivalence relation. This equivalence relation is similar to that in Figure 1.5, but instead of a simple conjugation of elements, $\pi_1(X)$ has a group action on

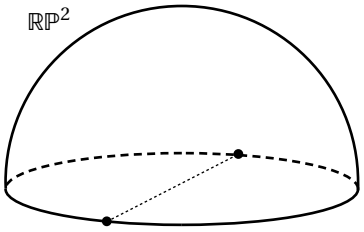

Figure 1.6: The real projective plane, $\mathbb{RP}^2$, the order parameter space for nematics. It can be thought of as a hemisphere with antipodal points on the equator identified. The non-orientability of this space leads to the presence of line defects in nematics.

all other homotopy groups, and it is this action that forms the equivalence relation. Finally, note that there is a relationship between the dimension of the surrounding sphere s, the defect r and the ambient space d, namely $s + r = d - 1$

Before we use this theory to understand three-dimensional nematics, we note that for a space of dimension d, $\pi_d(X)$ (and its associated equivalence relation) can be used to understand topologically non-trivial non-singular states [28]. If one has a system described by a field $\phi(x) : \mathbb{R}^d \to X$ which tends to a constant as $|x| \to \infty$, then the domain can be compactified to obtain a map $S^d \to X$, which can be classified with the homotopy theoretic techniques. A variety of topological solitons, such as baby Skyrmions and Hopf solitons can arise in this way.

Applying the theory to three dimensional nematics, the first challenge is to identify the order parameter space. Again we have a nematic described by a line field $\mathbf{n}$. At any point in space the possible lines are given by points in S^2 with antipodal points identified. This space is the real projective plane $\mathbb{RP}^2$, and can be visualised as a hemisphere with antipodal points on the equator identified, as shown in Figure 1.6[1]. The homotopy groups of this space are well known, and are given in Table 1.1, one finds that, as mentioned above, three dimensional nematics contain both point and line defects.

For line defects in three dimensional nematics, the appropriate homo-

[1]Because it is a closed non-orientable surface, it does not embed in three dimensional space, and so any visual representation necessarily contains cuts or self-intersections.

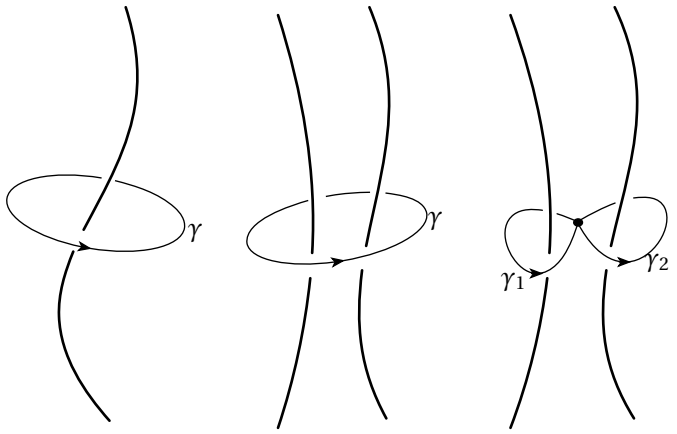

Figure 1.7: Combining line defects. Two line defects, of type a and b in $\pi_1(X)$ can combine to form a defect of type ab. In the case of disclinations in nematics, two line defects merging will always mutually annihilate, as $1+1 \equiv 0 \bmod 2$.

topy group is $\pi_1(\mathbb{RP}^2)$, which is the two element group, $\mathbb{Z}_2$. This is abelian and so described the line defects in three dimensional nematics. The trivial element (0) represents a loop encircling no (or an even number of) defect(s) and the non-trivial element (1) represents a loop encircling an odd number of disclination lines. This simple classification (in fact it is the simplest possible classification of defects) reflects the fact that we uncovered earlier: there is only one local structure for disclination lines in nematics, and that they may mutually annihilate, as shown schematically in Figure 1.7.

Point defects are a little more complicated. As indicated by Table 1.1 the second homotopy group is given by $\pi_2(\mathbb{RP}^2) \cong \mathbb{Z}$. However, we need to take into account the action of π_1 on π_2. In this case the action sends $x \to -x \in \mathbb{Z}$ and hence the classification of point defects is given by $\mathbb{Z}/(x \sim -x) \cong \mathbb{N}$, the natural numbers [21]. Essentially, because the nematic is unoriented one cannot distinguish between a point defect of type $\mathbf{n} = \mathbf{e}_r$ and $\mathbf{n} = -\mathbf{e}_r$. This raises potential issues. Suppose one has a system containing two point defects of type $p, q \in \mathbb{N}$. What happens when they are brought together? In the two dimensional case it is easy, the answer was $p+q$, but the three dimensional case is more complex. The answer may be $|p+q|$ or $|p-q|$. This ambiguity can only be solved by extending the homotopy theory to allow for

	H	π_1	π_2	π_3
Ferromagnet	$SO(2)$	1	$\mathbb{Z}$	$\mathbb{Z}$
Nematic	$O(2)$	$\mathbb{Z}_2$	$\mathbb{Z}$	$\mathbb{Z}$
Frame Field	1	$\mathbb{Z}_2$	1	$\mathbb{Z}$
Biaxial	D_2	Q	1	$\mathbb{Z}$

Table 1.1: Homotopy groups for the quotient of $SO(3)$ by various symmetry subgroups, H. Q denotes the group generated by $\langle i, j \rangle$ under quaternionic multiplication.

global information, connecting the two defects, which is explored in Chapter 2.

1.4 The General Theory

In the 70's the theory of topological defects in ordered materials was put on a general footing within the paradigm of broken symmetry. The classic text in this field is the review article by Mermin [26], but we will give a recapitulation since the ideas will play a role throughout this thesis.

One supposes that the system has some symmetry group G which is spontaneously broken in the ground state to a subgroup H. The canonical example and one which is relevant for us is ferromagnetism in three dimensions. The Hamiltonian of a ferromagnet is invariant under the action of $SO(3)$, corresponding to rotations of the system, the ground state of the system is a unit vector which breaks the $SO(3)$ symmetry and is only invariant under an $SO(2)$ subgroup of $SO(3)$ corresponding to rotations about the axis of the ferromagnetic order.

In this picture distinct ground states are labelled by elements in the quotient space G/H, which can be thought of as the order parameter space. The local description of topological defects is then given by homotopy classes of maps from measuring spheres into G/H. We will suffer through two trivial examples before discussing an interesting one, all are detailed in Table 1.1 and Figure 1.8. The first trivial example is the aforementioned case of the ferromagnet. Here we have an initial $SO(3)$ broken to an $SO(2)$ which pre-

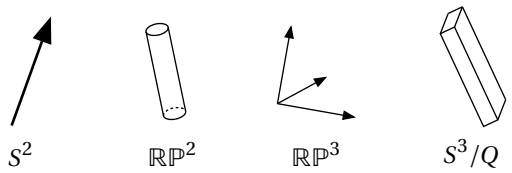

Figure 1.8: Visualisation of various types of order. From left to right: ferromagnetic order, described by a point in S^2, can be viewed as a unit vector; nematic order, given by $\mathbb{RP}^2$ can be visualised as a field of cylinders or lines; $SO(3)$ order can be viewed as a field of oriented triads and has $\mathbb{RP}^3 \cong SO(3)$ as an order parameter space; biaxial nematics, viewed as a brick invariant under π rotations about the principal axes, have the manifold S^3/Q as their order parameter space, where S^3 is viewed as the unit quaternions.

serves an oriented axis. The quotient space $SO(3)/SO(2)$ is S^2, so the local topology of defects in ferromagnets is given by homotopy groups of S^2. Nematics are similar, however the symmetry is broken to $O(2)$, since we need only preserve an unoriented axis. The quotient space $SO(3)/O(2)$ is the real projective plane, as discussed above, which leads to the presence of disclination lines.

1.5 Biaxial Nematics

One of the most interesting applications of the homotopy theory of defects is to biaxial nematics. This example is well known as being one of the simplest to exhibit more elaborate topological phenomena [21, 29]. We discuss it because it is interesting and because one of the main focuses of this thesis, the topology of cholesterics, has previously been approximated as that of biaxial nematics [12]. In these materials the local order is given by three principal unoriented directions, $\mathbf{e}_1$, $\mathbf{e}_2$ and $\mathbf{e}_3$. One can think of this as a brick, invariant under π rotations about each of the principal axes, as illustrated in Figure 1.8. More formally we identify the subgroup H of $SO(3)$ as consisting of rotations of π about each of the principal axes. So now we need to consider the order parameter space $SO(3)/H$. It is easier in this situation to use the $SU(2) \to SO(3)$ homomorphism and regard $SU(2)$ as the unit quater-

nions whence H becomes the subgroup $Q = (\pm 1, \pm i, \pm j, \pm k)$. As a manifold $SU(2) \cong S^3$ and so to understand line defects in biaxial nematics we are required to calculate $\pi_1(SU(2)/Q)$. Fortunately, there is a theorem [26,27] that says if G is a simply connected Lie group (such as $SU(2)$) and H a discrete subgroup, then $\pi_1(G/H) \cong H$. Therefore $\pi_1(SU(2)/Q) \cong Q$. Of course, as discussed above, to get the full classification one must consider conjugacy classes of Q. There are 5 such classes, corresponding to $\{1\}$, $\{-1\}$, $\{i,-i\}$, $\{j,-j\}$, $\{k,-k\}$. The first of these is the trivial element, corresponding to no defect. The last three correspond to singularities in each of the three principle directions. The second type, the $\{-1\}$, is associated to the fact that $SO(3)$ is not simply connected.

There are many subtleties coming from this formalism, we will highlight one which will be relevant to our discussion of cholesterics in Chapter 4. As observed by Poénaru and Toulouse [29], because Q is non-Abelian, defect lines may not necessarily be able to cross. If one has two line defects of type a and $b \in \pi_1(G/H)$, then their attempted crossing will result in a tether defect whose type is equivalent to the commutator $[a,b] = aba^{-1}b^{-1}$, as indicated in Figure 1.9. In biaxials, then, defects of type $\{i,-i\}$, $\{j,-j\}$ and $\{k,-k\}$ may not cross without leaving a tether of type -1, *e.g.* $(i)(j)(-i)(-j) = k^2 = -1$. We will show in Chapter 4 that an entirely different theory can reproduce these rules.

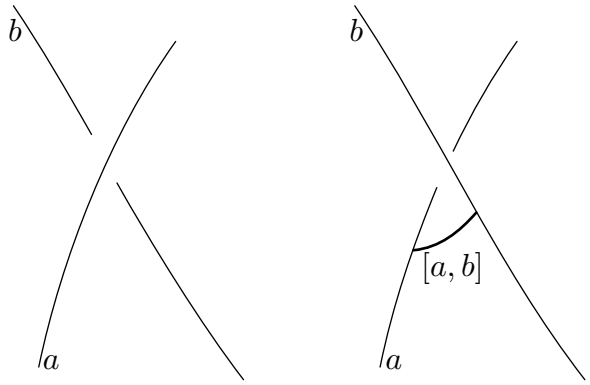

Figure 1.9: Crossing of defect lines. The attempted crossing of defect lines of types a and b will result in a tether of type $[a,b] = aba^{-1}b^{-1}$.

Chapter 2

Global Theory of Topological Defects in Nematic Liquid Crystals

In this chapter we will study the topological properties of defects in nematic liquid crystals from a global perspective. The traditional method of classification, outlined in the introduction, is performed by examining homotopy classes of maps $S^n \to \mathbb{RP}^2$, where the sphere S^n encircles a line defect $n = 1$ or surrounds a point defect $n = 2$, with distinct homotopy classes representing distinct defect types. The limitation of this analysis is that it is fundamentally local in nature and cannot capture any more subtle, global information about the topology of the texture. For example, from this perspective the topology of a disclination line is essentially unique; there are two classes of maps $S^1 \to \mathbb{RP}^2$, which we can denote 0 and 1, and which (roughly) correspond to disclination not present or present respectively, and so a disclination simply corresponds to the class 1. A little thought should make it clear, however, that this is not the only topological invariant of a line defect. For example, a line defect should possess a point defect charge. To see this, consider a small isolated disclination loop in a three dimensional nematic, so the material domain is all of $\mathbb{R}^3$ with free boundaries. In nematics, Derrick's theorem holds, which states that any uniform scale transformation of the director $\mathbf{n}(x) \to \mathbf{n}(\lambda x)$, $\lambda > 1$, acts to reduce the Frank free energy. As a con-

sequence such a defect loop will shrink until it becomes a point[1]. This point defect should then be classified by the invariants for point defects, which in this case is a natural number, $q \in \mathbb{N}$. The value of this invariant is fully determined by the structure of $\mathbf{n}(x)$ as $|x| \to \infty$, and can indeed by computed via the explicit integral

$$q = \left| \frac{1}{4\pi} \int_{S^2} \mathbf{n} \cdot \partial_\theta \mathbf{n} \times \partial_\phi \mathbf{n} d\theta d\phi \right| \tag{2.1}$$

where the sphere S^2 surrounds the defect and θ and ϕ are standard angular coordinates. As the defect shrinks to a point, the deformations of the texture on this sphere are smooth, and so cannot change the value of q. So clearly the defect loop must have possessed the same value of q, and so has a point defect charge as well as the $\mathbb{Z}_2$ invariant coming from $\pi_1(\mathbb{RP}^2)$.

This amendment seems simple enough, one should just say that disclination loops may carry a hedgehog charge. But then what happens if one has linked disclination loops? The disclination lines cannot be unentangled now, and it is not clear if one can associated a point defect charge separately to each of them, or a single point defect charge to the combination, or something else entirely. As we will show in this chapter, the answer is somewhere in the middle. Two linked defect lines possess only one point defect charge, but they also possess an additional $\mathbb{Z}_2$ topological invariant. The possible values this invariant may take depend upon the specific knot or link type of the defect line, for example a trefoil knot has a $\mathbb{Z}_3$ invariant, and an Olympic chain of N rings has a $\mathbb{Z}_2^{N-1}$ invariant. These indices reflect topologically distinct ways that the nematic can be ordered on the complement of the particular defect set. In the same way that there are many topologically distinct ways of ordering a nematic the exterior of a point defect, indexed by $\mathbb{N}$, there are topologically distinct ways of ordering a nematic in the exterior of knots and links. These additional invariants associated to knotted and linked defects are fundamentally global in nature, and as such cannot be captured

[1] This is more properly a cobordism.

by the traditional local approach. These invariants and their associated nematic textures are topological in the sense that they only depend on the knot or link type of the defect line, and not on specific profiles or any other local structure (as in the case of the self-linking numbers of Čopar [30]). However, because they are associated to specific knot and link types, they are not robust under changes of defect topology such as strand crossings[2].

For a collection of knotted and linked disclinations $\mathcal{L}$, the natural description of these states is in terms of the split components of $\mathcal{L}$, which are the number of distinct entangled components of a link. Formally, the split components form a partition of $\mathcal{L}$ so that each split component can be surrounded by a sphere, without any of the other components either in the interior of the sphere or intersecting the surface. For example, two linked loops have one split component, whereas two unlinked loops have two split components. The topological states associated a given split component, L_i are given by elements in the set

$$\left(\mathbb{Z} \oplus H_1(\Sigma(L_i))\right) / (x \sim -x), \tag{2.2}$$

where $H_1(\Sigma(L_i))$ is the first homology of the branched double cover of L_i, $\Sigma(L_i)$, which is a manifold associated to the split component. The elements of this set describe distinct topological states, corresponding to homotopy classes of textures in the complement of the defect set. The first factor of $\mathbb{Z}$ enumerates the possibles hedgehog charges for the split component, the second factor is more subtle and enumerates a set of internal topological states. Finally, the equivalence relation $x \sim -x$ is inherited from the $q \sim -q$ equivalence in the case of point defects and is applied to both sets ($\mathbb{Z}$ and $H_1(\Sigma(L_i))$ simultaneously.

As an example, take two linked loops, the Hopf link. In this case $H_1(\Sigma(L)) \cong$

[2] We note, however, that a full understanding of how the topology is affected by the dynamics makes for a very interesting project. An initial formulation is to create a cobordism from one defect to another and study maps relative to two fixed homotopy classes on the boundary manifolds (so one has a 4-manifold with corners). One should then for an obstruction to the creation of such a map.

$\mathbb{Z}_2$, so the possible states are given by

$$(\mathbb{Z} \oplus \mathbb{Z}_2/\sim) \cong \mathbb{N} \times \mathbb{Z}_2 \tag{2.3}$$

The first factor corresponds to the hedgehog charge, while the second $\mathbb{Z}_2$ factor is an internal state, which we shall see can be roughly interpreted as a statement about the signed linking numbers of the defect lines, a statement which is made explicit in Chapter 6. This is an intriguing result, nematic order is unoriented – a fact that is almost its defining property – but yet if one has linked defect lines, then the nematic order imparts a relative (not absolute) orientation to them, which is realised by homotopically distinct nematic textures on the complement of the defect set. As a consequence, every set of linked defects that has been made in the laboratory so far has possessed an invariant of this form, either 0 or 1 (or ± 1 if one wants to think about linking numbers). This invariant is the simplest possible internal state for a knotted and linked defect line and has not been explored or investigated experimentally, let alone the huge number of intricate structures associated to more complex knots and links. In Chapter 6 we give derive formulae for field configurations representing these two different configurations, for completeness we will quote them here. If one takes the two complex scalar fields

$$f_1(x,y,z) = \left(1 + \frac{8(1+x^2) - 8(1+x^2+y^2+z^2)}{(1+x^2+y^2+z^2)^2}\right) + i4\left(\frac{2xy - z(x^2+y^2+z^2-1)}{(1+x^2+y^2+z^2)^2}\right), \tag{2.4}$$

and

$$f_2(x,y,z) = \left(\frac{8(x^2+y^2)}{(1+x^2+y^2+z^2)^2} - 1\right) + i4\left(\frac{x(x^2+y^2+z^2-1) - 2yz}{(1+x^2+y^2+z^2)^2}\right). \tag{2.5}$$

Then the director fields

$$\mathbf{n}_i = (\cos\phi_i, 0, \sin\phi_i) \tag{2.6}$$

where $\phi_i = \Im \log {f_i}^{1/2}$ are homotopically distinct director fields with identical defect sets, both $\mathbf{n}_i$ have the same disclinations on a pair of linked rings defined by the constraints: $L_1 = \{x = z\} \cap \{2y = x^2 + y^2 + z^2 - 1\}$ and $L_2 = \{x = -z\} \cap \{-2y = x^2 + y^2 + z^2 - 1\}$. Both of these textures have $\lim_{|x|\to\infty} \mathbf{n}_i = (0, 0, 1)$, and so both have zero hedgehog charge.

In more complex situations comprising more than one split component the relation $\sim$ is still only applied globally, across all components and the full statement of the global classification of nematic textures can be stated as follows. Let $\mathbf{n}$ be a director field for a nematic liquid crystal in $\mathbb{R}^3$ with a defect set $\mathcal{D}$, we can split $\mathcal{D}$ up as $\mathcal{D} = \mathcal{P} \cup \mathcal{L}$ where $\mathcal{P}$ is the set of point defects and $\mathcal{L}$ is the set of line defects. Furthermore, $\mathcal{L} = \cup_i L_i$ where each of the L_i is a non-split knot or link. Then the topology of the texture $\mathbf{n}$ is given by an element of the set

$$\left(\bigoplus_{p_i \in \mathcal{P}} \mathbb{Z}\right) \oplus \left(\bigoplus_{L_j \in \mathcal{L}} (\mathbb{Z} \oplus H_1(\Sigma(L_j)))\right) / \sim . \tag{2.7}$$

The translation of this is the following. To specify the topological type of a texture containing point defects and a set of entangled defect loops, one needs to specify an integer charge for each point defect and each split component of the defects loops. In addition, one should specify an internal state for each split component, where the internal states live in a group ($H_1(\Sigma(L_i))$) that depends on the link type. Finally, one should consider states x and $-x$ as equivalent.

As an example of this, one can consider the colloidal system with two spherical colloids with an accompanying entangled Hopf link disclination line, as realised by the Ljubljana group [5]. In terms of the above notation, this system contains two point defects $\mathcal{P} = \{p_1, p_2\}$, represented by the col-

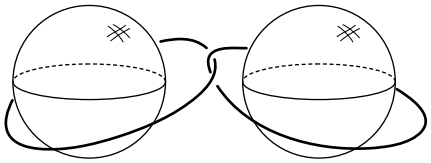

Figure 2.1: The colloidal Hopf link system. *A priori* the topological state is given from (2.32) by an element in the set $\mathbb{Z}\oplus\mathbb{Z}\oplus\mathbb{Z}\oplus\mathbb{Z}_2/\sim$. The system has specific boundary conditions, the colloids have homeotropic anchoring and the texture is uniform at large distances. This serves to fix the first three integers to be ±1, ±1 and ∓2 respectively, so all that remains is a $\mathbb{Z}_2$ invariant. Therefore, up to homotopy this system supports two distinct nematic textures.

loids, and one split component line defect $\mathcal{L}=\{L_1\}$, which takes the form of a Hopf link. *A priori* the topological state is therefore given from (2.32) by an element in the set $\mathbb{Z}\oplus\mathbb{Z}\oplus\mathbb{Z}\oplus\mathbb{Z}_2/\sim$. However, the system has specific boundary conditions, the colloids have homeotropic anchoring and the texture is uniform at large distances. This serves to fix the first three integers to be ±1, ±1 and ∓2 respectively, so all that remains is a $\mathbb{Z}_2$ invariant. This invariant, likely related to the self-linking numbers found in these systems [30], is a true topological invariant of the system and, to our knowledge there has not yet been an analysis of the values this invariant takes in these systems. An important point to note regarding these invariants is that any particular identification of homotopy classes of textures with elements in this set is not canonical, there is no canonical 0 and 1 in the $\mathbb{Z}_2$ for the Hopf link, though one can always fix the class of a set of reference textures to avoid any ambiguity. Figure 2.1 below shows the the Hopf link - colloidal system. Even with the specific boundary conditions on the colloids, there is an additional $\mathbb{Z}_2$ invariant which describes the topology of the system.

Given this result, there are two principal physical questions (which are related to each other): what do these states mean physically and how to I measure them. After establishing the result below, much of the remainder of this thesis concerns variations on these questions. As well as relative orientations mentioned above, aspects of the internal state can be interpreted as Skyrmion tubes, or in cholesterics λ lines, discussed at length in Chap-

ters 3 and 4, entangling the knot or link. Interestingly, if (as is typically the case) the set of internal sets is finite, then it is not amenable to Chern-Weil theory and so cannot be found by performing an integral such as (2.1). Experimental identification of these textures should be achievable through the Pontryagin-Thom construction as applied to nematics [9], though we have not fully formalised the process.

As alluded to, there have been a series of fascinating experiments in which such knotted defect lines have been created experimentally through the use of colloidal particles [5], knotted colloids [6] and toroidal droplets [7]. We hope that our work will help understand these experimental results, and motivate future work. Being able to identify and control these invariants would be of considerable interest.

2.1 Statement of the Problem

We will now give the precise setup for our problem. We consider a nematic liquid crystal in a domain Ω. Typically we will assume Ω is all of $\mathbb{R}^3$ minus a defect set, but this is not required for the calculations. For example, for a single point defect at the origin, the domain is $\mathbb{R}^3 - N(0)$ and for a knotted or linked defect, L, the domain is $\mathbb{R}^3 - N(L)$, where N denotes an open neighbourhood, which makes things more convenient technically, as well as modelling the finite size of nematic defects. To be more specific, in the case of the point defect at the origin the domain is given by $\{x \in \mathbb{R}^3 : |x| \geq \epsilon\}$, where ϵ is the defect radius, typically of order 10^{-8}m [1], though as we are concerned with the topology of the configuration, the actual size of the defects will not change the result. We impose free boundary conditions (up to a topological class) on all defects in the system. We note that other domains without defects (or where not every feature of the domain is a defect) can be encompassed in this approach, such as colloidal systems or other interesting geometries. Finally, we only consider 'tame' domains, such that may be

realisable experimentally[3].

The global problem is therefore to classify homotopy classes of maps $[\Omega, \mathbb{RP}^2]$, which gives the number of topologically distinct nematic textures in the domain Ω. Unlike the standard local approach [21, 26] this global approach throws away no information and avoids the usual ambiguities involved in the interaction of defects in nematics. Previous work on the topology of linked defects in nematics [29–32] has also not taken this global approach. Because Ω is a subset of $\mathbb{R}^3$, it will be homotopy equivalent to an orientable 2-complex [33] [4], $X(\Omega)$ (or just X), and so one need only consider homotopy classes of maps $[X, \mathbb{RP}^2]$. The mathematical problem is therefore homotopy classes of maps from a orientable 2-complex into $\mathbb{RP}^2$. We note that this also includes closed surfaces, for example a torus enclosing a defect line. There is an important physical consequence to the choices we have made. Because we can reduce the domain to an orientable 2-complex, our classification will not identify any phenomena associated to Hopf solitons, whose origin lies in $\pi_3(\mathbb{RP}^2)$. Such a situation could be achieved by fixing boundary conditions on all defects as well as at infinity, which would represent an interesting extension to our work.

2.2 Solution Through Obstruction Theory

The enumeration and classification of homotopy classes of maps $[X, \mathbb{RP}^2]$ have been addressed through the tools of obstruction theory in the work of Olum [34] and a discussion is also given by Eells and Lemaire [35], as well as in a note by Adams [36]. and draws upon the formulation for the case of maps into S^2 [37–40]. The result is that if X is an orientable 2-complex, the homotopy classes of maps $w_1(\mathbf{n}) : X \to \mathbb{RP}^2$ are determined by two invariants, the first is an orientation invariant $w_1(\mathbf{n})$, which can be thought

[3] At this point, one should quote Mermin [26], "[I] invite readers possessing the appropriate blend of ingenuity and perversity to add whatever assumptions of regularity are needed to exclude whatever pathological counterexamples they may come up with".

[4] See footnote 3.

of as a homomorphism $\pi_1(X) \to \mathbb{Z}_2$, which measures whether each loop in the domain preserves or reverses orientation, we note that this can be thought of as a discrete gauge field. Given $w_1(\mathbf{n})$, the free homotopy classes of maps are then in correspondence with elements of the set $H^2(X;\mathbb{Z}^w)/\sim$, where $H^2(X;\mathbb{Z}^w)$ is the twisted cohomology with the local coefficient system $\mathbb{Z}^w$ given by $\mathbb{Z}$ along with the map $\rho : \pi_1(X) \to \mathrm{Aut}(\mathbb{Z})$, equivalent to w_1.

These two invariants are related to $\pi_1(\mathbb{RP}^2)$ and $\pi_2(\mathbb{RP}^2)$ respectively, and measure properties relating to the orientation and to Skyrmions and point defects in the texture respectively. The result (2.32) is a computation of the second invariant for the case of a set of knotted and linked and indeed in general our problem can be solved by giving a computation of the twisted cohomology for a given choice of Ω and w_1. While we could begin immediately with this computation we will first give a discussion of the origins of these invariants.

2.2.1 First Invariant

The first invariant is related to the non-orientability of the texture. The director field $\mathbf{n} : \Omega \to \mathbb{RP}^2$ induces a homomorphism on the fundamental groups

$$\theta : \pi_1(\Omega) \to \pi_1(\mathbb{RP}^2) = \mathbb{Z}_2, \tag{2.8}$$

which measures whether $\mathbf{n}$ preserves or reverses orientation upon traversal of each loop in Ω. The primary example in this case is if γ is a loop encircling a disclination line, then $\theta(\gamma) = 1$. Note also that as $\mathbb{Z}_2$ is Abelian, this is equivalent to a map $w_1(\mathbf{n}) : H_1(\Omega) \to \mathbb{Z}_2$, and thus defines an element $w_1(\mathbf{n}) \in H^1(\Omega;\mathbb{Z}_2)$. As another explicit example, if Ω is $\mathbb{R}^3 - \mathcal{L}$, a set of $|L|$ line defects, then $H^1(\mathbb{R}^3 - \mathcal{L};\mathbb{Z}_2) = \mathbb{Z}_2^{|L|}$ and $w_1(\mathbf{n})$ is the element $(1,1,\ldots,1) \in \mathbb{Z}_2^{|L|}$. If instead the first line defect is actually a toroidal colloid, and $\mathbf{n}$ is orientable around it, then $w_1(\mathbf{n}) = (0,1,1,\ldots,1)$. The invariant $w_1(\mathbf{n})$ is an extension to the global case of local measurements around each defect line in a system. The observation one makes from the above exam-

ples is that this extension is trivial – the global information is simply given by specifying the local information around each closed loop in the system.

Of some later use will be the perspective of $\mathbf{n}$ not as a map $\Omega \to \mathbb{RP}^2$ but as a vector bundle. Nematic order associates to each point in the domain the linear subspace of vectors which point tangentially to the order. It therefore defines a one-dimensional subbundle $L_{\mathbf{n}}$ of the tangent bundle $T\Omega$. The invariant $w_1(\mathbf{n})$ is the first Stiefel-Whitney class of this bundle.

To show that this is indeed a homotopy invariant we will consider maps on the 1-skeleton of the complex, X, associated to Ω. Let X_n be the n-skeleton of X. First fix a particular point $p \in \mathbb{RP}^2$, and a map $X_0 \to \mathbb{RP}^2$ that maps each 0-cell in X_0 to p. Extending this map to X_1, keeping the map on X_0 fixed, is given up to homotopy by a choice of element in $\pi_1(\mathbb{RP}^2)$ for each edge in X_1, and so defines an element $c \in C^1(X_1;\mathbb{Z}_2) \cong C^1(X;\mathbb{Z}_2)$. This map can be extended onto X_2 only if the map is orientable around the boundary of each 2-cell, and so requires $\delta c = 0$.

Now consider two maps $f, g : X_1 \to \mathbb{RP}^2$ as defined above. We will try and construct a homotopy between them. To do this we take the complex $Y = X \times [0,1]$ and try to find a map $h : Y \to \mathbb{RP}^2$ such that h restricted to 0 resp. 1 is f resp. g. First consider the map restricted to $Y_1 = [0,1] \times X_0$, denoted h_1. Y_1 consists of two copies of the vertices of X, with each vertex joined to its pair by an edge. By construction h_1 restricted to each copy of the vertices must map to the point p, so as before h_1 is specified by an element $c^0 \in C^1(Y_1;\mathbb{Z}_2) \cong C^0(X;\mathbb{Z}_2)$, determining whether the homotopy is trivial or orientation reversing along each edge connecting the vertex pairs.

Extending the map h_1 onto Y_2, requires extending onto the the faces of Y_2, each of which corresponds to an edge in X_1. The boundary of each face in Y_2 consists of four edges. Two of these edges are a pair in $X_1 \times 0$ and $X_1 \times 1$. The other two edges connect the vertices in $X_1 \times 0$ to their corresponding partner in $X_1 \times 1$. The homotopy class of maps on the first two of these edges is determined by the maps f and g, and on the second two by h_0. The

extension to Y_2 can only be made if the map along the boundary of this face is orientable, this requires that $c_f - c_g = \delta c_0$, for $c_0 \in C^0(X;\mathbb{Z}_2)$. It follows that the pointed homotopy classes of maps on X_1 is given by elements of $H^1(\Omega;\mathbb{Z}_2)$.

2.2.2 Second Invariant

The second invariant ultimately has its origins in the fact that $\pi_2(\mathbb{RP}^2) \cong \mathbb{Z}$, along with the action of π_1 sending $x \to -x \in \pi_2$. From an abstract perspective one can construct the second invariant as follows. First one takes the twisted cohomology of $\mathbb{RP}^2$, $H^2(\mathbb{RP}^2;\mathbb{Z}^w) \cong \mathbb{Z}$. The map $\Omega \to \mathbb{RP}^2$ allows us to pull back the generator of this twisted cohomology to obtain a class in $H^2(\Omega;\mathbb{Z}^w)$ which is a homotopy invariant.

More geometrically, if the first invariant vanishes, $w_1(\mathbf{n}) = 0$, then the nematic texture is orientable and one can lift to a map $\hat{\mathbf{n}} : \Omega \to S^2$. The topological classification of orientable nematics on Ω is then given by the classification of unit magnitude vector fields, or maps into S^2, with the equivalence relation that the map $\hat{\mathbf{n}}$ and thus its homotopy class is identified with that of $-\hat{\mathbf{n}}$. This is a well-known result, and is simply given by the second cohomology group $H^2(\Omega)$ along with the equivalence relation $\sim$. Heuristically the result in the non-orientable case is similar, one attempts to orient the director, and classify with the second cohomology group, but because the nematic is non-orientable the sign of the element in H^2 can change upon traversal of a cycle, this is the origin of the twisted cohomology.

To proceed we will first orient a non-orientable texture. To do this we must pass to a covering space for our domain Ω. One can think of this space, $\widehat{\Omega}$ as containing two copies of Ω, with each copy containing one of the two possible orientations of the director field. To construct the cover, we observe that connected covering spaces for a given space Ω are classified by conjugacy classes of subgroups of the fundamental group $\pi_1(\Omega)$ [27]. So which covering space do we choose for our nematic domain Ω? The purpose of our

covering space is to allow us to orient $\mathbf{n}$. The obstruction to doing this is the first invariant $w_1(\mathbf{n}) : H_1(\Omega) \to \mathbb{Z}_2$ being non-zero. The criterion for $\mathbf{n}$ to be orientable on the covering space $\widehat{\Omega}$ is as follows. $H_1(\Omega)$ is the commutator subgroup of $\pi_1(\Omega)$. Thus, for a covering space, $\widehat{\Omega}$, there is an induced map $h \circ p : \pi_1(\widehat{\Omega}) \to H_1(\Omega)$, where h, the Hurewicz map, is equivalent to Abelianisation. This can then be composed with w_1 to form a map $\pi_1(\widehat{\Omega}) \to \mathbb{Z}_2$. $\mathbf{n}$ is orientable on $\widehat{\Omega}$ if this map is trivial.

The idea is to construct the 'smallest' covering space on which $\mathbf{n}$ is orientable, corresponding to the subgroup consisting of all loops in $\pi_1(\Omega)$ which map to $0 \in \mathbb{Z}_2$. To do this, look at the kernel, K, of the homomorphism $w_1 \circ h : \pi_1(\Omega) \to \mathbb{Z}_2$. Then it is an elementary result that K is a normal subgroup of $\pi_1(\Omega)$, and furthermore, since $w_1 \circ h$ is non-trivial, the index of K must be 2. So $\widehat{\Omega}$ is constructed from the subgroup corresponding to the kernel of $w_1 \circ h$. Note that our covering space is equipped with an order two deck automorphism

$$t : \widehat{\Omega} \to \widehat{\Omega}, \quad t^2 = 1 \tag{2.9}$$

that simply permutes the sheets of the cover.

As an example we will consider possible covering spaces when the domain is the torus, T^2, show in Figure 2.2. We have $\pi_1(T^2) = \mathbb{Z}^2$, which is generated by two elements e_1, e_2 that correspond to a meridian and longitude of the torus respectively. Then there are three non-trivial possibilities:

1. e_1 is non-orientable under the map w_1 and e_2 is orientable, *i.e.* $w_1(e_1) = 1$ and $w_1(e_2) = 0$.
2. e_2 is non-orientable ($w_1(e_2) = 1$) and e_1 is orientable ($w_1(e_1) = 0$).
3. Both e_1 and e_2 are non-orientable ($w_1(e_2) = w_1(e_1) = 1$) .

Our covering space corresponds to the subgroup of $\mathbb{Z}^2$ which is the kernel of the map to $\mathbb{Z}_2$. In case 1, this is the subgroup $\langle 2e_1, e_2 \rangle$. In case 2, it is the subgroup $\langle e_1, 2e_2 \rangle$ and in case 3 it is the subgroup $\langle e_1 + e_2, e_1 - e_2 \rangle$. In all these cases the resulting covering space $\widehat{\Omega}$ is once again a torus.

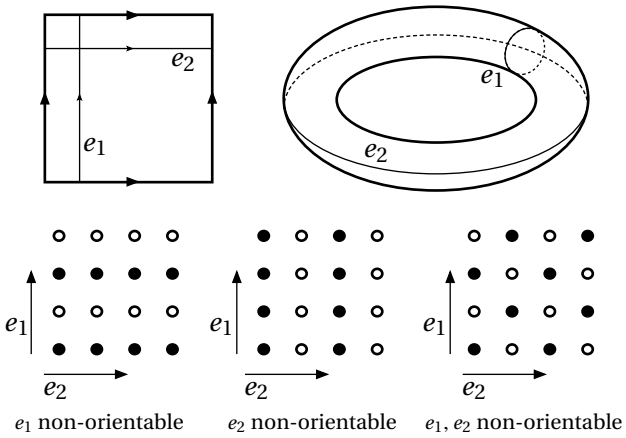

Figure 2.2: Nematic covering spaces when the domain is the torus. *Top left*: schematic of the torus as a square with opposite sides identified, with generators for $\pi_1(T^2)$ illustrated. *Top right*: as top left, but with the torus drawn as an embedding in $\mathbb{R}^3$. *Bottom left*: subgroup of $\mathbb{Z}^2$ in the case that $\mathbf{n}$ is non-orientable along e_1. $\mathbb{Z}^2$ is drawn as a lattice, filled in circles correspond to the elements that are part of the subgroup. Note that it is all group elements corresponding to cycles on the torus along which $\mathbf{n}$ is orientable. *Bottom middle* & *bottom left*: the same but for the other two cases. Note that in all cases the resulting covering space is another torus.

Now that we have our covering space $\widehat{\Omega}$ we can lift to an orientable map. By construction, the induced map $\widehat{\Omega} \to \mathbb{RP}^2$ is orientable, and one can lift to a map $\hat{n} : \Omega^{w_1} \to S^2$, with consistency demanding the following diagram commute

$$\begin{array}{ccc} \widehat{\Omega} & \xrightarrow{\hat{\mathbf{n}}} & S^2 \\ \downarrow p_1 & & \downarrow p_2 \\ \Omega & \xrightarrow{\mathbf{n}} & \mathbb{RP}^2 \end{array} \tag{2.10}$$

which can also be phrased as the equivariance condition $\hat{\mathbf{n}}(tx) = A(\hat{\mathbf{n}}(x))$, where t is the deck automorphism of $\widehat{\Omega}$ and A is the antipodal map on S^2. Note that for any given director field, there are two possible lifts, related by the antipodal map. As such one finds an equivalence between homotopy classes of nematic textures and of equivariant homotopy classes of maps $[\widehat{\Omega}, S^2]_{eq}/\sim$, where $\sim$ is the equivalence relation induced by the antipodal map on the target S^2. Note that if $\mathbf{n}$ is orientable (*i.e.* $w_1 = 0$), then Ω^{w_1} simply consists of two disjoint copies of Ω.

Now we show that $[\widehat{\Omega}, S^2]_{eq} \cong H^2(\Omega; \mathbb{Z}^w)$. Let $\widehat{X}$ be the corresponding double cover of X. Then we can equivalently study equivariant homotopy classes of maps $\hat{\mathbf{n}} : \widehat{X} \to S^2$.

It is clear from the discussion of the first invariant that the map $\hat{\mathbf{n}}$ restricted to the 1-skeleton, denoted $\hat{\mathbf{n}}_1$, is unique up to homotopy, and determined by the requirement that the projection from $\widehat{X} \to S^2$ to $X \to \mathbb{RP}^2$ has the specified $w_1(\mathbf{n})$. We choose $\hat{\mathbf{n}}_1$, such that its image is an equatorial $S^1 \subset S^2$. To specify $\hat{\mathbf{n}}_1$, one can instead consider the original complex X and the map $\mathbf{n}_1 : X_1 \to \mathbb{RP}^2$, and demand that $\mathbf{n}_1$ lies in the corresponding equatorial $\mathbb{RP}^1$. Such a choice is specified by an integer winding number for each edge, which can be reduced modulo 2 by allowing homotopies through the full $\mathbb{RP}^2$, such that the winding around the boundary of each face and the winding along any closed loop reduced modulo 2 matches w_1. Choose $\mathbf{n}_1$ so that the winding numbers of the lifted map $\hat{\mathbf{n}}_1$ are zero around the boundary of each face[5]. In general the extension of this map to the two skeleton, $\widehat{X}_2$, is given by a choice of element of $\pi_2(S^2, S^1)$ for each face such that the map on the boundary agrees with $\hat{\mathbf{n}}_1$. As shown below, $\pi_2(S^2, S^1) \cong \mathbb{Z} \oplus \mathbb{Z}$ and so the homotopy classes of extensions are given by an integer for each face. Since the map on the boundary of each face is null-homotopic, this integer can be identified as a degree for each face, and thus determines a cochain in $C^2(\widehat{X}_2; \mathbb{Z})$. Because our map must be equivariant, this cochain must be of the form $c - t_\sharp c$, where $t_\sharp$ is the map on cochains induced by the deck automorphism, t, of $\widehat{X}$, which is nothing other than an element of the cochain group $C^2(X; \mathbb{Z}^w)$ [27]; the minus sign associated to $t_\sharp$ is simply due to the action of the antipodal map.

Now, as in the case of the 1-skeleton, we consider two maps on $\widehat{X}_2$ that agree on the 1-skeleton, and try to construct a homotopy between them. By identical reasoning as in the case of the 1-skeleton, one can observe that a homotopy can only be constructed if the difference between the two cochains

[5]This is always possible, and given by the restriction of any choice of map $X \to \mathbb{RP}^1$ that satisfied the constraints on w_1 to X_1

representing the maps, c_1 and c_2 ca be written as $c_1 - c_2 = \delta e$, where $e \in C^1(X;\mathbb{Z}^w)$. It follows that $[\Omega, S^2]_{eq} \cong H^2(\Omega;\mathbb{Z}^w)$.

THE RELATIVE HOMOTOPY GROUP $\pi_2(S^2, S^1)$

In the argument above we are required to compute the relative homotopy group $\pi_2(S^2, S^1)$, where S^1 is an equator in S^2. There is a short exact sequence for a pair (X, A)

$$\longrightarrow \pi_n(A) \longrightarrow \pi_n(X) \longrightarrow \pi_n(X, A) \longrightarrow \pi_{n-1}(A) \longrightarrow \tag{2.11}$$

With the standard homotopy groups for the spheres, we find the short exact sequence

$$0 \longrightarrow \mathbb{Z} \xrightarrow{a} \pi_2(S^2, S^1) \xrightarrow{b} \mathbb{Z} \longrightarrow 0 \tag{2.12}$$

An element of $\pi_2(S^2, S^1)$ is a mapping $D^2 \to S^2$, such that the boundary of D^2 maps into S^1. The map b is then the degree of this restriction. Now we construct a map going the other way. Choose a point $x \in S^2$ not in the equatorial S^1, then for each $p \in S^1$ there is a unique great circle γ_p connecting x and p. Let a_p denote the shortest arc segment of γ_p connecting x to p, then given a map $S^1 \to S^1$, we can extend it to a map $D^2 \to S^2$ by mapping the origin of D^2 to x, and mapping straight line in D^2 connecting the origin to the boundary to a given a_p. Denote the resulting map c. Then it is clear that bc is the identity on $\pi_1(S^1)$, and it follows that (2.12) is right split, and $\pi_2(S^2, S^1) \cong \mathbb{Z} \oplus \mathbb{Z}$ (there are no non-trivial extensions of the integers with themselves). We note that the most natural way to think about this group is that each factor of $\mathbb{Z}$ corresponds to a the map covering each hemisphere of S^2. It follows that the maps in (2.12) are $a : x \to (x, x)$ and $b : (x, y) \to x - y$.

2.3 Orientable Textures

We will now give some example computations of homotopy classes of nematic textures in the orientable case, that is $w_1(\mathbf{n}) = 0$. In this case we have $H^2(\Omega;\mathbb{Z}^w) \cong H^2(\Omega;\mathbb{Z})$ and we need only compute the regular cohomology. In this case the only difference between a nematic and a unit vector field is a global sign ambiguity of $\mathbf{n} \sim -\mathbf{n}$, the implications of which have been discussed at length in the literature [21].

As a simple example consider Ω to be $\mathbb{R}^3$ minus the origin, as illustrated in Figure 2.3. This can be thought of as modelling the region surrounding a single point defect at the origin. Now $\mathbb{R}^3 - \{0\}$ is homotopy equivalent to S^2, and so one simply has to compute classes of maps $[S^2, \mathbb{RP}^2]$. All maps of this type are orientable (all point defects are orientable, a fact one can deduce by noting that $\pi_1(S^2) = 0$) and so from the above discussion we know that

$$[S^2, \mathbb{RP}^2] \cong H^2(S^2, \mathbb{Z})/\sim \cong \mathbb{N} \tag{2.13}$$

as previously established. This tells you that the topology of this system is purely determined by the local topology (or 'charge') of the defect, there is no more structure.

Things become more interesting when one looks at more complicated domains. Take now Ω to be $\mathbb{R}^3 - \{p_1, p_2\}$ where $\{p_1, p_2\}$ are two distinct points, illustrated in Figure 2.4. This is now modelling the topology of a system consisting of two distinct point defects. This example illustrates a well-known difficulty [21] with liquid crystal topology, corresponding to the 'addition of charges' for point defects. If one takes only local information, then each of the two defects, located at p_1 and p_2 are assigned an integer $q_i \in \mathbb{N}$. The ambiguity arises when one considers the result of bringing the two defects together, which is either $|q_1 + q_2|$ or $|q_1 - q_2|$. The resolution involves incorporating global information about the texture that connects

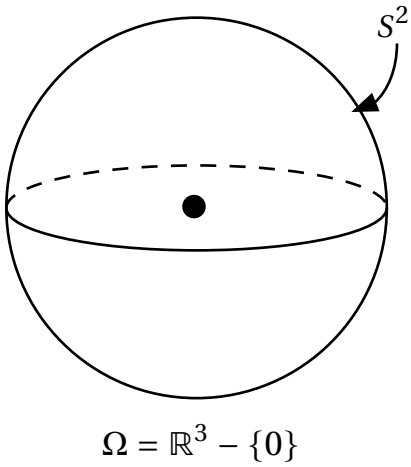

Figure 2.3: Domain corresponding to all of $\mathbb{R}^3$ minus a point at the origin. It is homotopy equivalent to a sphere; the topology of a nematic texture consisting of a single point defect is simply determined by the defect type.

the two neighbourhoods of p_1 and p_2. This can be, and has been, done in a number of ways. For example, one can consider a common basepoint for both local neighbourhoods or use the Pontryagin-Thom construction. With our method we take our domain to be $\mathbb{R}^3 - \{p_1, p_2\}$. This space deformation retracts to a wedge sum of spheres, $S^2 \vee S^2$, consisting of two spheres with a pair of points, (x_0, y_0), one from each sphere, identified. So now we must consider free homotopy classes of maps $[S^2 \vee S^2, \mathbb{RP}^2]$. It is true [27] that for pointed maps[6] $[A \vee B, C]_* \cong [A, C]_* \times [B, C]_*$. Hence we know $[S^2 \vee S^2, S^2]_* \cong \mathbb{Z} \times \mathbb{Z}$. Now our goal, $[S^2 \vee S^2, \mathbb{RP}^2]$, is simply found by acting on $[S^2 \vee S^2, S^2]_*$ with the equivalence relation. So we have

$$[S^2 \vee S^2, \mathbb{RP}^2] \cong \mathbb{Z} \times \mathbb{Z}/\sim \cong \mathbb{N} \times \mathbb{Z} \tag{2.14}$$

and therefore we find that including global information removes any ambiguity. The classes of maps are given by the set $\mathbb{N} \times \mathbb{Z}$, *i.e.* the ambiguity is a global sign ambiguity, we can fix the charge of the defect at, say, p_1, but then all the charges relative to that defect are fixed, and so the absolute value of

[6] A pointed map f is defined by choosing basepoints (p, q) in both the domain and target spaces, such that $f(p) = q$. One then restricts to homotopies of f that preserve this basepoint mapping property.

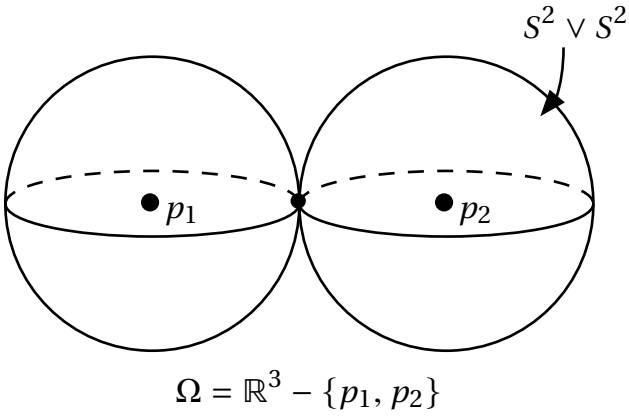

Figure 2.4: Domain corresponding to all of $\mathbb{R}^3$ except two points which one supposes to be point defects. The space is homotopy equivalent to the wedge sum of two spheres. The topology of the nematic in the surrounding area is given by free homotopy classes of maps from $S^2 \vee S^2$ to $\mathbb{RP}^2$. The result is the set $\mathbb{N} \times \mathbb{Z}$. The factor of $\mathbb{Z}$ says that if one assumes that the charge of the first defect is positive (given by $\mathbb{N}$), then the sign of the second can be either positive or negative, removing the ambiguity in adding the signs.

their sum is unambiguously defined. This extends naturally to the case of N point defects, where the distinct states are labelled by elements in the set $\mathbb{N} \times \mathbb{Z}^{N-1}$.

2.4 Non-orientable Textures

We now turn to the computation in the case of non-orientable textures. Our task is to compute the cohomology group $H^2(\Omega; \mathbb{Z}^w)$. We will pass through twisted Poincaré-Lefschetz duality [41] and consider instead the twisted relative homology group

$$H^2(\Omega; \mathbb{Z}^w) \cong H_{d-2}(\Omega, \partial\Omega; \mathbb{Z}^w) \tag{2.15}$$

Where d is the dimension of Ω. To compute this homology we can once again turn to the double cover, $\widehat{\Omega}$, and compute the equivariant homology of $\widehat{\Omega}$, $H_\bullet(\widehat{\Omega}, \partial\widehat{\Omega}; \mathbb{Z})_{eq}$ which is the homology of the sub chain complex consisting of all chains in $C_\bullet(\widehat{\Omega})$ that are of the form $c - t^* c$, where t^* is the action of the

deck transformation on chains. As an example, if one represents a 0-chain as a point p in $\widehat{\Omega}$, then t^*p would be equal to the corresponding point on the other sheet of the cover to whichever sheet p happened to be in. To give a detailed computation of the homology we will need the notion of branch sets for nematic domains.

2.4.1 Branch sets for a nematic domain

Associated to each choice of map w_1 are a class of branch sets, which can be thought of as an analogue of the familiar branch cuts in complex analysis. These branch cuts will be central to furthering our discussion, so we develop them here. We will define an admissible branch set for a nematic domain to be an orientable submanifold representing the Poincaré dual of $w_1(\mathbf{n})$. In a three dimensional domain $PD(w_1(\mathbf{n})) \in H_2(\Omega, \partial\Omega; \mathbb{Z}_2)$, and so the branch sets are surfaces. To understand their topological significance note that in a d dimensional domain there is an intersection pairing in homology

$$H_1(\Omega) \times H_{d-1}(\Omega, \partial\Omega) \to \mathbb{Z} \tag{2.16}$$

which, if one represents homology cycles as submanifolds, counts the intersection between the two submanifolds with sign. Choosing a particular class $[\mathcal{B}] \in H_{d-1}(\Omega, \partial\Omega)$ and reducing the final $\mathbb{Z}$ modulo 2 creates a map $b_{[\mathcal{B}]} : H_1(\Omega) \to \mathbb{Z}_2$. Branch sets are then orientable sets $\mathcal{B}$ for which $b_{[\mathcal{B}]} = w_1$ as maps on homology.

This construction then has a simple interpretation. One constructs a set $\mathcal{B}$, which is a surface if Ω is three dimensional or a line if Ω is two dimensional, such that if γ is a loop along which $\mathbf{n}$ is non-orientable, then γ must intersect $\mathcal{B}$ an odd number of times. Examples of branch sets for a given domain are shown in Figure 2.5.

Note that if we lift the requirement that $\mathcal{B}$ is orientable, then we could work in a theory with $\mathbb{Z}_2$ coefficients. While doing this is a more general

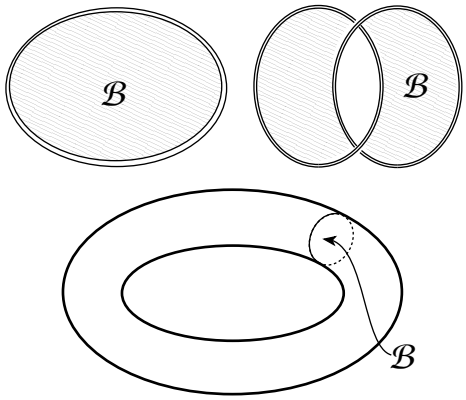

Figure 2.5: Examples of branching sets. *Top left*: The loop is a defect line around which $\mathbf{n}$ is non-orientable. A branching set $\mathcal{B}$ consists of the disk whose boundary is the defect. Note that because the domain has a boundary (the defect line), the set set $\mathcal{B}$ can be thought of as a cycle in relative homology. *Top right*: The same situation as the top left, only now the defect lines are linked. *Bottom*: the case where Ω is a torus. Here $\mathbf{n}$ is non-orientable along the cycle e_2 from Figure 2.2, the branch set $\mathcal{B}$ is homologous to e_1.

approach, it gives the same answer, so we will not adopt it[7]. In this non-orientable setting one can obtain a canonical set of branch sets through the Pontryagin-Thom construction [9, 20]. Take a director field $\mathbf{n}$ and pick a generic fixed direction, if one is in $\mathbb{R}^3$ then one may choose the vertical direction. Plot all points where $\mathbf{n}$ points orthogonal to this direction, this defines a surface in the domain where $\mathbf{n}$ is orthogonal to some direction. On S^2 the set of directions orthogonal to a given direction forms a great circle, which projects to a non-trivial cycle, α, in $\mathbb{RP}^2$. Suppose now that γ is a loop along which $\mathbf{n}$ is non-orientable. Then along γ $\mathbf{n}$ must map to a non-contractible loop in $\mathbb{RP}^2$. The image of γ on $\mathbb{RP}^2$ and the cycle and α must intersect an odd number of times, illustrated in Figure 2.6, and so γ must pass through the surface an odd number of times, satisfying the requirement in the definition of $\mathcal{B}$.

Branch sets have a connection to the covering space $\widehat{\Omega}$ which will be essential in what follows. Intuitively the idea is that the set $\mathcal{B}$ can be thought

[7] As a point of interest, taking this approach leads to the definition of something similar to a Gordon-Litherland form rather than a Seifert matrix when considering knotted defect lines, though this is only a computational observation, and does not confer any physical relevance

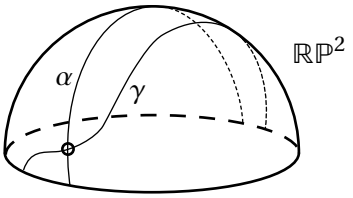

Figure 2.6: Two non trivial cycles α and γ on $\mathbb{RP}^2$ must intersect an odd number of times.

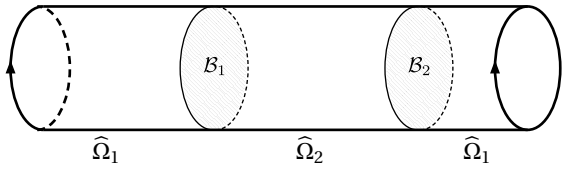

Figure 2.7: Schematic illustration of the relationship between a branch set $\mathcal{B}$ and the double cover $\widehat{\Omega}$. Lifting to the cover, $\mathcal{B}$ has two components, $\widehat{\mathcal{B}}_1$ and $\widehat{\mathcal{B}}_2$, which separate the two sheets of the cover, Ω_1 and Ω_2.

of as a 'portal'. Going through this portal takes you between the two sheets of $\widehat{\Omega}$. Formally, let $\mathcal{B}$ be a branch set for a nematic domain Ω, with covering space $\widehat{\Omega}$ and projection p. Then the lift $\widehat{\mathcal{B}} = p^{-1}(\mathcal{B}) \subset \widehat{\Omega}$ has two components, denoted $\widehat{\mathcal{B}}_1$ and $\widehat{\mathcal{B}}_2$, as illustrated in Figure 2.7. Cutting $\widehat{\Omega}$ along $\widehat{\mathcal{B}}$ defines two submanifolds $\widehat{\Omega}_1$ and $\widehat{\Omega}_2$ such that $\widehat{\Omega}_1 \cup \widehat{\Omega}_2 = \widehat{\Omega}$ and $\widehat{\Omega}_1 \cap \widehat{\Omega}_2 = p^{-1}(\mathcal{B})$. Furthermore, for a given $x \in \Omega$, $p^{-1}(x)$ will be two points, one in $\widehat{\Omega}_1$ and one in $\widehat{\Omega}_2$ unless $x \in \mathcal{B}$ in which case $p^{-1}(x)$ will be two points in the intersection of $\widehat{\Omega}_1$ and $\widehat{\Omega}_2$.

There is a final subtlety regarding orientation. Given an matching orientation for each component of $\widehat{\mathcal{B}}$ and matching orientations for the sheets $\widehat{\Omega}_1$ and $\widehat{\Omega}_2$ the orientation of $\widehat{\mathcal{B}}_1$ will match that of (say) $\widehat{\Omega}_1$ and not $\widehat{\Omega}_2$ and *vice versa* with $\widehat{\mathcal{B}}_2$.

2.4.2 Mayer-Vietoris for Equivariant Homology

Now that we have defined our branch sets, we can compute the equivariant homology. From before, we are required to compute $H_{d-2}(\widehat{\Omega}, \partial\widehat{\Omega}; \mathbb{Z})_{eq}$. To do this, choose a branch set $\mathcal{B}$, as defined above. Then, if $d = 3$ we can write down an equivariant Mayer-Vietoris sequence (with integer coefficients understood)

$$\begin{aligned} H_{d-2}(\mathcal{B}, \partial\mathcal{B})_{eq} &\xrightarrow{i} \left(H_{d-2}(\widehat{\Omega}_1, \partial\widehat{\Omega}_1) \oplus H_{d-2}(\widehat{\Omega}_2, \partial\widehat{\Omega}_2)\right)_{eq} \longrightarrow \\ \longrightarrow \quad & H_{d-2}(\widehat{\Omega}, \partial\widehat{\Omega})_{eq} \longrightarrow H_{d-3}(\mathcal{B}, \partial\mathcal{B})_{eq} \end{aligned} \tag{2.17}$$

Note that if the domain has dimension 2, then the last term is zero. We note the following about these groups. Because $\mathcal{B}$ has two components, $\mathcal{B}_1$ and $\mathcal{B}_2$, the homology splits $H_\bullet(\mathcal{B}, \partial\mathcal{B}) \cong H_\bullet(\mathcal{B}_1, \partial\mathcal{B}_1) \oplus H_\bullet(\mathcal{B}_2, \partial\mathcal{B}_2)$. The equivariant homology of $\mathcal{B}$ is then elements of $H_\bullet(\mathcal{B}, \partial\mathcal{B})$ that are of the form $(x, -x)$. Similarly in the case of $\left(H_1(\widehat{\Omega}_1, \partial\widehat{\Omega}_1) \oplus H_1(\widehat{\Omega}_2, \partial\widehat{\Omega}_2)\right)_{eq}$, we know that the two sheets of the cover, $\widehat{\Omega_1}$ and $\widehat{\Omega}_2$ are homeomorphic spaces, and so have isomorphic homologies. The equivariant elements of this group are then, again, elements of the form $(y, -y)$. The inclusion map takes into account the orientations of the pieces, and thus works as follows. Consider the map restricted to $\widehat{\mathcal{B}}_1$, denoted i_1. Given an element $x \in H_1(\mathcal{B}_1, \partial\mathcal{B}_1)$, $i_1 : x \mapsto$ Then $i_1 : x \mapsto (x, -x)$ (say) and correspondingly $i_2 : x \mapsto (-x, x)$, and so the composite map acts as $i : (z, -z) \mapsto (2z, -2z)$.

2.4.3 Computation for closed surfaces

We will now give a full computation of the homotopy classes of nematic textures when the domain is an orientable closed surface. As mentioned before, the classic example of this is a torus enclosing a defect loop, which is a classic calculation in the study of defect topology [20, 21, 32, 42]. Orientable closed surfaces are classified by their genus, g, and their first cohomology group is simply $H^1(\Sigma_g; \mathbb{Z}_2) \cong \mathbb{Z}_2^{2g}$, which gives the possible values for the first invari-

ant of the texture. If $w_1(\mathbf{n}) = 0$, then the map is orientable, and one can lift to find a map from an orientable surface into S^2. These are classified by degree, and so taking into account the ambiguity of the lift, one finds orientable nematic textures on a closed surface are classified by a natural number, $\mathbb{N}$. If $w_1(\mathbf{n}) \neq 0$, then we form the double cover $\widehat{\Omega}$, and we are required to compute the group $H_0(\Omega, \mathbb{Z}^w)$ (note the we do not use relative homology because Ω is closed). We may choose the branch set $\mathcal{B}$ to be a single circle, and from the sequence above we find

$$\begin{array}{ccccccc} (\mathbb{Z}\oplus\mathbb{Z})_{eq} & \longrightarrow & (\mathbb{Z}\oplus\mathbb{Z})_{eq} & \xrightarrow{i} & H_0(\Omega,\mathbb{Z}^w) & \longrightarrow & 0 \\ (x,-x) & \xrightarrow{i} & (2x,-2x) & & & & \end{array} \tag{2.18}$$

It follows from the exactness of the sequence that $H_0(\Omega, \mathbb{Z}^w) \cong \mathbb{Z}_2$, and so for any given non-trivial $w_1(\mathbf{n})$ there are two homotopy classes of texture, as found by Jänich in the case of the torus. One can give a pictorial representation of this structure, shown in Fig. 2.8. Equivariant elements of H_0 can be realised a set of point charges living on the double cover of the domain. Equivariance demands that the total charge on both sheets sums to zero. Individual point charges can be moved between sheets and annihilated. However, this must be done equivariantly, with the result being that there is a $\mathbb{Z}_2$ invariant for the total number of charges on each sheet. Equivalently, one can view this as point charges on the domain, along with a choice of branch set. If a point charge passes through the branch set, then its charge reverses.

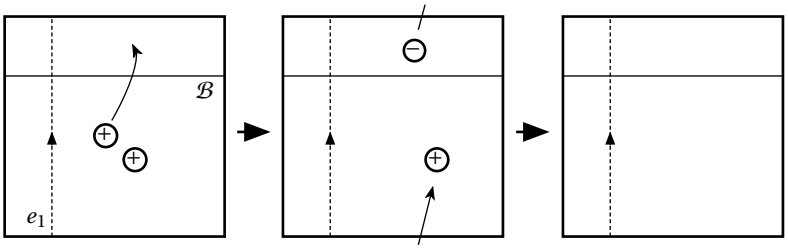

Figure 2.8: Nematic textures on T^2. The homotopy classes of nematic textures can be found by putting point charges on the torus. If the point charge passes through the branch cut, its sign flips, giving an overall $\mathbb{Z}_2$ invariant.

The Relationship with Jänich's Index

Jänich [32] introduced an index $\nu \in \mathbb{Z}_4$ used to characterise the tubular neighbourhood of a defect line. This index has been used by several authors to understand the topology of defect lines [21, 30]. We will show how this index relates to the homotopy classification of maps we have constructed. Suppose one has a defect loop in $\mathbb{R}^3$. Consider $\mathbf{n}$ restricted to the boundary of a tubular neighbourhood of the defect line. This will give a map $T^2 \to \mathbb{RP}^2$ that is non-orientable along the meridian. So we need to classify homotopy classes of maps $\mathbf{n} : T^2 \to \mathbb{RP}^2$ that are non-orientable along the meridian. The first step is determining the orientability of the map. The map is non-orientable along the meridian, and it may or may not be non-orientable along the longitude. Let $\mu_1 \in \mathbb{Z}_2$ denote whether or not $\mathbf{n}$ is non-orientable along the longitude. In each case there is a further index $\mu_2 \in \mathbb{Z}_2$, as illustrated above, that counts the mod 2 reduction of the number of framed 0-dimensional submanifolds representing $\mathbf{n}$. Hence the topological classes of maps is given by an element in the set $\mu = \mu_1 \times \mu_2 = \mathbb{Z}_2 \times \mathbb{Z}_2 \cong \mathbb{Z}_4$, where the last isomorphism is one of sets (there is no group structure on the maps), this, up to an automorphism of $\mathbb{Z}_4$ is exactly Jänich's index. Finally we should give the physical interpretation of this index, where we follow Alexander *et al.* [21]. The first factor, saying whether $\mathbf{n}$ is non-orientable along the longitude of T^2 counts, modulo two, the number of defect lines linking the one inside the torus. The second index is more subtle. It can be thought of as counting, modulo two, the number of point defects inside the T^2 neighbourhood.

2.5 Homotopy Classification of Knotted Defects

We now come to the central calculation of this chapter, that of the number – up to smooth deformation – of nematic textures surrounding a given set of line defects. We will be precise in our formulation of this problem. We will

consider a nematic texture in $\mathbb{R}^3$ with a prescribed set of line defects and no other singularities. Furthermore, we will assume that $\lim_{|x|\to\infty}\mathbf{n}(x) = \mathbf{n}_0$, a constant – we will relax this assumption later. Given this setup, we ask for the number of distinct nematic textures with this defect set. Our assumption that $\mathbf{n}$ is uniform at infinity allows us to compactify the domain and consider maps $\mathbf{n} : S^3 - N(L) \to \mathbb{RP}^2$, where $N(L)$ is a small neighbourhood of the defect lines.

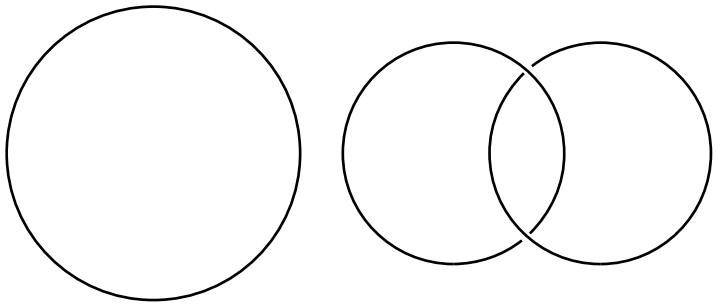

Figure 2.9: *Left*: An unknot, there is a unique nematic texture on the complement if the unknot is a defect. *Right*: A Hopf link, assuming that the lines are defects the complement of this link supports two distinct nematic textures.

While in the calculation of textures on surfaces we chose which cycles were non-orientable under w_1, in this case our choice is made for us: the texture is non-orientable around the defect lines. To be precise the first homology group of a link complement, $S^3 - L$, is given as $H_1(S^3 - L) = \mathbb{Z}^{|L|}$, where $|L|$ is the number of components of the link. We demand that the map $w_1 : H_1(S^3 - L) \to \mathbb{Z}_2$ sends each generator to the generator of $\mathbb{Z}_2$, in other words each link component represents a defect line. Before we do the calculation proper we will consider two toy cases: that of a simple circle (the 'unknot') and the case of two linked rings (the Hopf link) and solve them with different methods, before we turn to the general case.

The case of the unknot is simple. Let U be an unknot, then the complement $S^3 - U$ deformation retracts to S^1. Then the question is simply reduced to studying maps $S^1 \to \mathbb{RP}^2$, these are indexed by $\mathbb{Z}_2$, simply whether the texture is orientable or not. But we already know, by assumption, that the

texture is non-orientable, so there is no more freedom left and we find that there is a unique nematic texture associated to the complement of an unknotted defect in the 3-sphere[8]. One might be tempted to ask at this point about the relationship to Jänich's $\mathbb{Z}_4$ index, and how this relates to the statement that there is only one type of unknotted defect. The answer is that any of Jänich's indices other than 0 imply the existence of other defects in the system.

Consider now the Hopf link. The complement of the Hopf link in S^3 is fibered over S^1 with fibre a genus zero surface with two boundary components. This fibre deformation retracts onto a circle, so the complement of the Hopf link deformation retracts to the product of two circles, or the two-torus T^2. Hence the number of nematic textures in the complement of a Hopf link is equivalent to the number of nematic textures on a torus which are non-orientable along both e_1 and e_2, which is just two. As we will see, these two different textures on the Hopf link can be interpreted as having linking number plus or minus one, which is visualised in Chapter 6.

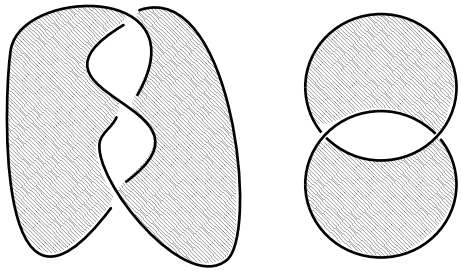

Figure 2.10: Examples of Seifert surfaces for the trefoil knot and the Hopf link. These serve as branch sets $\mathcal{B}$ if the lines are thought of as defects.

Now we will compute the homotopy classification of nematic textures in the general case of a knotted or linked line defect. Our domain is given as $\Omega = \mathbb{R}^3 - N(L)$, for a given link L. A branch set, $\mathcal{B}$ for this domain is a Seifert surface for L, as shown in Figure 2.10. The double cover $\widehat{\Omega}$ is now the double

[8]To save time we will be sloppy and often say 'there is a unique unknot' or similar when we are really talking about classes of maps.

cyclic cover [33], and each sheet $\widehat{\Omega}_{1,2}$ is a copy of Ω cut along $\mathcal{B}$. Note that $\partial\widehat{\Omega}_{1,2}$ consists of a copy of $|L|$ tori, the boundaries of the neighbourhoods of each link component, cut along a longitude that marks the location of $\mathcal{B}$, as indicated in Figure 2.11.

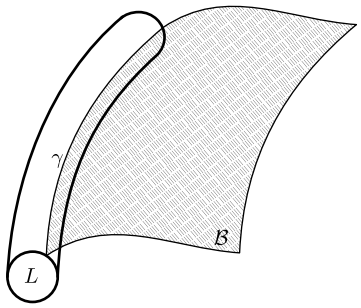

Figure 2.11: The boundary of $\widehat{\Omega}_{1,2}$ consists of tori for each link component ,L, each of which are cut along contours γ which form $\partial\mathcal{B}$. Note that the branch set is not in the boundary of $\widehat{\Omega}_{1,2}$

Now we use the equivariant Mayer-Vietoris sequence, obtaining the sequence

$$\begin{array}{ccccc} H_1(\mathcal{B},\partial\mathcal{B})_{eq} & \xrightarrow{\ i\ } & \left(H_1(\widehat{\Omega}_1,\partial\widehat{\Omega}_1)\oplus H_1(\widehat{\Omega}_2,\partial\widehat{\Omega}_2)\right)_{eq} & \longrightarrow & \\ \longrightarrow & & H_1(\widehat{\Omega},\partial\widehat{\Omega})_{eq} & \longrightarrow & 0 \end{array} \tag{2.19}$$

so our group is given by

$$H_1(\Omega,\partial\Omega;\mathbb{Z}^w)\cong\left(H_1(\widehat{\Omega}_1,\partial\widehat{\Omega}_1)\oplus H_1(\widehat{\Omega}_2,\partial\widehat{\Omega}_2)\right)_{eq}/\mathrm{Im}(i) \tag{2.20}$$

Our branch set, $\mathcal{B}$ consists of two copies of a Seifert surface for the link L, which we will assume has genus g. Because $\mathcal{B}$ is a surface with boundary, $H_0(\widehat{\mathcal{B}},\partial\widehat{\mathcal{B}})_{eq}$ is trivial. The first homology group $H_1(\widehat{\mathcal{B}},\partial\widehat{\mathcal{B}})_{eq}$ is the subgroup consisting of elements of the form $(x,-x)$ in $\mathbb{Z}^{2g+|L|-1}\oplus\mathbb{Z}^{2g+|L|-1}$. A basis for this in terms of cycles on one component of $\mathcal{B}$ is shown in Figure 2.12. The basis is of the form $\{b_i\}\cup\{e_i\}$ where the b_i run from $i=1$ to $i=2g$ and the e_i run from $i=1$ to $i=|L|-1$. Note that the additional b_i, $i>2g$ are null-homologous, but useful for calculations.

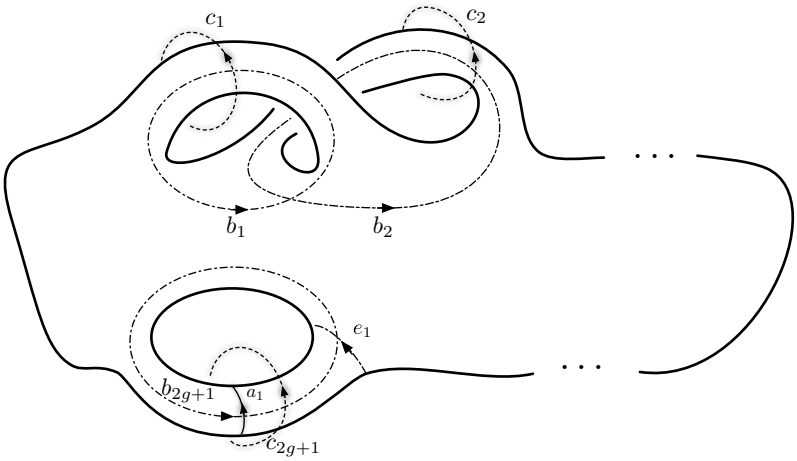

Figure 2.12: Various cycles relating to $\mathcal{B}$ and L. $\mathcal{B}$ is represented as a surface with g sets of double handles along the top and $|L|-1$ sets of loops along the bottom. The basis a gives set of tethers that connect the link components. The cycles b gives a basis for $H_1(\mathcal{B})$, and the cycles $\{b_i\}\cup\{e_j\}$ for $i\in[1,2g]$ and $j\in[1,|L|-1]$ give a basis for $H_1(\mathcal{B},\partial\mathcal{B})$. The basis c is generates for $H_1(S^3-L)$. $\{a_i\}\cup\{c_i\}$ gives an overcomplete basis for $H_1(S^3-\mathcal{B},\partial\mathcal{B})$. The bases $\{b_i\}$ and $\{c_i\}$ are chosen such that $\mathrm{Lk}(c_i,b_j)=\delta_{ij}$.

Now we must characterise $H_1(\widehat{\Omega}_{1,2},\partial\widehat{\Omega}_{1,2})$. An over-complete basis for this group is given as the set $\{a_i\}\cup\{c_i\}$, as illustrated in Figure 2.12, where the basis sets are chosen so that $\mathrm{Lk}(c_i,b_j)=\delta_{ij}$ and the a_i are a set of tethers connecting link components, with $p^+e_i=a_i$. As before, the equivariant form appearing in (2.20) will be of the form $(x,-x)$. From this, it follows that

$$H_1(\Omega,\partial\Omega;\mathbb{Z}^w)\cong H_1(\widehat{\Omega}_1,\partial\widehat{\Omega}_1)/R \tag{2.21}$$

where R is the set of relations coming from the inclusion i. Because the computation can be done only with information from one sheet, we can instead write

$$H_1(\Omega,\partial\Omega;\mathbb{Z}^w)\cong H_1(\Omega-\mathcal{B},\partial(\Omega-\mathcal{B}))/R' \tag{2.22}$$

Where the relations R' are of the form $p^+b_i+p^-b_i=0$ and $p^+e_i+p^-e_i=0$, where $p^\pm$ denotes the positive (negative) push-off of cycles from the branch set $\mathcal{B}$ into Ω. The relations on the generators $\{a_i\}\cup\{c_i\}$ fall into three distinct types, which we denote A, B and C. Types A and C come from the inclusion

map i whereas type B consists of setting all longitudes (with respect to the framing given by $\mathcal{B}$) of link components to zero. The relations of type C, of which there are $|L|-1$, can be found by considering cycles e_i, which give $p^+e_i + p^-e_i = 0$. From the diagram it is clear that $p^+e_i = a_i$ and $p^+e_i - p^-e_i = c_{2g+i}$, and so we conclude that $2a_i = c_{2g+i}$, as illustrated in Figure 2.13. Finally, relations of type A, of which there are $2g$ come from setting $p^+b_i + p^-b_i = 0$.

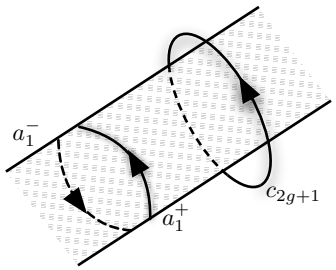

Figure 2.13: The relationship $a_i^+ - a_i^- = c_{2g+i}$.

Now, there are $2g$ relations of type A, and $|L|-1$ relations of type B and C. Each of the three can be written out as

$$A_i := b_i^+ + b_i^- = \sum_{j=1}^{2g+|L|-1} \mathrm{Lk}(b_j, b_i^+) + \mathrm{Lk}(b_j, b_i^-) = 0 \tag{2.23}$$

$$B_i := b_{2g+i}^+ = \sum_{j=1}^{2g+|L|-1} \mathrm{Lk}(b_j, b_{2g+i}^+) = 0 \tag{2.24}$$

$$C_i := 2a_i - c_{2g+i} = 0 \tag{2.25}$$

and combined into a block matrix, where the horizontal blocks correspond to the first $2g$ $\{c_i\}$, the last $|L|-1$ $\{c_i\}$ and the $\{a_i\}$ and the vertical blocks

correspond to relationships of type A, B and C, as

$$\begin{pmatrix} A^{(1)} & A^{(2)} & 0 \\ B^{(1)} & B^{(2)} & 0 \\ 0 & 1 & -2 \end{pmatrix}. \tag{2.26}$$

This is just a presentation matrix for an Abelian group. By taking into account relationships of type C, it is clear that an equivalent group is given by the matrix

$$M_1 = \begin{pmatrix} A^{(1)} & 2A^{(2)} \\ B^{(1)} & 2B^{(2)} \end{pmatrix}. \tag{2.27}$$

Now let S be the Seifert matrix for the link L, then in our notation the matrix

$$M_2 = S + S^T = \begin{pmatrix} A^{(1)} & A^{(2)} \\ 2B^{(1)} & 2B^{(2)} \end{pmatrix} \tag{2.28}$$

is a presentation matrix for the first homology of the branched double cover of $S^3 - L$ which we denote $H_1(\Sigma(L))$. The Abelian group given by a presentation matrix is determined by its Smith normal form. Two matrices X and Y have the same Smith normal form if $X - \lambda I$ is similar to $Y - \lambda I$. Since M_1 and M_2 have the same diagonal elements, it then follows from this that if they are similar then they present the same Abelian group. By construction M_2 is symmetric, so $2B^{(1)} = A^{(2)}$. Then the following is true

$$M_1 = PM_2P^{-1} \tag{2.29}$$

where

$$P = \begin{pmatrix} \sqrt{2} & 0 \\ 0 & \frac{1}{\sqrt{2}} \end{pmatrix}, \tag{2.30}$$

and so M_1 and M_2 present the same group, $H_1(\Sigma(L))$, the first homology group of the branched double cover of the link complement.

Finally we can say the following. Suppose one has a nematic texture in

$\mathbb{R}^3$ with uniform boundary conditions at infinity and a set of line defects L. Then the number of topologically distinct nematic textures associated to that defect set is given by elements of $H_1(\Sigma(L))/\sim$, where the equivalence relation is $x \sim -x$. We are almost at our goal, (2.32), we just need to take account of a few more things. The first is the case of split links. A split link in S^3 is a link for which you can find an embedded sphere separating two or more components. The idea is to model a collection of defects. Indeed if one can surround a defect with a sphere, then it ought to have a charge as if it were a point defect, since on the sphere one cannot tell what type of defect, point, line knot *etc.* is inside the sphere. This is the case, and it is a standard result [43] that for a link L with N split components, then

$$H_1(\Sigma(L)) = \mathbb{Z}^{N-1} \oplus \bigoplus_i H_1(\Sigma(L_i)). \tag{2.31}$$

The factors of $\mathbb{Z}$ at the front can be thought of as corresponding to the point-defect charges of the split components. There are $N-1$ of them rather than N because our uniform boundary conditions demand that the total charge is zero, which reduces the degrees of freedom by one. We can lift this condition by supposing that there is a point defect 'at infinity' in S^3, the charge of this point defect compensates for the charges of all the other defects. Finally we can also add an arbitrary number of point defects into our system. Doing this we obtain the result quoted at the beginning of this chapter. Let $\mathbf{n}$ be a director field for a nematic liquid crystal in $\mathbb{R}^3$ with a defect set $\mathcal{D}$, then $\mathcal{D} = \mathcal{P} \cup \mathcal{L}$ where $\mathcal{P}$ is the set of point defects and $\mathcal{L}$ is the set of line defects. Furthermore, $\mathcal{L} = \cup_i L_i$ where each of the L_i is a non-split knot or link. Then the topology of the texture $\mathbf{n}$ is given by an element of the set

$$\left(\bigoplus_{p_i \in \mathcal{P}} \mathbb{Z} \right) \oplus \left(\bigoplus_{L_j \in \mathcal{L}} (\mathbb{Z} \oplus H_1(\Sigma(L_j))) \right) / \sim \tag{2.32}$$

2.5.1 Interpretation of the Topology of Knotted Defects

The interpretation of this result is difficult. Broadly speaking the internal states fall into two classes as follows. Given an element $x \in H_1(\Sigma(L))$, one can compute $2x \in H_1(\Sigma(L))$. As we will show below, elements for which $2x = 0$ have a different physical interpretation from those which do not. Furthermore, much of the work in Chapters 3 and 4 can be used to show that in cholesterics many internal states for which $2x \neq 0$ can be realised as λ lines entangling the knotted defect. In nematics, of course, one does not have λ lines and the analogous phenomena is that of a Skymrion tube entangling the knot or link. In Chapter 6 we discuss how those textures for which $2x = 0$ can be thought of as inducing different relative orientations on the link components.

To begin our investigation, we note that for a knot, the quantity $|H_1(\Sigma(L))|$ is always a finite odd integer, and is a well known invariant termed the determinant of the knot. Table 2.1 shows $H_1(\Sigma(L))$ for all torus links up to $(20, 20)$, and one may observe that if p, q are coprime, so that the torus link is in fact a knot[9], then the order of the group is odd. Because the group is of odd order it can have no elements x such that $2x = 0$ and as a consequence, all internal states in knotted, but not linked defects, can be thought of as involving Skyrmion tubes entangling the knot.

The distinction between elements of order 2 and otherwise can be related to the inversion symmetry of the nematic. Suppose one had a knotted texture, then by the method detailed above, one must lift this to an orientable map on a covering space. A reasonable question is: when does the result not depend on the choice of lift from $\mathbb{RP}^2$. The answer is when there are elements of order two. Under $\mathbf{n} \to -\mathbf{n}$ the appropriate element in $H_1(\Sigma(L))$ also changes sign. Order two elements are precisely those which are invariant with respect to this symmetry. For an example, take the Hopf link, it has $H_1(\Sigma(L)) = \mathbb{Z}_2$ which contains two elements 0 and 1. Under $x \to -x$ we

[9] A (p,q) torus link has gcd(p, q) components.

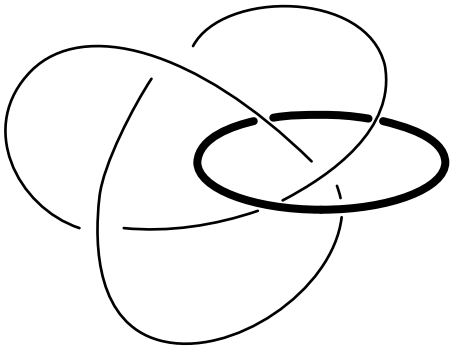

Figure 2.14: Skyrmion tube (thick line) entangling a trefoil knot defect. The creation of this line takes the state from 0 to 1 in $\mathbb{Z}_3$.

have $0 \to 0$ and $1 \to 1$. As a counter example take the trefoil knot. It has $H_1(\Sigma(L)) = \mathbb{Z}_3$, with three elements 0, 1 and -1. But under $x \to -x$ we have $0 \to 0$, $1 \to -1$ and $-1 \to 1$, so only one of the elements is invariant. This suggests we should partition states associated to a link based on their response – either symmetric or antisymmetric – to inversion symmetry. In fact, for any knot there is only ever one internal state which is invariant under this symmetry, and so for a knot there is a canonical topological 'groundstate', and one would guess that almost all of the experimentally realised knotted defects would be in this groundstate.

We have stated that one can think of elements for which $2x \neq 0$ as corresponding to Skyrmion tubes entangling the knot. One might ask how such a conclusion is reached. Consider the following question 'given a director field, can I find another director field always orthogonal to the first?' As we will discuss in later chapters, the answer to this question is given in terms of the (twisted) Euler class of the orthogonal 2-plane bundle defined by $\mathbf{n}$, and it is precisely those textures that are order 2 that allow such an orthogonal direction to exist [44]. Physically, if one also demands that $\mathbf{n}$ is a cholesteric, then symmetric states are those that can be realised without the presence of additional λ lines. More generally, for a nematic, one can think of states which are anti-symmetric with respect to inversion as containing Skyrmion tubes entangling the knot or link (shown in Figure 2.14), whereas the sym-

metric states have no such tubes.

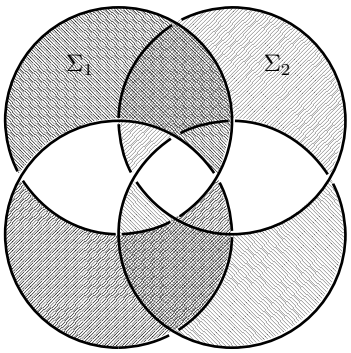

Figure 2.15: Disconnected spanning surface for the $(4,4)$ torus link. One can think of it has two linked Hopf links. If this link represents a defect set in a nematic, then $\mathbf{n}$ is orientable on a closed torus surrounding either of the connected components of the surface. Since one can find a closed, non-contractible surface on which $\mathbf{n}$ is orientable, one can compute the degree of $\mathbf{n}$ on the surface. This gives a full integer and the effect is responsible for the integer summands given in Table 2.1.

Though we do not yet have a proof, it is likely that the order 2 states all have planar representatives, by which is meant that one can write down a representative of the texture such that the director is always in, say, the $x-y$ plane. In chapter 6 we show that this is true for the Hopf link. Interestingly, in the case of the Hopf link the two planar textures are related by a symmetry transformation, which implies that that have equivalent energetic properties in a nematic (but not a cholesteric). One might speculate whether this degeneracy would lead to interesting entropic properties for large collections of tangled knotted and linked defects. This symmetry also implies that in the case of order 2 elements one cannot canonically identify the states with elements of $H_1(\Sigma(L))$. Because of their symmetry, it is reasonable to suggest that planar textures should typically be easier to produce experimentally, and indeed one may even be able to produce a device that can sustain multiple topologically distinct textures that have the same defect structure.

Now we turn to links for which $|H_1(\Sigma(L))|$ is infinite. Algebraically the implication of this is clear. For a closed 3-manifold M we know that $H_2(M) =$

$H_1(M)$/torsion and hence the groups of infinite order imply that the branched double cover of S^3 over L has non-trivial second homology group. This has a nice geometric interpretation [33], in terms of the existence of disconnected spanning surfaces for the particular link, as shown in Figure 2.15. If such a link represents a defect set in a nematic, then $\mathbf{n}$ is orientable on a non-contractible closed surface surrounding a part of the link. Since one can find a closed, non-contractible surface on which $\mathbf{n}$ is orientable, one can compute the degree of $\mathbf{n}$ on the surface. This gives a full integer and the effect is responsible for the integer summands given in Table 2.1.

$p \setminus q$	2	3	4	5	6	7	8	9	10	11	12	13	14	15	16	17	18	19	20
2	2	3	4	5	6	7	8	9	10	11	12	13	14	15	16	17	18	19	20
3	3	2^2	3	1	$\mathbb{Z}^2$	1	3	2^2	3	1	$\mathbb{Z}^2$	1	3	2^2	3	1	$\mathbb{Z}^2$	1	3
4	4	3	$2 \times \mathbb{Z}^2$	5	12	7	$4 \times \mathbb{Z}^2$	9	20	11	$6 \times \mathbb{Z}^2$	13	28	15	$8 \times \mathbb{Z}^2$	17	36	19	$10 \times \mathbb{Z}^2$
5	5	1	5	2^4	5	1	5	1	$\mathbb{Z}^4$	1	5	1	5	2^4	5	1	5	1	$\mathbb{Z}^4$
6	6	$\mathbb{Z}^2$	12	5	$2 \times \mathbb{Z}^4$	7	24	$3 \times \mathbb{Z}^2$	30	11	$4 \times \mathbb{Z}^4$	13	42	$5 \times \mathbb{Z}^2$	48	17	$6 \times \mathbb{Z}^4$	19	60
7	7	1	7	1	7	2^6	7	1	7	1	7	1	$\mathbb{Z}^6$	1	7	1	7	1	7
8	8	3	$4 \times \mathbb{Z}^2$	5	24	7	$2 \times \mathbb{Z}^6$	9	40	11	$12 \times \mathbb{Z}^2$	13	56	15	$4 \times \mathbb{Z}^6$	17	72	19	$20 \times \mathbb{Z}^2$
9	9	2^2	9	1	$3 \times \mathbb{Z}^2$	1	9	2^8	9	1	$3 \times \mathbb{Z}^2$	1	9	2^2	9	1	$\mathbb{Z}^8$	1	9
10	10	3	20	$\mathbb{Z}^4$	30	7	40	9	$2 \times \mathbb{Z}^8$	11	60	13	70	$3 \times \mathbb{Z}^4$	80	17	90	19	$4 \times \mathbb{Z}^8$
11	11	1	11	1	11	1	11	1	11	2^{10}	11	1	11	1	11	1	11	1	11
12	12	$\mathbb{Z}^2$	$6 \times \mathbb{Z}^2$	5	$4 \times \mathbb{Z}^4$	7	$12 \times \mathbb{Z}^2$	$3 \times \mathbb{Z}^2$	60	11	$2 \times \mathbb{Z}^{10}$	13	84	$5 \times \mathbb{Z}^2$	$24 \times \mathbb{Z}^2$	17	$12 \times \mathbb{Z}^4$	19	$30 \times \mathbb{Z}^2$
13	13	1	13	1	13	1	13	1	13	1	13	2^{12}	13	1	13	1	13	1	13
14	14	3	28	5	42	$\mathbb{Z}^6$	56	9	70	11	84	13	$2 \times \mathbb{Z}^{12}$	15	112	17	126	19	140
15	15	2^2	15	2^4	$5 \times \mathbb{Z}^2$	1	15	2^2	$3 \times \mathbb{Z}^4$	1	$5 \times \mathbb{Z}^2$	1	15	2^{14}	15	1	$5 \times \mathbb{Z}^2$	1	$3 \times \mathbb{Z}^4$
16	16	3	$8 \times \mathbb{Z}^2$	5	48	7	$4 \times \mathbb{Z}^6$	9	80	11	$24 \times \mathbb{Z}^2$	13	112	15	$2 \times \mathbb{Z}^{14}$	17	144	19	$40 \times \mathbb{Z}^2$
17	17	1	17	2	17	1	17	1	17	1	17	1	17	1	17	2^{16}	17	1	17
18	18	$\mathbb{Z}^2$	36	5	$6 \times \mathbb{Z}^4$	7	72	$\mathbb{Z}^8$	90	11	$12 \times \mathbb{Z}^4$	13	126	$5 \times \mathbb{Z}^4$	144	17	$2 \times \mathbb{Z}^{16}$	19	180
19	19	1	19	1	19	1	19	1	19	1	19	1	19	1	19	1	19	2^{18}	19
20	20	3	$10 \times \mathbb{Z}^2$	$\mathbb{Z}^4$	60	7	$20 \times \mathbb{Z}^2$	9	$4 \times \mathbb{Z}^8$	11	$30 \times \mathbb{Z}^2$	13	140	$3 \times \mathbb{Z}^4$	$40 \times \mathbb{Z}^2$	17	180	19	$2 \times \mathbb{Z}^{18}$

Table 2.1: $H_1(\Sigma(L))$ for (p,q) torus links with $2 \leq (p,q) \leq 20$. x implies a group $\mathbb{Z}_x$, integer summands are given as usual.

Chapter 3

Umbilic Lines and the Geometry of Orientational Order

The pure topological perspective explored in the previous chapter is illuminating, the abstraction allows one to see and say much. However, one also throws much away in doing this; a physical system is much more than its topology. This chapter is an exploration of the geometry of physical systems described by orientational order and ultimately how this geometry reflects the topology we have been discussing. In this way, in part, one can think of this chapter as a bridge between some of the abstract objects in the previous chapter and structures in physical systems. Seen in another light, this chapter is an attempt at a unification and elucidation of much of the lore concerning 'double twist cylinders' and their myriad companions in chiral systems. Still further, one might think of this chapter as a simple exercise in the geometry of vector fields.

In this chapter we are concerned with geometric features of orientational order. By this we mean systems which are described by either a unit vector or line field, such as magnetic or nematic systems. These systems typically contain line-like geometrical features, the centres of vortex like distortions identified as λ lines and related structures in cholesteric liquid crystals [10, 45–48]. However, their appearance is not just confined to these systems, indeed they arise in superfluids as the cores of vortices [49–52], and they

can be identified in the Skyrmion[1] textures of chiral ferromagnets [53–57] and Bose-Einstein condensates [58–63]. We will show that these lines can be identified as a set of natural geometric singularities in a unit vector field, which we call umbilic lines. These lines convey the global structure of the vector field through their role as Poincaré dual to the Euler class of a natural vector bundle associated to the order. Later in this thesis we will show that how the identification of umbilics with λ lines and related structures in cholesteric liquid crystals [10, 45–48] allows one to give a global description of cholesteric topology. We name them umbilics since if the orientational order defines a foliation, then the umbilic lines correspond to the lines traced out by the umbilical points of the leaves of the foliation.

The umbilics we describe are generic traits, exhibited by any vector or line field, and closely analogous to several other structural degeneracies, for instance the lines of circular polarisation (C lines) in a generic electromagnetic field [64–67] and the umbilic points of surfaces [68, 69] and random fields [70–77], from which the terminology derives.

While we will give a detailed discussion of their relevance to cholesterics in Chapter 4, in general umbilic lines acquire extra significance in any material where the ground state has non-zero gradients where typically the vortex configurations surrounding umbilics correspond to local minima of the free energy. So for concreteness one can consider this chapter as concerning a system governed by the free-energy such as

$$F = \frac{K}{2}\int_{\mathbb{R}^3} |\nabla \mathbf{n}|^2 + 2q_0 \mathbf{n}\cdot\nabla\times\mathbf{n} dV, \tag{3.1}$$

where K is an elastic constant and q_0 is the strength of the chirality, or magnitude of spin-orbit coupling. This is the Frank free energy [1] for a bulk cholesteric under the one elastic constant approximation and also the Hamiltonian for elastic distortions in a chiral ferromagnet with a Dzyaloshinskii-

[1] We use the word 'Skyrmion' in the context of textures observed in chiral magnets, rather than in its original context of a non-linear field theory of pions.

Moriya interaction [78, 79]. We note that there is a connection of our local description with the work of Efrati and Irvine [80] on chiral shapes and structures. In their work they introduced a chirality pseudotensor to characterise the direction of twisting and sense of chirality of various materials. We demonstrate a general connection with the shape operator for a surface or vector field, from which their chirality pseudotensor can be derived, and show that natural benefits are gained by considering both operators. Finally, analogous geometrical structures to the umbilics we describe have been discussed by Thorndike *et al.* [81], Čopar *et al.* [82], and Beller *et al.* [83], although not with the topological aspect that we give here.

3.1 Local Geometry of Orientational Order

Three dimensional orientational order in a material can be given the following generic characterisation. At every point in space there is a local symmetry corresponding to rotations which preserve $\mathbf{n}$. Under the action of this rotation the gradient tensor $\nabla\mathbf{n}$ decomposes into irreducible representations as

$$\nabla_i n_j = n_i n_k \partial_k n_j + \frac{\nabla\cdot\mathbf{n}}{2}(\delta_{ij} - n_i n_j) + \frac{\mathbf{n}\cdot\nabla\times\mathbf{n}}{2}\epsilon_{ijk}n_k + \Delta_{ij}. \tag{3.2}$$

The first of these corresponds to the gradients along $\mathbf{n}$, known as bend distortions. The remaining parts correspond to gradients along directions orthogonal to $\mathbf{n}$, the first two of which are isotropic and comprise splay and twist distortions, known as the mean curvature and the mean torsion [84,85] respectively, and correspond to scalar and pseudoscalar parts of the transformation. The last part is a deviatoric, or spin 2, component, Δ, that conveys the local 'shear'. Its eigenvectors can be used to define principal directions of the curvature of the local orientation. In the case where $\mathbf{n}$ is the normal to a surface, the transformation (3.6) is the derivative of the Gauss map, or shape operator of the surface, and the principal directions alluded

to are the directions of principal curvature. The final component, Δ_{ij} corresponds to the anisotropic orthogonal gradients of $\mathbf{n}$, and contains saddle-splay distortions. We will assume for now that $\mathbf{n}$ is a vector, rather than a director. The local description of line fields is exactly the same, as can be seen by introducing a local orientation for the director field, and we defer a more thorough discussion until later. The decomposition in (3.2) carries over into the energy through expressions for the norm $|\nabla\mathbf{n}|^2$, which we write in the well-known form [1]

$$|\nabla\mathbf{n}|^2 = \frac{1}{2}(\nabla\cdot\mathbf{n})^2 + \frac{1}{2}(\mathbf{n}\cdot\nabla\times\mathbf{n})^2 + \big((\mathbf{n}\cdot\nabla)\mathbf{n}\big)^2 + 2|\Delta|^2, \tag{3.3}$$

where (the choice of normalisation for the norm of Δ is motivated by subsequent considerations)

$$\begin{aligned} |\Delta|^2 = &\left(\frac{\nabla\cdot\mathbf{n}}{2}\right)^2 + \left(\frac{\mathbf{n}\cdot\nabla\times\mathbf{n}}{2}\right)^2 \\ &- \frac{1}{2}\nabla\cdot\Big[\mathbf{n}\big(\nabla\cdot\mathbf{n}\big) - \big(\mathbf{n}\cdot\nabla\big)\mathbf{n}\Big]. \end{aligned} \tag{3.4}$$

Local minima of free energies such as (3.1) can then be expressed in terms of this decomposition. In particular, if $\big((\mathbf{n}\cdot\nabla)\mathbf{n}\big)^2 = \nabla\cdot\mathbf{n} = |\Delta|^2 = 0$, then the local energy density of (3.1) is given by

$$\frac{K}{2}\left(\frac{1}{2}(\mathbf{n}\cdot\nabla\times\mathbf{n})^2 + 2q_0\mathbf{n}\cdot\nabla\times\mathbf{n}\right) \tag{3.5}$$

and achieves an optimal lower bound of $-Kq_0^2$ for $\mathbf{n}\cdot\nabla\times\mathbf{n} = -2q_0$ [86, 87]. The local minima of (3.1) are thus characterised by having zero splay, zero bend, twist equal to -$2q_0$, and $|\Delta|^2 = 0$. We define points where $|\Delta|^2 = 0$ as umbilics of the orientational order; they therefore correspond to regions of the material where the orthogonal gradients of $\mathbf{n}$ are isotropic. In computational settings, umbilic lines can be identified by plotting isosurfaces of $|\Delta|^2$, which are shown as blue tubes throughout. In some cases, such as Figs. 3.5, 3.6 and 3.8, there is significant variation in the size of the tubes. In

part this reflects the structure of the orientational order around the umbilic, although some features such as the shrinking to zero size in Fig. 3.5 are artefacts of the finite difference schemes used in the computer simulations and do not represent any physical phenomena. If $\mathbf{d}_1, \mathbf{d}_2$ are arbitrary unit vectors orthogonal to $\mathbf{n}$, such that $\{\mathbf{d}_1, \mathbf{d}_2, \mathbf{n}\}$ form a right-handed set, then the orthogonal gradients can be expressed in this local basis as a 2×2 real matrix with the decomposition

$$\begin{aligned}\nabla_\perp \mathbf{n} = \frac{\nabla\cdot\mathbf{n}}{2}\begin{bmatrix}1 & 0\\ 0 & 1\end{bmatrix} + \frac{\mathbf{n}\cdot\nabla\times\mathbf{n}}{2}\begin{bmatrix}0 & -1\\ 1 & 0\end{bmatrix}\\ + \begin{bmatrix}\Delta_1 & \Delta_2\\ \Delta_2 & -\Delta_1\end{bmatrix},\end{aligned} \tag{3.6}$$

where

$$\Delta_1 = \frac{1}{2}\big(\partial_1 n_1 - \partial_2 n_2\big), \quad \Delta_2 = \frac{1}{2}\big(\partial_1 n_2 + \partial_2 n_1\big). \tag{3.7}$$

The vanishing of Δ is then analogous to the Cauchy-Riemann equations. Indeed, director configurations whose stereographic projection is a meromorphic function have $\Delta_1 = \Delta_2 = 0$ everywhere; they are totally umbilic. As shown by Belavin and Polyakov [88], these arise naturally as the minimisers of (3.1) with $q_0 = 0$ when the domain is two-dimensional. However, this situation, where a two-dimensional surface is totally umbilic, is not generic and in general umbilics occur at isolated points in two dimensions and along lines in three. This is simply because Δ is two-dimensional, and one requires both $\Delta_1 = 0$ and $\Delta_2 = 0$, meaning umbilics are codimension 2. The presence of chirality ($q_0 \neq 0$) or spin-orbit coupling in the free energy (3.1) yields the generic situation.

Their dimensionality, coupled with the isotropic nature of $\nabla_\perp \mathbf{n}$ on umbilic lines, means that umbilics are associated with the centres of vortex-like distortions. For chiral free energies such (3.1), the preference for twist leads to umbilic profiles such as those shown in Fig. 3.1(a,c,e), typically seen in

materials with chiral interactions. For chiral vortices there is an immediate correspondence with 'double twist' [86], traditionally written as $\partial_i n_j = -q_0 \epsilon_{ijk} n_k$, which is equivalent to the condition of being on an umbilic line, with only twist deformations. Typical double twist configuration, such as shown in Fig. 3.1(e), are axisymmetric and contain an umbilic line along their centreline, however this umbilic is not generic. In the generic case the umbilics are non-axisymmetric, such as the two λ lines in the dislocation shown in Fig. 3.1(a). They can still correspond to regions where the free energy is lower than that of the helical state, as long as the other aspects of the gradient tensor, splay and bend, are sufficiently small. Umbilic lines with local structures dominated by splay and bend distortions, Fig. 3.1(d), can also be energetically favourable for systems with a term of the form [89]

$$\mathbf{E} \cdot \big((\mathbf{n} \cdot \nabla)\mathbf{n} - \mathbf{n}(\nabla \cdot \mathbf{n}) \big), \tag{3.8}$$

for an external field $\mathbf{E}$, replacing the chiral term in (3.1). This term corresponds to the flexoelectric effect in liquid crystalline systems [90] and to Rashba spin-orbit coupling in magnetic systems [89]. By an analogous argument to that given above, it is easy to see that umbilics with splay and bend distortions can correspond to local minima of a free energy with such a term. In this way the existence of Skyrmion lattices, such as those shown in Fig. 3.4, can be interpreted as due to the energetic preference for umbilic lines, and the association between umbilic lines and Skyrmions, given by (3.19).

The geometric character of the orientational order is conveyed by the generic local description (3.2). The twist, $\mathbf{n} \cdot \nabla \times \mathbf{n}$, encodes the chirality of the order with surfaces of zero twist separating regions of different handedness, and also indicates whether $\mathbf{n}$ is the normal to a system of layers. The splay, $\nabla \cdot \mathbf{n}$, measures how the flow of $\mathbf{n}$ preserves volume, and $(\mathbf{n} \cdot \nabla)\mathbf{n}$ gives the geodesic curvature of the integral lines. Zeros of the deviatoric part of $\nabla_\perp \mathbf{n}$ occur along lines in three dimensions – they require both Δ_1 and Δ_2

to vanish and hence are codimension two – and correspond to degeneracies of the principal curvatures, or singularities of the principal curvature directions. They are the umbilics of the orientational order. At such points the transverse gradients are isotropic meaning that umbilics are naturally associated with the centres of vortex-like structures. A basis-independent expression can be given for these zeros purely in terms of the director; they correspond to the vanishing of the non-negative quantity

$$|\Delta|^2 = \left(\frac{\nabla\cdot\mathbf{n}}{2}\right)^2 + \left(\frac{\mathbf{n}\cdot\nabla\times\mathbf{n}}{2}\right)^2 - \frac{1}{2}\nabla\cdot\Big[\mathbf{n}\big(\nabla\cdot\mathbf{n}\big) - \big(\mathbf{n}\cdot\nabla\big)\mathbf{n}\Big], \tag{3.9}$$

this being the 2-norm of Δ. In the vicinity of an umbilic we may write

$$\Delta = |\Delta| \begin{bmatrix} \cos\theta & \sin\theta \\ \sin\theta & -\cos\theta \end{bmatrix}, \tag{3.10}$$

and around the umbilic the angle θ winds by an integer multiple of 2π. An umbilic is said to be generic if it has a winding number of ± 1. Umbilics with higher winding do occur, and indeed those with winding $+2$ are often observed in vortices, double twist cylinders and (baby) Skyrmions, with the degeneracy coming from an imposed axisymmetry. This can persist in certain experimental settings, either where there is axisymmetry or hexagonal symmetry, however, from a structural point of view they can be seen as a composite of winding ± 1 umbilics, into which they break apart under generic perturbation.

Illustrations can be given for a number of simple field conformations corresponding to textures observed in systems such as superfluid vortices, magnetic Skyrmions and the λ lines of cholesteric liquid crystals, shown in Figure. 3.1. We show two-dimensional sections of the full textures on surfaces intersecting the umbilics transversally. The eigenvectors of Π, which will be defined presently, are shown in (b) and identify the profiles of the

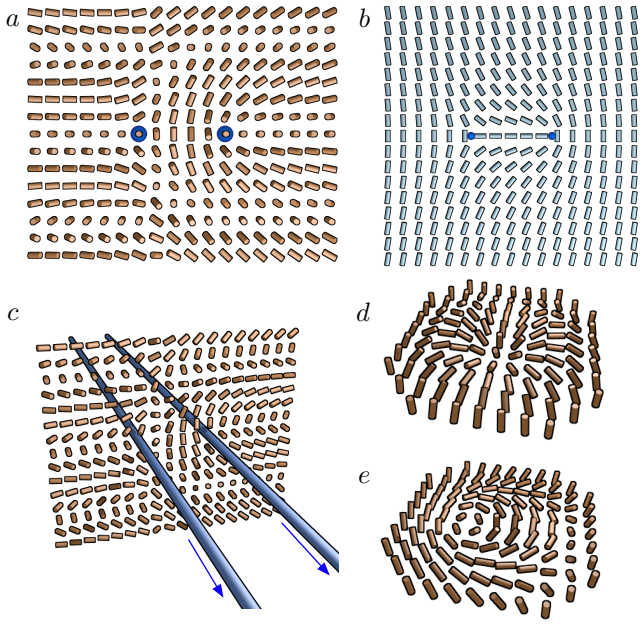

Figure 3.1: Umbilic lines. (a) λ^+ λ^- dislocation in a cholesteric. It contains two generic umbilics. This combination of two generic umbilics can be identified as half a Skyrmion, or a meron. (b) Eigenvector field of Π for the dislocation. The two umbilics have opposite windings of the eigenvectors, but are counted with the same sign as $\mathbf{n}$ rotates by π when passing from one to the other. (c) Umbilic lines can be oriented in three dimensions. (d) & (e) Typical centres of vortices, based on curvature and torsion distortions respectively, that correspond to winding number 2 non-generic umbilics.

umbilics in (a).

As we will show, the windings that we have just described are equivalent to the indices of the umbilics up to a sign, which arises because the orientation of $\mathbf{n}$ 'reverses' from one umbilic to another. (The discrepancy is therefore absent if $\mathbf{n}$ is the normal to a surface, since then there is no reversal of its orientation between umbilics, and the index is simply the local winding of the eigenvectors of Δ.) The sum of the indices of the umbilics yields a topological invariant, equal to four times the Skyrmion number of the texture on the two-dimensional surface. This calculation of the Skyrmion number is dual to the usual method of integrating a curvature form [28, 88]

$$q = \frac{1}{8\pi} \int_{\Sigma} \epsilon_{abc} n^a \partial_i n^b \partial_j n^c \, dx^i \wedge dx^j, \tag{3.11}$$

which computes the degree of the map $\mathbf{n} : \Sigma \to S^2$. The duality can be viewed as entirely analogous to that in the classical differential geometry of surfaces between the Gauss-Bonnet theorem – integral of the Gaussian curvature – and the calculation of the Euler characteristic using umbilic points of the surface.

Two additional aspects of the local description are worth bringing out before giving a global treatment. First, the complex structure $J = \left[\begin{smallmatrix} 0 & -1 \\ 1 & 0 \end{smallmatrix}\right]$ acts on the shape operator (3.6) by simple composition to produce an equivalent linear transformation

$$\begin{aligned} \chi = J \circ \nabla_{\perp} \mathbf{n} = -\frac{\mathbf{n} \cdot \nabla \times \mathbf{n}}{2} \begin{bmatrix} 1 & 0 \\ 0 & 1 \end{bmatrix} + \frac{\nabla \cdot \mathbf{n}}{2} \begin{bmatrix} 0 & -1 \\ 1 & 0 \end{bmatrix} \\ + \begin{bmatrix} -\Delta_2 & \Delta_1 \\ \Delta_1 & \Delta_2 \end{bmatrix}. \end{aligned} \tag{3.12}$$

This transformation, although equivalent to the shape operator, is independent from it in the sense that they are orthogonal with respect to the natural inner product between matrices, $\mathrm{Tr}(\chi^T \nabla_{\perp} \mathbf{n}) = 0$, a property that turns out

to be of some importance in the analysis of the topology of umbilics. χ is the chirality pseudotensor given by Efrati and Irvine [80] in their study of chiral materials. The spin 2 component $\Pi = J \circ \Delta$ carries equivalent information to Δ. Its eigenvectors can be thought of as defining directions of principal torsion (or twist) and are simply rotated relative to those of Δ by $\pi/4$ about the director. Nonetheless, for materials with chiral interactions or structure, it is these directions, rather than the eigenvectors of Δ, that are often more visibly recognisable, as is elegantly illustrated in the experiments of Armon *et al.* [91] on the opening of chiral seed pods, and those of Efrati and Irvine [80] on stretched elastic sheets.

Second, if the umbilic forms a closed loop then the winding of the angle θ along the contour length of the umbilic (a longitude) conveys a second integer invariant. Of course, this latter depends on both the choice of longitude and the homotopy class of the local trivialisation $\{\mathbf{d}_1, \mathbf{d}_2\}$. We describe this in detail later.

3.2 Global Definition of Umbilics and their Topology

The umbilic lines we have identified convey topological information about the vector field $\mathbf{n}$, specifically the Euler class of the orthogonal 2-plane bundle, ξ, through a combination of the Gauss-Bonnet-Chern theorem [92–95] and Poincaré duality. The curvature of a vector bundle represents a characteristic cohomology class that can be integrated over homology cycles to produce topological invariants. By Poincaré duality this can be viewed as a homology class and the umbilics furnish a representative of this Poincaré dual. We shall develop this general topology of orientational order in terms of a natural connection on the vector bundle that the spin 2 transformation Δ takes values in.

As before, let $\mathbf{n}$ be a unit vector field in $\mathbb{R}^3$; then it defines a splitting of

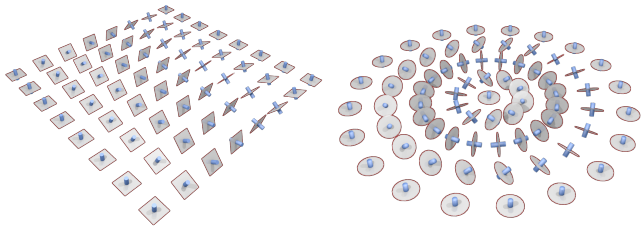

Figure 3.2: The splitting $T\mathbb{R}^3 \cong L_{\mathbf{n}} \oplus \xi$ induced by orientational order. *Left:* A simple helical director profile, corresponding to the ground state of a cholesteric liquid crystal or helimagnet. *Right:* An idealised, axisymmetric Skyrmion profile, the central portion of which is a standard idealised model of double twist cylinders in blue phases.

the tangent bundle

$$T\mathbb{R}^3 \cong L_{\mathbf{n}} \oplus \xi, \tag{3.13}$$

into a real line bundle, $L_{\mathbf{n}}$, of vectors parallel to $\mathbf{n}$ and a rank 2 real vector bundle, ξ, of vectors orthogonal to $\mathbf{n}$. Examples of this splitting are shown in Figure 3.2. The gradients of $\mathbf{n}$ take values in $T\mathbb{R}^{3\,*} \otimes \xi \cong (L_{\mathbf{n}}^* \otimes \xi) \oplus (\xi^* \otimes \xi)$, with the first part containing the bend deformations and the second the perpendicular gradients given locally in (3.6). By complete analogy with the classical differential geometry of surfaces we call these perpendicular gradients the shape operator of the orientational order and think of it as a linear transformation on the orthogonal 2-planes.

The shape operator decomposes in the following way. Local rotations about the director field correspond to a local symmetry and endow the bundle ξ with a natural $SO(2)$ action, under which the tensor product $\xi^* \otimes \xi$ splits into a direct sum $\mathcal{I} \oplus \mathcal{J} \oplus E$, where $\mathcal{I}$ and $\mathcal{J}$ are trivial line bundles and E is a rank 2 vector bundle. Correspondingly, the shape operator has the decomposition

$$\nabla_\perp \mathbf{n} = \frac{\nabla \cdot \mathbf{n}}{2} \mathbb{I}_\xi + \frac{\mathbf{n} \cdot \nabla \times \mathbf{n}}{2} J + \Delta, \tag{3.14}$$

given previously in (3.6). Here, $\mathbb{I}_\xi$ is the identity transformation and $J = \mathbf{n}\times$ is a complex structure on ξ, now defined globally, while Δ has the global

definition

$$\Delta(\mathbf{v}) = \frac{1}{2}\Big[(\mathbf{v}\cdot\nabla)\mathbf{n} + \mathbf{n}\times(\mathbf{n}\times\mathbf{v}\cdot\nabla)\mathbf{n}\Big], \tag{3.15}$$

for any $\mathbf{v}$ that is a section of ξ. The umbilics are identified with the zeros of Δ; they encode the topology of the orientational order.

Without repeating too much of the local description given previously, we note that composition with the complex structure again yields the chirality pseudotensor [80], $\chi = J\circ\nabla_\perp\mathbf{n}$, and that the spin 2 component of this, $\Pi = J\circ\Delta$, can be expressed globally as

$$\Pi(\mathbf{v}) = \frac{1}{2}\Big[\mathbf{n}\times(\mathbf{v}\cdot\nabla)\mathbf{n} - (\mathbf{n}\times\mathbf{v})\cdot\nabla\mathbf{n}\Big], \tag{3.16}$$

for any $\mathbf{v}$ that is a section of ξ, and is also a section of E. We reiterate that although Π and Δ may be obtained one from the other by composition with the complex structure, they are orthogonal with respect to the natural inner product $\langle\Pi,\Delta\rangle = \frac{1}{2}\mathrm{Tr}(\Pi^T\Delta)$. At the same time, they share the same magnitude and the same zero set, the umbilics $\mathcal{U}$. Thus, away from umbilic lines, Π and Δ represent two non-zero orthogonal sections of E, and so they provide a basis for $E|_{\mathbb{R}^3-\mathcal{U}}$ and also define a natural connection 1-form

$$A = \frac{\langle\Pi,\nabla\Delta\rangle}{\langle\Delta,\Delta\rangle}. \tag{3.17}$$

This 1-form conveys the fundamental topology of the orientational order.

We give in (3.17) a global definition of A that emphasises its naturality and makes clear how it arises. In a local chart it can be represented in terms of the eigenvectors, $\mathbf{p}^+$ and $\mathbf{p}^-$, of Δ and has components $A_i = 2p_a^-\partial_i p_a^+$, an expression perhaps closer in form to the usual way of writing Berry connections. However, one must keep in mind that this representation is only local in the present context; otherwise it only serves to obfuscate the natural structure. The exterior derivative of A, $\Omega_E = dA$, is the (Berry) curvature of the vector bundle E. It is equal to twice the curvature of ξ on account of

E being a spin 2 subbundle of $\xi^* \otimes \xi$. (This is also evident from the local expression in terms of the eigenvectors $\mathbf{p}^{\pm}$.)

A fundamental property of an umbilic is given by the integral of the connection 1-form (3.17) around any simple closed loop γ encircling the umbilic. Let Σ be an oriented surface with boundary γ, as in Figure 3.3. If Σ is generic then the umbilics will intersect it transversally in some number of distinct points. Let $\{D_i\}$ be disjoint small discs in Σ about each of these intersection points and denote their boundaries by $\{C_i\}$. Then $|\Delta|$ is nowhere zero on $\Sigma - \{D_i\}$ and $\partial(\Sigma - \{D_i\}) = \gamma \sqcup \{\overline{C}_i\}$ so that by Stokes' theorem

$$\int_\gamma A - \sum_i \int_{C_i} A = \int_{\Sigma - \{D_i\}} dA = \int_{\Sigma - \{D_i\}} \Omega_E. \tag{3.18}$$

To extend the analysis over the umbilics, we can introduce a local trivialisation of $L_{\mathbf{n}} \oplus \xi$ on each of the D_i, which we denote by the orthonormal basis $\{\mathbf{n}, \mathbf{d}_1, \mathbf{d}_2\}$. Then $\mathbf{e}_1 = \mathbf{d}_1 \otimes \mathbf{d}_1 - \mathbf{d}_2 \otimes \mathbf{d}_2$ and $\mathbf{e}_2 = \mathbf{d}_1 \otimes \mathbf{d}_2 + \mathbf{d}_2 \otimes \mathbf{d}_1$ form a local basis for E. In such a basis $\Delta = |\Delta| \cos\theta\, \mathbf{e}_1 + |\Delta| \sin\theta\, \mathbf{e}_2$ and $A = d\theta + 2\omega$ where $\omega_i = (\mathbf{d}_2)_a \partial_i (\mathbf{d}_1)_a$ is the connection 1-form on ξ for this basis (the factor of two accounts for E being a spin 2 bundle). With this, one finds at once the Gauss-Bonnet-Chern theorem [96] in the form

$$\begin{aligned} \frac{-1}{2\pi} \int_\Sigma \Omega_E + \frac{1}{2\pi} \int_\gamma A &= \sum_i \frac{1}{2\pi} \int_{C_i} d\theta, \\ &= \sum_i \text{index}_\Sigma\, U_i, \end{aligned} \tag{3.19}$$

which defines the index of an umbilic, an integer associated to its intersection with a surface. Note that, as alluded to earlier, the index of an umbilic is not simply the winding number of the angle θ that characterises the local profile as that is measured relative to a local basis for ξ, while the index uses the orientation on the surface Σ; there is, therefore, an additional sign according to whether $d\theta$ is cooriented with C_i or not.

It is instructive to contrast this situation, where the type of profile does

not carry topological information, with that of umbilical points of surfaces where it does. This occurs because in the case of surfaces $\mathbf{n}$ is fixed to be the normal to Σ, and so $d\theta$ is always cooriented with C_i.

One can understand this relation between the profile and index in terms of oriented umbilics. The 1-form A circulates around umbilic lines, orienting them such that the circulation is right handed. If one orients umbilics in this way, the expression for the index in (3.19) is rewritten as

$$\text{index}_\Sigma\, U_i = s_i \text{Int}(U_i, \Sigma), \tag{3.20}$$

where $\text{Int}(U_i, \Sigma)$ is the signed number of intersections of U_i with Σ and $s_i \in \mathbb{N}$ is the absolute strength of the umbilic U_i. Examples illustrating this are shown in Figures 3.1 and 3.4; we describe only the latter (the former is essentially identical). Figure 3.4 shows a Skyrmion lattice, a well-known structure seen in a variety of systems [53–56, 61, 97–100]. The umbilics form a lattice, with $s = 2$ umbilics each surrounded by six $s = 1$ umbilics. The eigenvectors of Π show the central umbilic having a $+1$ profile, and the six outer umbilics a $-1/2$ profile. All the umbilics have the same orientation induced by A, and so their intersection numbers, and thus indices in (3.19), are all positive. For the $+1$ profile, $-1/2$ profile and the orientations to all be consistent, it is necessary that $\mathbf{n}$ rotates by π when passing from the central umbilic to an outer one.

The curvature of the bundle ξ can be expressed in terms of the director field as

$$\Omega_\xi = -\frac{1}{2}\epsilon_{abc} n^a \partial_i n^b \partial_j n^c dx^i \wedge dx^j. \tag{3.21}$$

This is because each 2-plane of the bundle ξ is explicitly embedded in $\mathbb{R}^3$ (see Figure 3.2) and the expression is just the extrinsic definition of curvature in terms of the (generalised) Gauss map, and so can be viewed as the pullback of the area 2-form on the target S^2 to the material domain. (3.21) also follows from an explicit calculation in local coordinates for any particular texture,

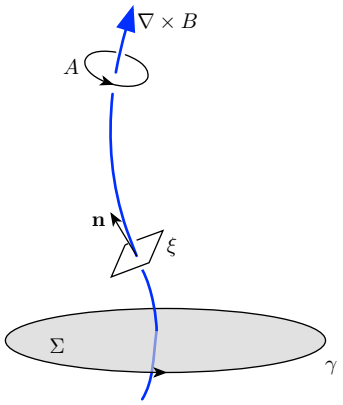

Figure 3.3: Anatomy of an umbilic line. *Top.* The vector $\nabla \times B$ is tangent to generic umbilic lines, giving them a natural orientation. This orientation is compatible with that induced by A. *Middle.* The vector field $\mathbf{n}$ and associated orthogonal plane ξ. Note that in general the tangent vector of the umbilic does not align with $\mathbf{n}$. ξ is oriented by $\mathbf{n}$ and so gives a natural cycle along which to measure the winding. For a generic umbilic if $\mathbf{n} \cdot \nabla \times B > 0$ then the eigenvectors of Δ have a $+1/2$ profile and if $\mathbf{n} \cdot \nabla \times B < 0$ the eigenvectors have a $-1/2$ profile. *Bottom.* A measuring cycle γ bounding a surface Σ. Whether γ measures the winding of the umbilic as positive or negative depends on whether the umbilic – oriented by $\nabla \times B$ – intersects Σ positively or negatively.

say a radial hedgehog. A third way to establish it is through a calculation in the style of the Mermin-Ho relation [49], a good account of which has been given by Kamien [101]. The curvature of E is equal to twice this, $\Omega_E = 2\Omega_\xi$, since E is a spin 2 subbundle of $\xi^* \otimes \xi$. Therefore, when Σ is closed, or the boundary term vanishes, we have

$$\sum_i s_i \text{Int}(U_i, \Sigma) = \frac{1}{2\pi} \int_\Sigma \epsilon_{abc} n^a \partial_i n^b \partial_j n^c dx^i \wedge dx^j = 4q, \tag{3.22}$$

or the sum of the indices of the umbilics piercing Σ is equal to four times the Skyrmion number. This then establishes a general relationship between Skyrmions and umbilics. This is illustrated in Figure 3.4 where each unit cell contains one $s = 2$ umbilic and six $s = 1$ umbilics, each of which are shared between three unit cells, giving a total count of $2 + 6 \times 1/3 = 4$, *i.e.* there is one Skyrmion in each unit cell.

This correspondence between Skyrmions and umbilics can be seen as a version of Poincaré duality, giving a natural way to localise Skyrmions to a

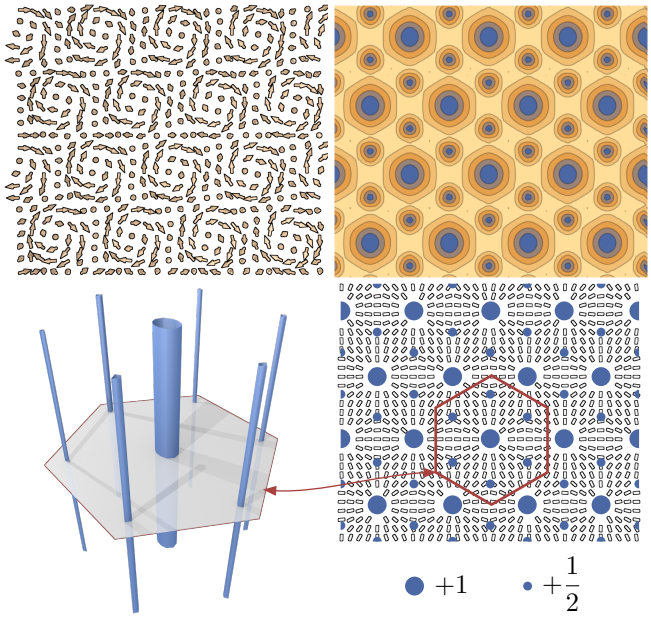

Figure 3.4: Skyrmion lattice simulated in a triply periodic cell using the free energy (3.1). Each unit cell possesses a single central $s = 2$ umbilic, with the six outer $s = 1$ umbilics each shared between 3 unit cells giving a total count of $2 + 6 \times 1/3 = 4$ umbilics $= 1$ Skyrmion per unit cell. *Top Left*: Unit vector field $\mathbf{n}$ in a Skyrmion lattice. *Top Right*: Contour plot of $|\Delta|$ showing the umbilic lines forming a lattice of tubes. *Bottom Right*: Eigenvector field of Π, illustrating the $+1$ winding around the central umbilics and $-1/2$ winding around the outer umbilics. Note that both are counted with the same sign as the orientation of $\mathbf{n}$ changes from one to another. *Bottom Left*: Umbilics form lines in three dimensions.

set of points or lines. The set of umbilics $\mathcal{U}$ in a three dimensional system M gives a representative of a cycle in $H_1(M)$. The Poincaré dual of this is the cocycle $e(E) \in H^2(M)$, the Euler class, which depends only on the topology of the bundle E and hence $\mathbf{n}$, and gives a global constraint on the total number of umbilic lines in the system in terms of the topology of $\mathbf{n}$. As a spin-2 vector bundle, $e(E) = 2e(\xi) = 4[\mathbf{n}]$, where $[\mathbf{n}] \in H^2(M)$ is the cocycle represented by $\mathbf{n}$[2]. In the absence of torsion in $H^2(M)$[3], there is a canonical representative of the cocycle $4[\mathbf{n}]$ as a 2-form which is given through the Chern-Weil homomorphism by $\mathrm{Pf}(-\Omega_E/2\pi)$, where Pf is the Pfaffian, which leads to (3.19).

An example of the Euler class as a global constraint on umbilics is given by the case of monopoles, illustrated in Figure 3.5. As realised in chiral ferromagnets, these are point defects in the magnetisation that mediate changes in the number of Skyrmions [57]. In the local neighbourhood of a point defect the topology of $\mathbf{n}$ is described by an integer $q \in \pi_2(S^2) \cong \mathbb{Z}$, the charge of the point defect. Through (3.22) one finds that a sphere surrounding this point defect must be pierced by umbilics of total index $4q$. In Figure 3.5 we show a simulation of two ± 1 point defects, or monopoles, in a chiral ferromagnet. There are four umbilics, each of generic type, ending on the point defects in a manner reminiscent of Dirac strings [92]. On a slice in the midplane of the cell $\mathbf{n}$ contains a Skyrmion, illustrating the well-known creation and annihilation of Skyrmions in terms of point defects, observed experimentally [57].

3.3 Local Profiles of Umbilic lines

Simple examples of umbilic lines, such as the Skyrmion lattice in Fig. 3.4, possess translational symmetry along the umbilic, with the tangent vector

[2] If $\mathbf{n}$ is considered as a map into S^2, then homotopy classes are given by an element in H^2 with additional data associated to the Hopf invariant.

[3] Here, torsion is meant in the sense of group theory – *i.e.* $H^2(M)$ contains elements of finite order – and not in the geometric sense.

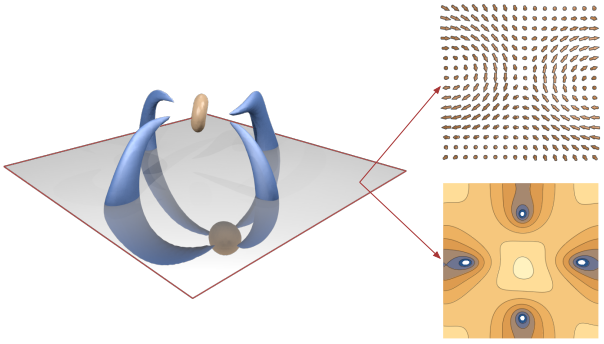

Figure 3.5: Transient monopoles and umbilic lines observed in a simulated quench of the free energy (3.1). *Left:* Contours of constant value of $|\Delta|$. The blue lines are umbilics, the beige spheres are monopoles (point defects). Each umbilic has winding $n = 1$. They are all oriented similarly, so that the sum of the umbilics entering/leaving the negative/positive point defect is 4, in accordance with (3.19) and corresponding to the Skyrmion created between the monopoles. *Top Right:* Cross-section showing $\mathbf{n}$ on the shaded plane. As a map from the plane to S^2, it has degree 1, indicating the presence of a Skyrmion. *Bottom Right:* Contour plot showing the magnitude of $\log(|\Delta|)$ on the shaded plane, the umbilics are clearly picked out.

of the umbilic pointing parallel to $\mathbf{n}$. Both these situations are not generic; the local profile of umbilic lines may change along their length and the tangent vector of the line does not have to be parallel to $\mathbf{n}$. To describe how these quantities can vary one needs to understand the local structure of umbilic lines, the focus of this section. Ultimately this local description will lead to the definition of global linking invariants or umbilic loops in the next section. This can be considered analogous to the situation earlier, where the local structure of umbilics in orientational order led to global invariants, namely Skyrmions.

Generic umbilic lines carry a canonical orientation through the vector B, defined as

$$B^i = \langle \Pi, \partial^i \Delta \rangle = \langle \Delta, \Delta \rangle \delta^{ij} A_j, \tag{3.23}$$

which assigns a tangent vector to the umbilic, provided it is generic, as follows. In an arbitrary local trivialisation, $\Delta = s_1 \mathbf{e}_1 + s_2 \mathbf{e}_2$ and an umbilic is defined as the intersection of the two surfaces $s_1 = 0$ and $s_2 = 0$ and so its tangent vector will be $\nabla s_1 \times \nabla s_2$. Note that while the values of s_1 and s_2 depend on the choice of basis, the tangent vector does not. In this local form

we can write

$$B = s_1 \nabla s_2 - s_2 \nabla s_1 + 2(s_1^2 + s_2^2)\omega, \tag{3.24}$$

where $\omega_i = (\mathbf{e}_2)_a \partial_i (\mathbf{e}_1)_a$, so that on an umbilic we have $\nabla \times B = 2\nabla s_1 \times \nabla s_2$ and hence the vector $\nabla \times B$ points along umbilic lines, canonically orienting them. As indicated in Fig. 3.3 this orientation is compatible with that induced by the circulation in A previously discussed. As alluded to in Figs. 3.1 and 3.4, the discrepancy between the type of profile and index of an umbilic depends on the relative orientation between $\mathbf{n}$ and the umbilic line. To measure whether the eigenvectors of a generic umbilic have winding $\pm 1/2$ one should integrate A along a contour γ chosen such that its orientation matches the orientation imparted to ξ by $\mathbf{n}$. One can then show that the local profile is $\pm 1/2$ depending on

$$\mathrm{Sgn}(\mathbf{n} \cdot \nabla \times B), \tag{3.25}$$

the analysis being identical to that given by Berry and Dennis for C lines in electromagnetic fields [70, 102]. The freedom between the relative orientations of umbilic lines and $\mathbf{n}$ means that $\mathbf{n} \cdot \nabla \times B$ can pass continuously through zero, changing the type of profile from $\pm 1/2$ to $\mp 1/2$, in a similar manner to nematic disclinations [21].

This quantity $\mathbf{n} \cdot \nabla \times B$ can be used to further characterise the local structure of umbilic lines. Along an umbilic Δ vanishes and generically we can expect it to vanish linearly. Its local profile is then given by the form of the linear order terms in Δ in the immediate vicinity of the umbilic. Equivalently, generically we can expect the gradients of Δ to be non-zero on the umbilic and the local profile is then given by the structure of $\nabla\Delta$ evaluated on the umbilic. As usual, we split the gradients into the components parallel to $\mathbf{n}$ and those perpendicular to it, and consider only the latter. The non-zero part of these transverse gradients, evaluated on the umbilics, takes values in $\xi^* \otimes E$, so it is this part that we need to focus on. A section of this bundle

characterising the local profile of the umbilic can be constructed from $\nabla\Delta$ as follows. If $\mathbb{I}_E$ is the projection onto E in $T\mathbb{R}^{3*}\otimes T\mathbb{R}^3$ then we define the differential operator ∇^ξ as $\nabla^\xi\Delta = \mathbb{I}_\xi\nabla\Delta\mathbb{I}_E$. By construction $\nabla^\xi\Delta$ is a section of the bundle $\xi^*\otimes E$. Under the action of $SO(2)$ the bundle $\xi^*\otimes E$ splits into two rank 2 subbundles, $F^+\oplus F^-$, where F^+ is the spin 1 bundle corresponding to $+1/2$ profiles and F^- is the spin 3 bundle corresponding to $-1/2$ profiles, and we decompose $\nabla^\xi\Delta$ according to this splitting as

$$\nabla^\xi\Delta = \nabla^\xi\Delta^+ + \nabla^\xi\Delta^-. \tag{3.26}$$

A short calculation shows that $\mathbf{n}\cdot\nabla\times B = |\nabla^\xi\Delta^+|^2 - |\nabla^\xi\Delta^-|^2$, so that if $|\nabla^\xi\Delta^+| > |\nabla^\xi\Delta^-|$ the umbilic has a local $+1/2$ profile, while if the converse holds the profile is of type $-1/2$.

This analysis allows us to give a description of the space of local profiles for a generic umbilic. Since $\nabla^\xi\Delta|_{\mathcal{U}}$ is non-zero for a generic umbilic, but otherwise arbitrary, the space of local profiles has the homotopy type of the three-sphere, which can be seen as analogous to the 'Poincaré T sphere' variables given in [72]. The position of the profile on this three-sphere can be obtained by normalising $\nabla^\xi\Delta|_{\mathcal{U}}$. The equality $|\nabla^\xi\Delta^+| = |\nabla^\xi\Delta^-|$ defines a Clifford torus which separates the three-sphere into two solid tori corresponding to the different profiles. A natural constraint on an umbilic loop is for its profile to be of constant type, *i.e.* for $\mathbf{n}\cdot\nabla\times B$ to be of constant sign or the profile to stay within a single solid torus. We call an umbilic loop which satisfies this constraint transverse, as its tangent vector is always transverse to the planes of ξ. This is not an unphysical constraint, transverse umbilic lines are commonly found in various chiral structures – typical λ lines in cholesterics have a local structure in which $\mathbf{n}$ is either parallel or antiparallel with the tangent vector to an umbilic. Figure 3.6 shows the transverse umbilic loop found in toron excitations in frustrated cholesterics [8,9], simulated using (3.1).

The condition of an umbilic being transverse therefore translates as one

of the two profiles having a higher 'weight' along the entire length of the umbilic. If this is the case then we have $|\nabla^\xi \Delta^\pm|^2 \neq 0$ with the sign depending on whether the umbilic is positively or negatively transverse. Suppose, for concreteness, that the umbilic is positively transverse. Then, in a local trivialisation, we will have $\nabla^\xi \Delta^+ = t_1 \mathbf{f}_1^+ + t_2 \mathbf{f}_2^+$, with $t_1^2 + t_2^2 \neq 0$, and the space of positively transverse umbilics has the homotopy type of a circle. The variation of the profile around a closed, transverse umbilic loop confers another integer winding number. This number depends on how the basis vectors of the trivialisation of F^+ wind around the umbilic. The ambiguity can be removed by demanding that each of the basis vectors in the trivialisation does not link with the umbilic. As we will show in the next section, this winding number can be interpreted as twice a self-linking number for the umbilic loop, and is related to a relative Euler class of E.

3.4 The Local Profile of Tensor Field Zeros in 2D

An understanding of the profiles of higher order umbilics can be phrased in terms of the local structure of zeros of a spin-2 field in two dimensions. This is a specific example of the more general case of zeros of an arbitrary spin field in two dimensions, which has an elegant structure when phrased in terms of vector bundles[4] and forms an amusing digression.

We will begin with a trivial calculation. Suppose we have two rank 2 vector bundles E and F on a 2-manifold Σ. They have spin N and M meaning that under the action of $SO(2)$ corresponding to rotations a section s of E transforms as

$$s_1 \mathbf{e}_1 + s_2 \mathbf{e}_2 \mapsto s_1(\cos(N\theta)\mathbf{e}_1 + \sin(N\theta)\mathbf{e}_2) + s_2(\cos(N\theta)\mathbf{e}_2 - \sin(N\theta)\mathbf{e}_1), \quad (3.27)$$

or, writing as a vector

$$s \mapsto R_\theta^N s, \quad (3.28)$$

[4] Of course, it can all be done in half the time by using complex numbers, but we would like to keep using vector bundles.

with a corresponding statement for F. Now consider the bundle $E \otimes F$. It has dimension four and under the rotation one finds that it splits into two irreducible two-dimensional subbundles as

$$E \otimes F \cong A \oplus B \tag{3.29}$$

where A consists of identity and antisymmetric tensors and has spin $N-M$ and basis $\mathbf{a}_1 = \mathbf{d}_1 \otimes \mathbf{e}_1 + \mathbf{d}_2 \otimes \mathbf{e}_2$ and $\mathbf{a}_2 = \mathbf{d}_2 \otimes \mathbf{e}_1 - \mathbf{d}_1 \otimes \mathbf{e}_2$; and B consists of traceless symmetric tensors, has spin $M+N$ and basis $\mathbf{b}_1 = \mathbf{d}_1 \otimes \mathbf{e}_1 - \mathbf{d}_2 \otimes \mathbf{e}_2$ and $\mathbf{b}_2 = \mathbf{d}_1 \otimes \mathbf{e}_2 + \mathbf{d}_2 \otimes \mathbf{e}_1$. Writing bundles with their spin as a subscript we have the equation

$$E_N \otimes F_M \cong A_{M-N} \oplus B_{M+N} \tag{3.30}$$

Now suppose we have a field $\sigma = s_1\mathbf{e}_1 + s_2\mathbf{e}_2$, a section of a rank-2 spin N vector bundle E. Now the first order derivative of σ will be a section of $T^*\Sigma \otimes E$, and by (3.30) this decomposes as

$$T^*\Sigma \otimes E_N \cong D^{(1)}E_{N-1} \oplus D^{(-1)}E_{N+1}, \tag{3.31}$$

since $T^*\Sigma$ has spin 1 and we have used the notation $D^{(a)}E_M$ to denote a subbundle corresponding to a spin M derivative of E, a is associated to the winding of a zero whose derivative only has values in the bundle, and will be explained below. To understand the full structure we will need to go one step further, and look at second derivatives. In this case we are looking at a section of the bundle

$$T^*\Sigma \otimes T^*\Sigma \otimes E_N \cong D^{(1,1)}E_{N-2} \oplus D^{(1,-1)}E_N \oplus D^{(-1,1)}E_N \oplus D^{(-1,-1)}E_{N+2}. \tag{3.32}$$

A short calculation in terms of basis vectors shows that the bundles $D^{(1,-1)}E_N$ and $D^{(-1,1)}E_N$ are the same. If we denote $\nabla^{\pm}$ to be the restriction of the

derivative to the appropriate subbundle, then this structure can be summed up by the diagram.

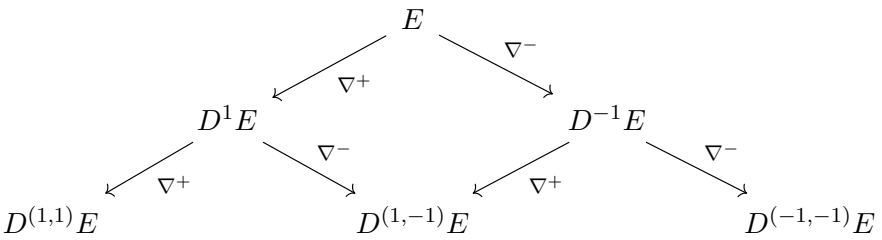

This diagram has a natural extension to arbitrary order, and it commutes up to the p^{th} row for a zero of order p. This is a consequence of the following. Suppose there is a point x such that $\sigma(x) = 0$. Then the order of the zero at x is the lowest p such that $\nabla^p \sigma \neq 0$. Now, if ω is a connection form for E then

$$\nabla\sigma = \partial\sigma + \omega_{ik}^{j}\sigma_j, \tag{3.33}$$

so that if we restrict the derivatives to be of order $\leq p$ we can consider the connection to be flat in the vicinity of the zero, since any terms coming from the connection will be multiplied by $\sigma(p) = 0$ or lower order gradients.

Now suppose there is a zero of order p, but that its p^{th} derivatives lie entirely in a single subbundle, as distinguished on symmetry grounds. Then, purely by symmetry, one can deduce the winding of the zero. To see this consider the field $\sigma(x)$ with $\sigma(0) = 0$. Then, if one considers a circuit around the zero, it is possible to deduce that the winding of a zero of a spin N field corresponding to a spin M subbundle is $N - M$. This is illustrated in Table 3.1. Finally, one can use this relationship to observe changes in the symmetry of a zero when one tries to change the symmetry of a field. The canonical example of this operation is decorating a line field with an orientation. Suppose one has a spin N field σ with a zero of spin M, then by trying to change the symmetry of the field, one creates a new field with spin N/p for an integer divisor p of N. One can see, then, that this will only be possible if the spin of the zero, M, is equal to pM'.

Order	Charge	Spin	Profile	Charge	Spin	Profile
1	$\frac{1}{2}$	1	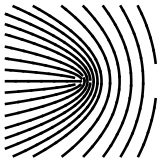	$-\frac{1}{2}$	3	
2	1	0	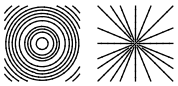	-1	4	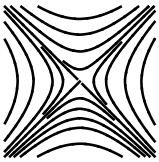
3	$\frac{3}{2}$	-1	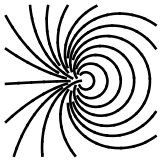	$-\frac{3}{2}$	5	
4	2	-2	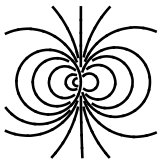	-2	6	
5	$\frac{5}{2}$	-3	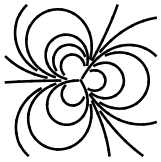	$-\frac{5}{2}$	7	
6	3	-4	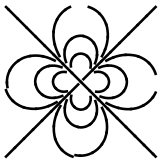	-3	8	

Table 3.1: Local structure of zeros for a spin 2 field in two dimensions up to order 6. The spins of the profile correspond to the spins of the associated vector bundles. Note that the sum of the spins in a given order is equal to twice the spin of the original field, in this case 4. Also note that the charge 1 profile has spin zero, meaning one can distinguish a star and a centre on symmetry grounds.

3.5 Umbilic Loops

The umbilics of three-dimensional orientationally ordered materials are extended line-like objects, however most of the properties we have described so far can be associated to isolated points along the umbilics. For example the points of transverse intersection with an appropriate surface (or slice through the material) count numbers of Skyrmions, merons, or λ defects. It is clear, however, that these locally measurable objects do not represent all the information encoded by umbilic lines; if one has a closed umbilic loop then, as discussed above, the local properties at each point must stitch together consistently along the loop conveying both geometric and topological information about the orientational order.

Umbilic loops have been observed in experimental systems [9, 10, 74], and a motivating set of examples are the so-called torons [8], illustrated in Figure 3.6. These soliton structures can be generated in a frustrated cholesteric cell, with the director held vertical along the top and bottom. As shown in Figure 3.6(a), they display a characteristic umbilic loop, in the form of a circle sitting in the midplane of the cell. This loop is of generic type, with the eigenvectors of Π having a monstar profile.

As with local properties of umbilic lines, much of the structure of loops is encoded in the 1-form A. Previously we have obtained local information about umbilics by integrating A around a meridian. The first step to understanding their global structure is to integrate A along a longitude. Since A is singular on an umbilic, we must define this integral as a limit. If U_i is an umbilic, then let U_i' be a curve close to U_i that has zero linking number with it. The integral of A over U_i' is well defined and if all the umbilics in the system are closed loops we can take the limit $U_i' \to U_i$ to obtain

$$\int_{U_i} A = 2\pi \sum_j s_j \mathrm{Lk}(U_i, U_j) + \int_\Sigma \Omega_E, \tag{3.34}$$

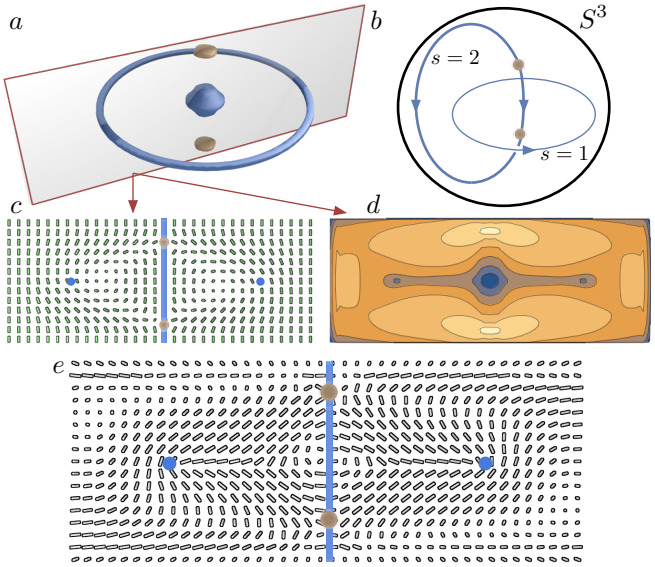

Figure 3.6: Umbilic lines in a toron. (a) Simulation results showing point defects and characteristic umbilic loop in a toron. The umbilic loop is transverse and has zero self-linking number. The point defects have opposite charge, due to lattice effects the simulation does not resolve the umbilic lines connecting them, though they are clear in the topology of the eigenvector field. (b) Diagram illustrating the umbilic structure of the toron in S^3 when the boundary of the cell is collapsed to a point, note that the umbilic loops connecting the point defects each have strength $s = 2$, for a total of 4, as required by (3.19). (c) Simulation results showing director field for the toron. (d) Contour plot showing the value of $|\Delta|$. (e) Eigenvector field of Π. Note that the umbilic loop is generic and has a monstar profile.

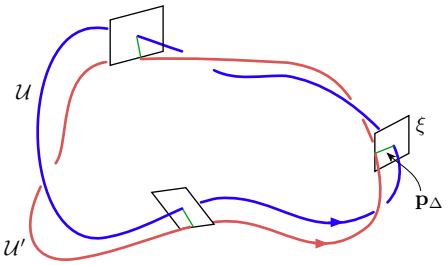

Figure 3.7: The self-linking number for transverse umbilic loops. The red curve U' is formed by pushing U along an eigenvector field $\mathbf{p}_\Delta$ of Δ. The self-linking number is then computed as the linking number of U with U'. The umbilic must be transverse to ensure that U' does not cross U. Because the eigenvectors are degenerate on the umbilic, one evaluates $\mathbf{p}_\Delta$ on a line close to U, $\hat{U}$, that has zero self-linking number with U. Such a line can be found by drawing an orientable surface whose boundary is U and pushing U into that surface. Note that because eigenvectors are line fields, the self-linking number can be a half-integer, corresponding to $\mathbf{p}$ being non-orientable along the longitude of U.

where Σ is an orientable surface bounded by U_i. The requirement that U_i' have zero linking with U_i ensures that the limit is well defined but in general the result depends upon this choice of framing. $\sum_j s_j \mathrm{Lk}(U_i, U_j) = e(U_i)$ in (3.34) is an integer associated to the umbilic line, the relative Euler class, and counts the number of umbilics linking U_i. There are two natural questions to ask of this quantity. The first is whether it corresponds to any local geometric structure of the umbilic line; the second is whether it relates to a global property of $\mathbf{n}$. On both counts the answer is yes. Geometrically (3.34) is related to both a self-linking number and the winding number defined in the previous section. Globally we will show that it is related to the Hopf invariant of $\mathbf{n}$.

To see this suppose U is a transverse umbilic loop, then let $\hat{U}$ be a loop close to U of zero linking number with U. Evaluate one of the eigenvectors of Δ, $\mathbf{p}_\Delta^+$ say, along $\hat{U}$ and then push U along this eigenvector field to form a new loop, U'. The linking number $\mathrm{Lk}(U, U')$ is then taken to define the self-linking number of the transverse umbilic, $\mathrm{Sl}(U)$. This construction is shown in Figure 3.7. Note that since $\mathbf{p}_\Delta^+$ is a line field, $\mathrm{Sl}(U)$ may be a half-integer corresponding to $\mathbf{p}$ being non-orientable along the longitude of U.

With this notion in hand the correspondence between the self-linking

number and the winding number coming from the variation of the local profile defined in the previous section can be established. Choose a trivialisation $\{\mathbf{d}_1, \mathbf{d}_2\}$ of ξ on a neighbourhood of U such that the linking number of U pushed off along $\mathbf{d}_1$ (say) is zero, then the winding of $\nabla^{\xi}\Delta^{+}$ with respect to the chosen trivialisation will give twice the self-linking number. Note that the geometric definition of the self-linking number did not depend on the zero of Δ being of linear order. The relationship between between the self-linking number and the relative Euler class of a transverse umbilic is then[5]

$$\mathrm{Sl}(U) = \overline{\mathrm{Sl}}(U) + \frac{1}{2}e(U). \tag{3.35}$$

There is a new term in this equation, $\overline{\mathrm{Sl}}(U)$, the transverse self-linking number of U. $\overline{\mathrm{Sl}}(U)$ is a geometric quantity, preserved under deformations that keep U transverse. A similar notion is studied in the context of contact topology [103] where it provides useful geometric information, but we do not know of a general discussion in the case of arbitrary $\mathbf{n}$.

We now turn to the relationship between the linking of umbilics and global properties of $\mathbf{n}$. Associated to the 1-form A is the Chern-Simons 3-form, $A \wedge dA$, and it is natural to ask whether the integral over the complement of $\mathcal{U}$,

$$\int A \wedge dA, \tag{3.36}$$

gives some information about umbilic lines and $\mathbf{n}$. This integral can be compared to the similar helicity integral for a fluid flow and the Abelian Chern-Simons action. Both these quantities are related to linking numbers, of vortex lines in the case of helicity [104–106] and Wilson loops in Chern-Simons theory [107, 108] and, as we will show, it is no different for umbilics, (3.36) connects the linking numbers of the umbilic loops with the Hopf invariant of $\mathbf{n}$. To proceed we will assume that the material domain is S^3, with no defects and that the zero set of Δ is one-dimensional. By a compactification,

[5] To see that (3.35) is correct it is enough to show that increasing $e(U)$ by 1 increases $\mathrm{Sl}(U)$ by $1/2$ coupled with standard arguments from contact topology [103].

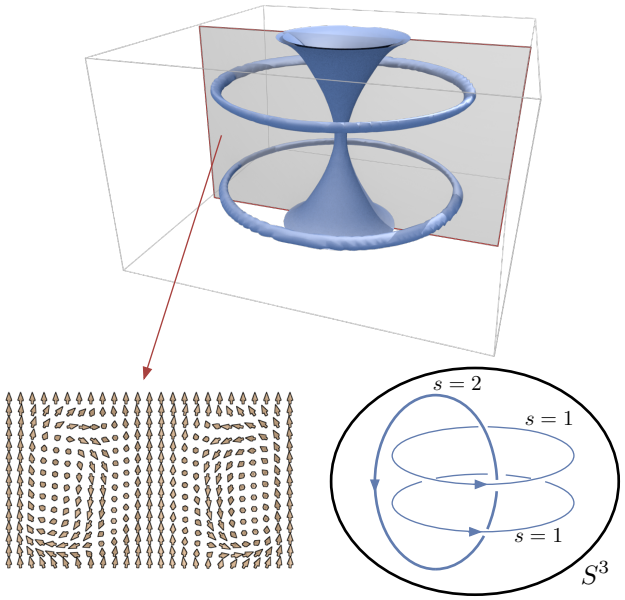

Figure 3.8: Umbilic lines in the Hopf fibration. *Top*: Umbilic lines given as isosurfaces of $|\Delta|$ for a simulated Hopf fibration. The two lines in the mid plane of the cell are both generic, with the same orientation. For symmetry reasons the central umbilic is not generic and has $s = 2$. On the boundary of the cell $\mathbf{n}$ is uniform, which means that the Hopf invariant is well-defined. Note that the system is totally umbilic on the boundary. If you compactify the domain by collapsing the boundary to a point, then one can interpret the central vertical umbilic line as passing through this point. *Bottom Left*: director field for the Hopf texture. *Bottom Right*: Schematic of the relationship between umbilic lines in S^3. Two generic $s = 1$ umbilic lines each link with one $s = 2$ umbilic line that passes through the point at infinity.

this assumption that the domain is S^3 is equivalent to examining a system in $\mathbb{R}^3$ for which $\lim_{x\to\infty} \mathbf{n}(x) = \mathbf{n}_0$, a constant. An example of such a system is illustrated by the Hopf fibration, which has been experimentally realised in frustrated cholesterics [9], illustrated in Figure 3.8, and the aforementioned toron. In both these systems $\mathbf{n}$ is constant on the boundary of the cell. Because of this $\Delta = 0$ on the boundary and one should consider these systems as having an umbilic line passing through the point 'at infinity', which in Figures 3.6 and 3.8 is just the boundary of the system.

Topologically the configuration in Figure 3.8 is unusual, it is non-singular but not homotopically equivalent to a constant. The difference is that it has a non-zero Hopf invariant. This integer invariant distinguishes topologically distinct non-singular textures in $\mathbb{R}^3$ which are constrained to tend to a con-

stant at infinity and is typically visualised in terms of linking of pre-images of two orientations using the Pontryagin-Thom construction [9]. In our setting however one can give a slight re-interpretation of the famous Whitehead integral formula [109], similar to that given by Arnol'd [106], to show that the Hopf invariant is also the Chern-Simons invariant of the bundle ξ. In our interpretation, if one takes a ω to be a connection form for ξ, then $d\omega$ is the curvature of ξ and the Chern-Simons integral

$$\frac{1}{(4\pi)^2}\int_{S^3}\omega\wedge d\omega \tag{3.37}$$

computes the Hopf invariant of $\mathbf{n}$.

Now we turn back to our integral (3.36). As discussed, we assume the material domain is S^3 (or $\mathbb{R}^3$ with uniform boundary conditions). This means that we can give a global trivialisation of ξ with connection ω and our 1-form A can be written as $A = d\theta + 2\omega$. This allows us to write

$$\int_{S^3-\mathcal{U}} A\wedge dA = 4\int_{S^3-\mathcal{U}}\omega\wedge d\omega + 2\int_{S^3-\mathcal{U}} d\theta\wedge d\omega \tag{3.38}$$

or, since $\mathcal{U}$ has measure zero

$$\int_{S^3-\mathcal{U}} A\wedge dA = 4(4\pi)^2 H + 2\int_{S^3-\mathcal{U}} d\theta\wedge d\omega \tag{3.39}$$

where H is the Hopf invariant of $\mathbf{n}$. Now we need to evaluate the integral of $d\theta\wedge d\omega$ over $S^3-\mathcal{U}$. We will first do a simpler integral, over $S^3-N(\mathcal{U})$, where $N(\mathcal{U})$ is a neighbourhood of the umbilic lines. By Stokes' theorem this can be reduced to an integral over the boundary of $N(\mathcal{U})$ as

$$\int_{S^3-N(\mathcal{U})} d\theta\wedge d\omega = \sum_i \int_{\partial N(U_i)}\omega\wedge d\theta. \tag{3.40}$$

The boundary of the neighbourhood of each umbilic line is a torus and because our domain is S^3 we can choose a preferred longitude for each torus that has zero linking with the umbilic at its centre. This allows us to specify

a decomposition of each boundary component into $S^1_M \times S^1_L$. If we choose $N(\mathcal{U})$ small enough, then along each meridian of the torus ω will be approximately constant and equal to its value on the umbilic line. The integral over each boundary component can then be written as:

$$\sum_i \int_{\partial N(U_i)} \omega \wedge d\theta = \sum_i \int_{S^1_L} \omega^* \left(\int_{S^1_M} d\theta^* \right) \tag{3.41}$$

where we have pulled the forms back to each S^1.

The integral of $d\theta$ is trivial, it evaluates to $s_i 2\pi$, where s_i is the strength of the i^{th} umbilic. Finally, we take a limit as $N(\mathcal{U}) \to \mathcal{U}$ and obtain a sum of Wilson loop integrals

$$\lim_{N(\mathcal{U})\to\mathcal{U}} \sum_i \int_{\partial N(U_i)} \omega \wedge d\theta = 2\pi \sum_i s_i \int_{U_i} \omega. \tag{3.42}$$

Now from the Gauss-Bonnet-Chern theorem (3.19) we can relate integrals of ω along umbilics to integrals of A. Putting this together with the above equations we obtain

$$\begin{aligned} \frac{1}{(4\pi)^2} \int_{S^3-\mathcal{U}} A \wedge dA - \frac{1}{8\pi} \sum_i s_i \int_{U_i} A \\ = 4H - \frac{1}{4} \sum_{ij} s_i s_j \text{Lk}(U_i, U_j) \end{aligned} \tag{3.43}$$

This equation relates analytic data, the integral of $A \wedge dA$ and Wilson loop integrals, to topological data, namely the linking number of the umbilic lines and the Hopf invariant. We hope that this relationship will allow for an interpretation of the creation and destruction of Hopf solitons in terms of umbilic lines, however we do not currently have a deep physical understanding of this relationship.

3.6 Examples of Line Fields: Blue Phases

So far in this chapter we have been concerned with the geometric properties of vector fields and our discussion of line fields has been confined to the observation that a local orientating of a director is always possible and so a local definition[6] of umbilics passes through to the non-orientable case, with the only effect of potential non-orientability relating to the global constraints on umbilic lines, which will be dealt with extensively in Chapter 4.

However, not all orientationally ordered systems are described by either a vector or a director field. In Chapter 1 we considered tensorial order parameters, in particular Q tensors, and it is natural to ask whether umbilic lines exist in these systems also. Much of this section is built around discussion of a beautiful set of examples, the cholesteric blue phases. These remarkable materials are characterised by periodic orientational order corresponding to crystalline space groups, while remaining three-dimensional fluids. Two distinct cubic structures, BPI with space group $O^{8-}(I4_132)$ and BPII with space group $O^2(P4_232)$, are observed on varying temperature or the amount of chiral dopant [86, 87, 110], while several other structures can be induced by applied electric field effects [111–113] or confinement [114], and there is also an amorphous phase, known as BPIII [115]. Their structure arises because the local optimal configuration for the chiral free energy is one of double twist (illustrated in Figures 3.1 and 3.2), but this is only locally favourable and the structure becomes energetically unstable if it extends too far. This leads to a frustrated arrangement where locally preferred regions of double twist form periodic arrays interwoven by a network of disclination lines [86, 87]. The blue phases have a long-standing association with Skyrmions in chiral magnets, with which they may be considered analogous, and this connection continues to stimulate considerable interchange of ideas between the two fields [10, 116–119].

[6] Here local has the rather tautological definition of a region in which $\mathbf{n}$ may be oriented, in liquid crystalline systems this will typically mean a region containing no disclination lines.

To begin our discussion of umbilic lines in Q tensors, we note that as $\xi^* \otimes \xi$ is a subbundle of $T\mathbb{R}^{3*} \otimes T\mathbb{R}^3$ the linear transformation Π, equation (3.16), can be embedded in a 3×3 matrix and expressed, in a Cartesian basis, as

$$\begin{aligned}\Pi_{ij} = &\frac{1}{4}\epsilon_{ilk}\Big[n_l\partial_k n_j + n_l\partial_j n_k - n_j n_l n_m \partial_m n_k\Big] \\ &+ \frac{1}{4}\epsilon_{jlk}\Big[n_l\partial_k n_i + n_l\partial_i n_k - n_i n_l n_m \partial_m n_k\Big].\end{aligned} \tag{3.44}$$

The issue at hand is what a suitable replacement should be if we express the orientational order using a Q-tensor rather than the director field. The usual approach to obtaining such a replacement is to adopt algebraic methods rather than geometric ones[7]; one constructs a list of potential expressions and selects on the basis of how they reduce when the Q-tensor is written in terms of the director field. Following this procedure, we find that the expression

$$\begin{aligned}\tilde{\Pi}_{ij} = &\frac{1}{4}\epsilon_{ilk}\Big[2Q_{lm}\partial_k Q_{jm} + Q_{jm}\partial_k Q_{lm} \\ &\qquad + Q_{lm}\partial_j Q_{km} - Q_{jl}\partial_m Q_{km}\Big] \\ &+ \frac{1}{4}\epsilon_{jlk}\Big[2Q_{lm}\partial_k Q_{im} + Q_{im}\partial_k Q_{lm} \\ &\qquad + Q_{lm}\partial_i Q_{km} - Q_{il}\partial_m Q_{km}\Big],\end{aligned} \tag{3.45}$$

reduces to Π_{ij} when the Q-tensor is uniaxial, with constant magnitude, $Q_{ij} \propto n_i n_j - \frac{1}{3}\delta_{ij}$. We subtract its trace and adopt it as an appropriate Q-tensor analogue of Π. In simulations, the umbilic lines can then be identified using isosurfaces where the norm of $\tilde{\Pi}$ drops below a threshold value.

Illustrations are given in Figure 3.9 for some standard blue phase textures. The umbilics coincide with structural motifs that have been identified previously, either through symmetry considerations [120] or by taking a singular value decomposition of the Q-tensor, as in the work of Čopar et

[7] We are reminded here of a sentiment put forth by Michael Atiyah: "*Algebra is the offer made by the devil to the mathematician. The devil says: 'I will give you this powerful machine, it will answer any question you like. All you need to do is give me your soul: give up geometry and you will have this marvellous machine.'*", from page 7 of M.F. Atiyah, *Mathematics in the 20th Century*, Bull. Lond. Math. Soc. **34**, 1-15 (2002).

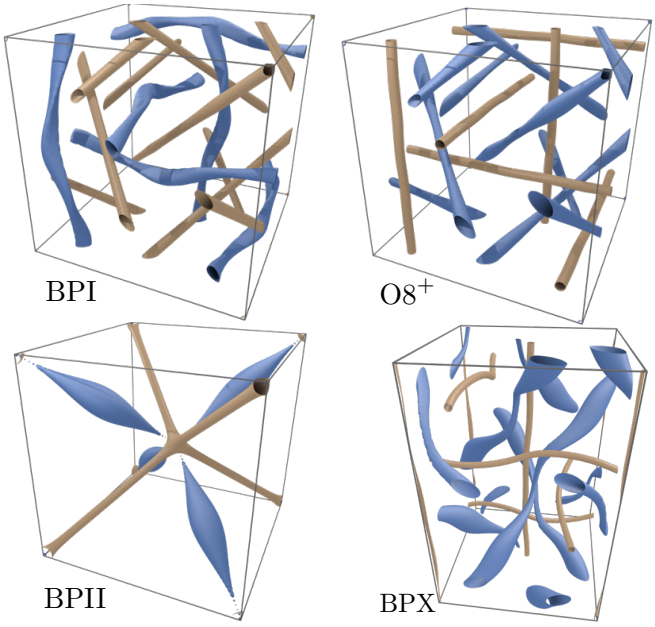

Figure 3.9: Umbilic lines in the blue phases. The umbilics are indicated by blue isosurfaces, while the network of disclination lines is shown by bronze isosurfaces. The textures BPI and BPII are the cubic structures observed experimentally. $O8^+$ is a cubic structure with the same space group as BPI but an interchange between disclination lines and umbilics. BPX is a tetragonal texture observed in an applied electric field. The arrangement of disclinations and umbilics is the same as in O^{8+}, although the symmetry is different.

al. [82]. These motifs are the axes of double twist cylinders [86, 87]. Two remarks are in order concerning this. First, the pattern of umbilic lines in BPII (see Figure 3.9) does not correspond to the array of double twist cylinders traditionally depicted in the literature. In the traditional depiction the double twist cylinders are taken along the 2-fold axes lying in the faces of the conventional unit cell and, indeed, inspection by eye reveals these lines to have the same general structure as model double twist cylinders [86] (see Figure 3.1). However, in a Q-tensor description of BPII these are not degeneracies where the local structure is axisymmetric, as in the standard idealised picture of a double twist cylinder; rather they are 2-fold lines where the Q-tensor is maximally biaxial [14, 82, 121]. Second, it is perhaps worth emphasising that the umbilics identified in all other blue phase textures also differ from the standard idealised picture of a double twist cylinder. This is because the idealised axisymmetry of the latter constrains it to be a degenerate winding $+2$ umbilic, whereas those that are found in periodic textures are generic umbilics, typically with a $-1/2$ profile for the eigenvectors of $\tilde{\Pi}$, *i.e.* a star umbilic.

We have given here only cursory illustrations for periodic blue phases with crystalline space groups. It would be of interest to also study the structure of the amorphous BPIII in terms of umbilics, as well as their behaviour in transitions and rheology. The Q-tensor version of the linear transformation Π that we introduced here was motivated on algebraic grounds rather than the geometrical considerations that the rest of our work is founded upon. It is clear that geometrical considerations can be developed for traceless symmetric tensors, parallel to our description of orientational order. It would be interesting to do so and compare the outcome with the algebraic construction we have given. We speculate that since the group of symmetries of the biaxial phase is discrete, the identification of an umbilic line in a Q tensor necessarily coincides with degeneracies in Q itself.

CHAPTER 4

SYNTHESIS: THE CASE OF THE CHOLESTERIC

In this chapter we will bring together ideas from the previous chapters, along with material from the field of contact topology and geometry to try to understand structures and defects in cholesteric liquid crystals.

Cholesterics are liquid crystals with chirality, typically though not always due to a chiral dopant. The result is a propensity for the cholesteric to twist, and the groundstate of such a system is given by

$$\mathbf{n} = \cos q_0 z \mathbf{e}_x + \sin q_0 z \mathbf{e}_y, \tag{4.1}$$

which is periodic with period π/q_0 ($\mathbf{n}$ is a director not a vector), a length-scale known as (half the) the pitch of the cholesteric [12]. The value of q_0 controls the rate of twisting, with the sign dictating whether the twisting is right or left handed. The value of q_0 is not only affected by chemical properties such as the amount of chiral dopant, but also physical variables such as temperature. Indeed it is possible to have helical sense inversion as a function of temperature, where the value of q_0 passes from being positive to negative. This process is continuous, and the system does not undergo any phase transition [1].

While this groundstate has a simple form, cholesterics themselves support a huge array of exotic twisted structures, particularly in confined environments, often accompanied by set of line-like features many of which

do not correspond to the singular disclination lines found in nematics, and are instead non-singular. These twisted structures include textures, soliton structures and other phenomena. Of interest to us include various solitons in frustrated cholesterics, including those related to topological objects such as baby Skyrmions [8,10] and the Hopf fibration [9] and textures displayed by cholesterics such as oily streaks, which consist of various line defects against a helical background, and the related fingerprint and fan textures [122,123].

Understanding these structures from the perspective of geometry and topology has long stood as a challenge, indeed in his 1979 review [26] Mermin described constructing a theory of defects in cholesterics as an "important challenge which the topological methods have yet to come to terms with" and while various descriptions have been given based on ideas such as the Volterra process [47] and applications of the homotopy theory [12,46, 124], it is arguable that none of these truly capture the essence of the problem.

In this chapter we illustrate two different, and hopefully complementary, approaches to the study of cholesterics. The first is a combination of the perspectives outlined in the previous two chapters, we discuss how umbilic lines form natural candidates for the familiar λ lines in cholesterics and other line-like features. In particular, we show how they arise out of a perspective based on the traditional notion of the pitch axis. As emphasised in Chapter 3 this gives a precise definition for these objects, and allows their properties to be better understood. Using the global perspective we developed in Chapter 2, we show how the internal topological states associated to knotted and linked defects can be used to give global constraints on the number of τ and λ lines in the system. To summarise briefly, in Chapter 2 we outlined how for the space of internal states $H_1(\Sigma(L))$ for a give link, there was a distinction between elements of order 2 and (x such that $2x = 0$) and other elements. In cholesterics one finds additional structure based on the existence of elements of order 4. The result we sketch states that, for an in-

ternal state x, then if $2x = 0$, the state can be represented in a cholesteric with only χ defect lines (regular disclinations), if $4x = 0$, then the state can be represented with only χ and τ lines and in all other cases one requires either τ lines, λ line or both.

The second approach is of a different nature altogether. The foundational idea in the study of topological defects is to consider configurations up to the equivalence relation of homotopy. In cholesterics, however, there is an alternative choice. This is to consider only deformations of the texture that preserve its handedness, that is $\mathbf{n} \cdot \nabla \times \mathbf{n} \neq 0$. One therefore looks for equivalence classes of twisted field configurations. It turns out that this constraint has been studied mathematically under the name of contact topology, and indeed the topological classification one finds in this case is far richer than in the regular nematic case. We give a preliminary exploration of this, and show how one can distinguish field configurations as cholesterics when they are topologically equivalent as nematics. It is important to note that the description we give here is only an outline, one would suspect that there is much more interesting physics to uncover in this area. Finally, we conjecture on a possible way to combine these two perspectives into a Floer homology theory

4.1 Observed Defects in Cholesterics

Defects in cholesterics have traditionally been studied in model settings such as Grandjean-Cano wedges [45, 48, 125–127]. In these systems a sample of cholesteric liquid crystal is placed between two plates with strong planar surface anchoring. If the plates are parallel then the cholesteric will form its helical phase, illustrated in Figure 4.1, with $\mathbf{n}$ undergoing an integer, p, number of twists from one plate to another. Note that if the separation of the plates L is not equal to an integer multiplied by π/q_0, then the cholesteric will not be at a minimum of the free energy and will be frustrated. The wedge is formed by arranging the plates such that they are at a small angle with re-

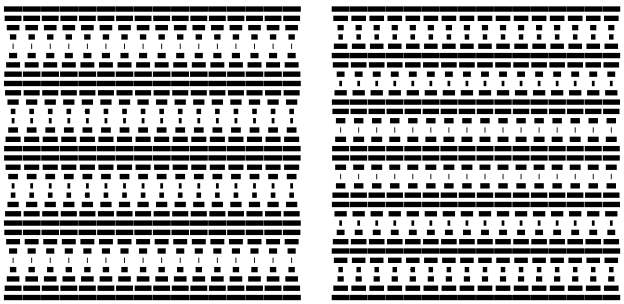

Figure 4.1: Two helical cholesterics in a slab of height L. The left has four twists and the right six.

spect to each other. At this point one observes a change from p twists to $p+1$ or $p+2$ twists as the separation increases. This change in the number of twists is typically mediated by a line defect, pointing in the direction orthogonal to that of increasing cell width. These defects may take several forms, and were first understood using the Volterra process by Kléman and Friedel [47] and were grouped into three categories, λ, τ and χ defect lines, some of which are shown in Figure 4.2.

While wedge and slab geometries provide a controlled setting for the study of defect lines in cholesterics, the same set of lines has, of course, been observed in many other contexts, for example, in simulations of cholesteric droplets [128], frustrated cholesteric cells [129] and in the work of Bouligand [122, 123].

4.2 The Theory of the Pitch Axis

Historically these line defects have been organised through a homotopy theoretic approach involving the introduction of an auxiliary direction in space known as the pitch axis [12, 46, 124]. The theory is centred around the observation that the helical groundstate of the cholesteric, (4.1) consists of $\mathbf{n}$ rotating about an axis, in (4.1) this is the z-axis, though in general it is an arbitrary direction $\mathbf{p}$, with $\mathbf{p}\cdot\mathbf{n} = 0$ and of course one can form a third direction

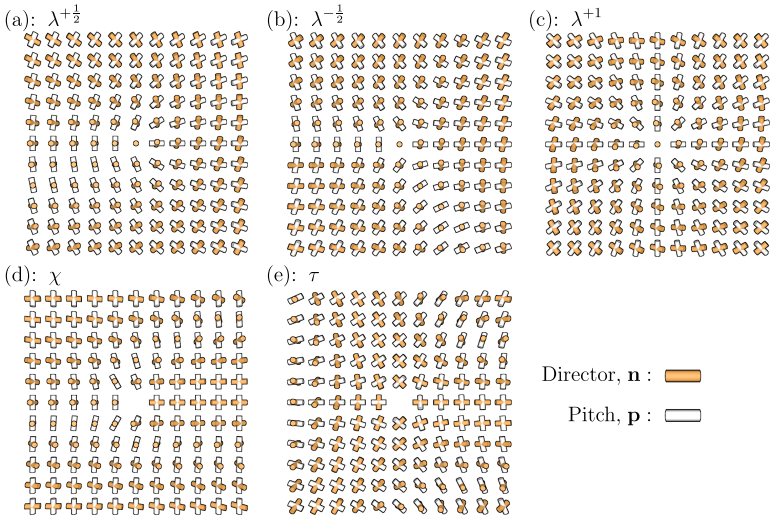

Figure 4.2: Defects in cholesterics and an associated pitch axis, constructed as an eigenvector of Δ. λ defects are defects in the pitch axis, or umbilic lines. χ defects are defects in $\mathbf{n}$. τ lines are defects in $\mathbf{n}$ around which the pitch axis is non-orientable.

as $\mathbf{n} \times \mathbf{p}$.[1] As such, one obtains a triad of directors $\mathbf{T}$. The direction $\mathbf{p}$ is also a director, rather than a vector, since directions of twisting are apolar[2], think of a helix or corkscrew, and do not distinguish a direction but only an axis. Though, of course, it is apolar for a different reason than $\mathbf{n}$ is apolar, and so one should also allow for a theory of the pitch axis in polar materials as well as liquid crystals.

With the direction $\mathbf{p}$ given, the theory of the pitch axis states that the triad $\mathbf{T}$ is an element in a regular order parameter space which, as a triad of directors, is the biaxial nematic order parameter space. This predicts then, that cholesterics contain no point defects, only line defects the type of which each correspond to a different type singularity in the biaxial order parameter space. This theory fits remarkably well with the structures found in oily streak cholesterics, as shown in Figure 1.7, where we see that λ lines, which are non-singular in $\mathbf{n}$, are associated with defects in the pitch axis, χ lines which are simply standard disclinations and τ lines which are singularities

[1] Some feel that this direction should be called $\not\mathbf{n}$ for 'not $\mathbf{n}$'.

[2] In fact a helix, which has a handedness and an apolar direction, is a nice example of an elementary object whose moduli space is a tensor, specifically a rank (in the sense of a matrix) 1 symmetric section of $T\mathbb{R}^{3\otimes 2}$.

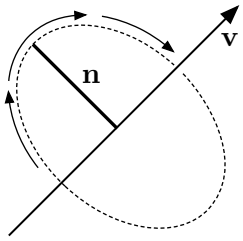

Figure 4.3: The twist of $\mathbf{n}$ along $\mathbf{v}$ can be thought of as the rate of change of $\mathbf{n}$ about $\mathbf{v}$ in the direction along $\mathbf{v}$.

in both the pitch axis and the director.

Despite the observational successes of this theory – which indicate that it should be along the right lines – it has a conceptual difficulty. The difficulty is precisely the one raised implicitly by Mermin [26] and Chen [20], in that the direction $\mathbf{p}$ cannot be incorporated into a regular order parameter as it is a quantity derived from $\mathbf{n}$ and as such cannot be varied independently from $\mathbf{n}$. One can only vary the director and examine the consequences on the pitch axis. Indeed, all one needs to define a cholesteric is a director field, which contains all the information about the phase. One should, therefore, be able to construct a coherent theory of these structures entirely in terms of singularities in the director.

4.2.1 Remedies for the Pitch Axis

To fix the difficulty with this theory, one should try to define the pitch axis as a properly derived quantity in terms of $\mathbf{n}$. The first point to note is that it is apolar, and as such should be an eigenvector of a particular tensor. Our heuristic notion was that the pitch axis should be 'the axis along which the cholesteric is twisting'. Following this intuition, one can define the twisting of $\mathbf{n}$ in a direction $\mathbf{v}$ to be the rate of change of $\mathbf{n}$ about $\mathbf{v}$, shown in Figure 4.3. In a similar vein to Efrati and Irvine's [80] work in chirality in materials, one can consider the twisting $T(\mathbf{v})$ as

$$T(\mathbf{v}) = (\mathbf{v}\cdot\nabla)\mathbf{n}\cdot(\mathbf{n}\times\mathbf{v}) \tag{4.2}$$

the pitch axis should then be considered as the unit vector $\mathbf{p}$ which maximises $T(\mathbf{p})$. This problem has a simple solution, in index notation one should maximise

$$T(\mathbf{p}) = p_i \partial_i n_j \epsilon_{jkl} n_k p_l - \lambda p_i p_i. \tag{4.3}$$

or

$$T(\mathbf{p}) = p_i M_{il} p_l - \lambda p_i p_i. \tag{4.4}$$

which has the solution

$$\frac{1}{2}(M + M^T) \cdot \mathbf{p} = \lambda \mathbf{p} \tag{4.5}$$

There is one additional assumption to make, that is that $\mathbf{p} \cdot \mathbf{n} = 0$. If one does not account for this then $T(\mathbf{p})$ is affected by the value of $(\mathbf{n} \cdot \nabla)\mathbf{n}$ which is a bend deformation (in particular one can show that (4.5) implies that $\mathbf{p} \cdot \mathbf{n} \propto (\mathbf{n} \cdot \nabla)\mathbf{n}$). Demanding this orthogonality condition one finds that $\mathbf{p}$ should be an eigenvector of the tensor

$$-\frac{1}{2}\big(\mathbf{n} \cdot \nabla \times \mathbf{n}\big) I_\xi + \Pi \tag{4.6}$$

where the tensors I_ξ and Π are defined in Chapter 3, and the tensor acts on ξ, the orthogonal 2-plane bundle. The pitch axis $\mathbf{p}$ should then be the eigenvector with largest (in magnitude) eigenvalue.

4.3 Umbilic Lines and Cholesteric Defects

With our definition of the pitch axis, we are in a position to describe the types of lines seen in cholesterics. The first, χ lines, are regular disclinations and discontinuities in $\mathbf{n}$. λ lines then become singularities in the pitch. These are degeneracies in the tensor $-(\mathbf{n} \cdot \nabla \times \mathbf{n}/2) I_\xi + \Pi$, and so are simply generic umbilics, and we can import our entire theory from the previous chapter. The last class of lines, τ lines, correspond to disclination lines around which

$\mathbf{p}$ is non-orientable. Note the slightly different definition in comparison with the τ lines found in the biaxial theory. Since the pitch axis is defined in terms of $\mathbf{n}$, one cannot evaluate the pitch axis along a disclination.

In terms of Π (or indeed Δ) we therefore obtain a consistent theory of defects in cholesterics, in which the various types of defects can all be explicitly derived from the gradients of the director $\mathbf{n}$[3]. As we will show, an advantage of this description is that we immediately obtain a global constraint of the λ and τ defects in the system from the Euler class of the orthogonal 2-plane bundle. Moreover, because we defined the defects in terms of the gradients in $\mathbf{n}$ we can always forget about this additional structure and examine the topology as a nematic.

The relationship between the Euler class and umbilics in simple cases such as in connection to point defects and baby Skyrmions has already been discussed in Chapter 3. Of more interest is the case where one has knotted and linked defect lines. Recalling Chapter 2, if one has a set of disclination lines L in $\mathbb{R}^3$ with $\mathbf{n}$ null-homotopic at infinity, then, ignoring the equivalence relation, the topological class of $\mathbf{n}$ is given by an element of $H^2(\Sigma(L))$, where $\Sigma(L)$ is the branched double cover of S^3 over L. We then suppose that the cholesteric defects in the system are described by the tensor Π, which is a section of the vector bundle E. The global constraint on the zeros of Π is then the Poincaré dual of the Euler class of E, which is $e(E) = 4[\mathbf{n}] \in H^2(\Sigma(L))$. If $H^2(\Sigma(L))$ consists wholly of integer summands then the situation is more or less as illustrated in Chapter 3. Of interest are the cases where $H^2(\Sigma(L))$ contains elements of order 2 and 4, since these correspond to no required zeros in Π (or a trivial Euler class).

Suppose one had a director field $\mathbf{n}$ containing a linked disclination set L such that $e(E) = 0$, *i.e.* the element in $H^2(\Sigma(L))$ describing $\mathbf{n}$ is of order 2 or 4. Furthermore, suppose that Π contains no zeros, that is there are no umbilic lines in the system. Our task is to analyse the cholesteric defects in

[3]Note that this also allows for 'orientable cholesterics' where $\mathbf{n}$ is a vector rather than a director, such as chiral ferromagnets.

this situation.

Now the vector bundle E is a subbundle of $\xi^* \otimes \xi$ consisting of symmetric tensors and therefore non-zero sections of E have corresponding eigenvectors, $\mathbf{p}_1$ and $\mathbf{p}_2$, previously identified as potential pitch axes. Since, by assumption, $\mathbf{n}$ does not contain any umbilic lines, these eigenvectors are globally defined and are sections of the projectivisation of ξ, $P(\xi)$. There are two possibilities: either the eigenvector fields are orientable, or they are not. If the eigenvector fields are orientable then one can find a non-zero vector field $\mathbf{v}$ parallel to $\mathbf{p}_1$. Since $\mathbf{v} \cdot \mathbf{n} = 0$, $\mathbf{v}$ is a section of ξ. Since $\mathbf{v}$ is non-zero, ξ must have vanishing Euler class. The Euler class of ξ is $2[\mathbf{n}]$, and so this corresponds to an element of order 2. Physically, this situation corresponds to no cholesteric defects – since Π is non-zero there are no λ lines and since its eigenvectors are orientable there are no τ lines. As an example take the Hopf link, for which $H^2(\Sigma(L)) \cong \mathbb{Z}_2$. Both these elements are of order two, so there is no obstruction to either of these textures being realised in a cholesteric without either τ or λ lines. Of course, in an actual realisation these may exist for energetic, kinetic or more subtle topological reasons which will be discussed below.

Now we consider the case where the eigenvectors are not orientable. By similar reasoning to that given above, we therefore conclude that $[\mathbf{n}]$ is an element of order 4. What of the cholesteric defects in this case? By assumption there are no umbilic lines in the system, and yet the eigenvectors of Π must be non-orientable. This implies that there are closed loops in $\mathbb{R}^3 - L$ around which these eigenvectors are non-orientable. The only closed loops in $\mathbb{R}^3 - L$ are those that encircle defect lines, hence there must be disclination lines around which Π is non-orientable – these are τ lines.

The natural question to ask at this point is: given a defect set L with an associated homotopy class which is an element of order 4, can one determine where the τ defect lines can be? If one has a system containing only disclination lines, some of which are τ lines, then the τ lines can be represented

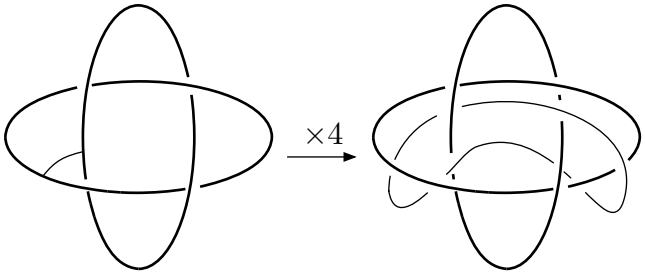

Figure 4.4: Solomon's Seal and τ lines in a cholesteric. For Solomon's Seal $H_1(\Sigma(L)) = \mathbb{Z}_4$, this implies that for textures corresponding to elements 1 and 3, there is no topological obstruction to the removal of umbilic lines, but that such a removal would result in the pitch axis being non-orientable, indicating the existence of τ lines. A generator of $H_1(\Sigma(L))$ is indicated on the left, as a tether connecting the two components. Multiplying this by 4, one finds a cycle that is cobordant to a longitude of either of the link components. Either of these, therefore can be realised as τ lines. Finally, note that if one would bring together the two defect lines, the result would be a λ line.

by a set of longitudes. The homotopy class of $\mathbf{n}$ can then be determined by deducing which element in $H_1(\Sigma(L))$ gives, up to cobordism, a longitude when multiplied by 4.

An example is shown in Figure 4.4. The $(4,2)$ torus link, known as Solomon's Seal, has an associated group $\mathbb{Z}_4$, which contains two elements of order 4 and one element of order 2, therefore there is no obstruction to every possible homotopy class of texture in its complement having no umbilic or λ lines. Textures corresponding to the two elements of order 4, however, must contain τ lines. To understand this, note that a generator of this group can be represented as a tether connecting the link components. Denote this tether by t, then $4t$ is equivalent to either of the longitudes. Hence, the elements of order 4 can be realised as one χ line (disclination) and one τ line. Note that if one would bring together the two defect lines, the result would be a λ line.

An amusing counterexample to this case is the Hopf link. One can ask whether it is possible to have a τ line linking with a regular disclination. This would imply that there was an element of order 4 in the group $H_1(\Sigma(L))$ for the Hopf link. But we know that in this case the group is $\mathbb{Z}_2$, which has maximum order 2, and so one cannot find a τ line linking a regular disclination.

This statement has its analogue in the theory of biaxial nematics (and thus the theory illustrated in §4.2), defects of type i and j may not link without a tether. The technical statement of this constraint is that there must exist a homomorphism from the fundamental group of the link complement onto the group Q [31]. Given this, it is natural to ask if other phenomena in the biaxial theory have their analogues in our construction. One natural question to ask is if a λ line may cross a disclination. In the biaxial case we know the following: recalling the definitions in Chapter 1, the fundamental group of the biaxial order parameter space is the set of quaternions generated by $\{i, j\}$ and has four classes of defects given by -1, $\pm i$, $\pm j$ and $\pm k$. The crossing of two defect lines of type x and y leaves a tether of type given by the commutator $xyx^{-1}y^{-1}$ (if the group is abelian then crossing of defect lines is possible). If one uses the theory of biaxials as a model for cholesterics, then it predicts that the crossing of λ defects and disclinations will lead to a tether. If one identifies a disclination (χ defect) as i and a λ line as j, then the tether created by their crossing is of type $i \cdot j \cdot -i \cdot -j = -1$.

Let us consider the corresponding situation where now the λ line is a generic umbilic. As discussed, the Euler class supplies a global constraint for the umbilics, and hence λ lines, in the system. The constraint is in the form of an element of the first homology of the double cover of the complement of the defect set. As such, one expects that λ lines should not be able to simply cross disclination lines in nematics, since this would change their homology class. In fact, considering λ lines as umbilic lines leads to precisely the same conclusion as the biaxial based theory. This is illustrated in Figure 4.5, which shows that an attempt to make a generic umbilic line cross a disclination creates a 'tether' comprising a non-generic umbilic. The standard non-generic umbilic corresponds exactly to the standard -1 disclination.

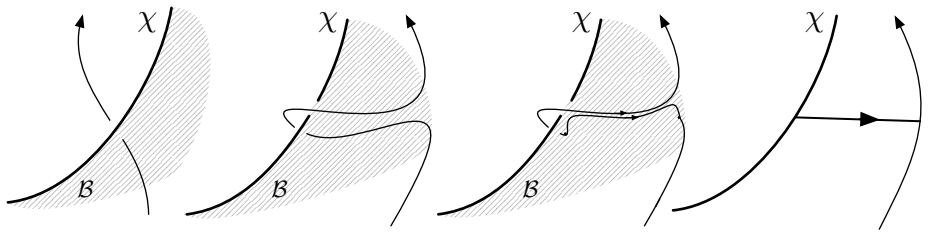

Figure 4.5: Umbilic Crossing a Disclination. From left to right. A disclination χ and an umbilic, $\mathcal{B}$ is a branch set for the disclination lines in the system. The umbilic line is moved in such a way as to preempt crossing the disclination line, because it does not cross $\mathcal{B}$ it can be given a consistent orientation. The umbilic line is homotoped so that it crosses $\mathcal{B}$, its orientation must be reversed at these crossing points. A further homotopy is performed, creating a $s = 2$ strength umbilic as a 'tether' connecting the two defect lines.

4.4 Two-dimensional Smectics

At this point, it is instructive to consider the topology of two-dimensional smectic liquid crystals [20, 130], with which our work shares many similarities. Smectics are liquid crystals with an additional layered structure, typically forming at lower temperatures than nematics, that is the system has 1 dimensional positional order, where d is the dimension of the space. This layered structure is such that the director in a smectic (type A) points in a normal direction to the layers. A naive approach to understanding this system is then to have two objects describing the order, a phase ϕ describing the layer structure, along with the regular director $\mathbf{n}$, and then studying the topology of each separately. As observed by Mermin [26], this fails because the director and the phase are related, $\mathbf{n} = \nabla\phi/|\nabla\phi|$, a condition that must be satisfied at all times. Indeed, as shown by Poénaru [131], this implies that a two dimensional smectic can have no defects of winding higher than $+1$.

The resolution of this problem can be phrased in many equivalent ways. $\mathbf{n}$ is completely determined by ϕ, which can be visualised as a surface [130], shown in Figure 4.6, and as such serves as the description of the order. Singularities in $\mathbf{n}$, or disclinations in the smectic, are then entirely determined by this surface, and can be thought of as an additional structure sitting on

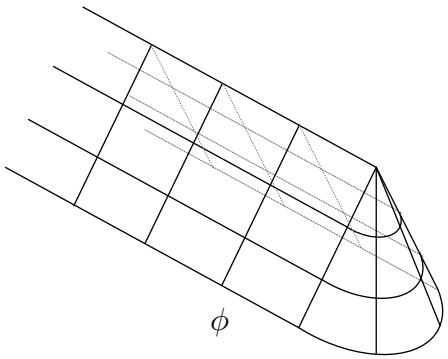

Figure 4.6: A surface corresponding to a phase field ϕ in a 2d smectic, the associated director $\mathbf{n} = \nabla\phi/|\nabla\phi|$ contains a $+1/2$ defect at the end of the ridge.

top of the basic description, which is simply the phase field ϕ. As discussed above we find an analogous situation in cholesterics, where the observed λ lines are described as umbilics. In the same way that disclinations in the 2d smectic are derived from ϕ, λ lines are derived from $\mathbf{n}$, which serves as the basic description of the order.

4.5 The Weakly Twisted Case

This perspective, in which the additional cholesteric defects sit on top of the basic nematic description, has an advantage when considering systems such as weakly twisted cholesterics. The identification of and emphasis on λ, τ and χ lines in experimental cholesteric systems comes from their easy optical identification in strongly twisted cells. Focussing on λ lines, which we have identified as umbilics, one might wonder whether all umbilic lines in a cholesteric always correspond to λ lines as they are identified experimentally. The answer to this question is no. Essentially this is because umbilics are perfectly well defined in nematics, and one can continuously transform a nematic into a cholesteric. Indeed, in weakly twisted systems ($Lq_0 \ll 1$, where L is the system size) one can observe bare charge 1 point defects in $\mathbf{n}$ [12]. While such a point defect necessarily has umbilic lines of total strength 4 emerging from it, they are not experimentally visible. A similar

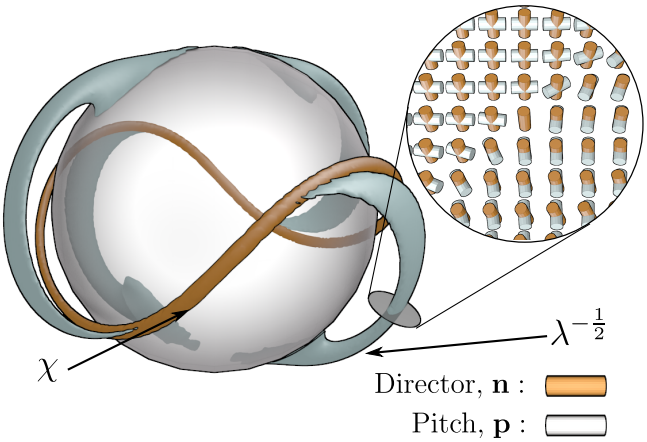

Figure 4.7: Simulation of umbilic lines in a Saturn's ring configuration, using the standard Landau-de Gennes free energy. Placing a colloid with homeotropic anchoring conditions into a cholesteric liquid crystal can induce the type of twisted disclination line seen here. From topological considerations, one expects (and observes) the existence of four generic umbilic lines, given in blue, connecting the disclination line to the colloid. These lines do not have a strong optical signature experimentally, as opposed to those that correspond to λ lines.

situation occurs for Saturn's ring structures. In cholesterics, with $Lq_0 \sim 1$ the familiar defect loop twists up around the colloid [132–134]. Optical images do not reveal any noticeable umbilic lines, though simulations, shown in Figure 4.7 show that they exist.

4.6 The Free Energy and Geometry of a Cholesteric

So far we have only discussed the identification of defects in the cholesteric. A more subtle question is that of topological equivalence of different configurations. Again making the analogy to the case of two dimensional smectics, we know that deformations of a texture can be visualised by deformations of the surface corresponding to ϕ. Our task is finding the equivalent structure in the case of cholesterics.

To do this, we must first examine the elastic energy of the cholesteric. One of the essential characteristics of the cholesteric is that in its ground-state the director field has non-zero gradients. A short inspection of possible elastic free energies reveals that, not only is the cholesteric the lowest order

extension of the nematic having a groundstate with non-zero gradients, but that the geometric characterisation of the cholesteric is $\mathbf{n} \cdot \nabla \times \mathbf{n} = -q_0$.

Since a cholesteric can be obtained from a nematic by varying temperature without a phase transition, the description of a cholesteric must reduce to that of nematic, and its description must be given completely in terms of a director field. Recalling our discussion in Chapter 1, we know that the free energy for a unit vector field, including only first order derivatives, can be written (excluding saddle-splay) as

$$F = \int \frac{K_1}{2}\big(\nabla \cdot \mathbf{n} + s_0\big)^2 + \frac{K_2}{2}\big(\mathbf{n} \cdot \nabla \times \mathbf{n} + q_0\big)^2 + \frac{K_3}{2}\big((\mathbf{n} \cdot \nabla)\mathbf{n}\big)^2 dV. \quad (4.7)$$

From this we can clearly see that the only two linear terms allowed correspond to s_0 and q_0 being non-zero, since these are identified with sections of line bundles. However, for a director field, we cannot have $s_0 \neq 0$, since we cannot distinguish $\mathbf{n}$ from $-\mathbf{n}$. Hence we find that for a director field, the lowest order adjustment to the gradients to ensure the groundstate is non-zero is to make $q_0 \neq 0$, at which point we find that $\mathbf{n} \cdot \nabla \times \mathbf{n} = -q_0$ characterises the propensity of the cholesteric to twist. This requirement has a natural geometric meaning, $\mathbf{n}$ is never the normal to a system of layers. To see this note the following. Suppose $\mathbf{n}$ is the normal to a system of layers. If Σ is an arbitrary patch of one of the layers, with boundary $\partial\Sigma$, then we know that

$$\int_{\partial\Sigma} \mathbf{n} \cdot d\mathbf{l} = 0, \quad (4.8)$$

but by Stokes' theorem we have

$$\int_{\partial\Sigma} \mathbf{n} \cdot d\mathbf{l} = \int_{\Sigma} \big(\mathbf{n} \cdot \nabla \times \mathbf{n}\big) dA. \quad (4.9)$$

Since Σ was arbitrary this gives $\mathbf{n} \cdot \nabla \times \mathbf{n} = 0$ as the requirement for $\mathbf{n}$ to be the normal to a foliation.

4.7 Cholesterics and Contact Structures

With the energetic and geometrical condition of $\mathbf{n} \cdot \nabla \times \mathbf{n} = -q_0 \neq 0$ of the cholesteric we can begin to understand the topology of deformations. Suppose that a cholesteric undergoes a deformation induced by, say, a change of boundary conditions, or an external field. Then, given the form of the static elastic energy, there is a strong energetic preference for $\mathbf{n} \cdot \nabla \times \mathbf{n} \approx -q_0$ throughout the material during this process. A simple scale-free constraint on the system is therefore to demand that $\mathbf{n} \cdot \nabla \times \mathbf{n} \neq 0$. Note that this constraint is natural both geometrically and energetically. In mathematics there is a similar class of objects known as contact structures [103], and we will consider the consequences of making this analogy. Contact structures are non-integrable rank 2 subbundles of the tangent bundles of a given manifold. Note that if one has a metric, as is in our case, then there is a simple equivalence between rank-2 subbundles and director fields. Contact structures are defined locally as (the kernel of) a one-form α such that $\alpha \wedge d\alpha > 0$. The local restriction here is the same as the fact that a director field can locally be thought of as a unit vector field.

Making the connection explicit, we will think of cholesterics as a unit vector field $\mathbf{n}$ such that the orthogonal 2-plane bundle ξ is non-integrable. The notion of equivalence between two cholesteric field configurations is then an isotopy, that is $\mathbf{n}$ and $\mathbf{n}'$ are isotopic if there is a one parameter family of director fields $\mathbf{n}_t$, $t \in [0,1]$, with $\mathbf{n}_0 = \mathbf{n}$ and $\mathbf{n}_1 = \mathbf{n}'$, such that for each t, the corresponding 2-plane bundle, ξ_t, is non-integrable [4], or that $\mathbf{n}_t \cdot \nabla \times \mathbf{n}_t \neq 0$.

This formulation has immediate consequences for the topological classification of cholesterics. Two director fields that are topologically equivalent as nematic textures can fail to be equivalent as cholesterics, that is to pass

[4] As a note we should mention that for contact structures on open manifolds, such as $\mathbb{R}^3$, it is common in the mathematical literature to consider proper isotopies, those that are induced by diffeomorphisms of the underlying manifold.

from one texture to another requires going through a state where at some point in the material $\mathbf{n} \cdot \nabla \times \mathbf{n} = 0$, which is energetically costly. The most elementary of these properties is that a helical state with $\mathbf{n} \cdot \nabla \times \mathbf{n} > 0$ is not equivalent to its mirror image with $\mathbf{n} \cdot \nabla \times \mathbf{n} < 0$ (though they are equivalent as nematics). Therefore, as one might hope, the handedness of the system is preserved in this theory and cholesterics of opposite chirality are considered distinct. This trivial distinction is always present, and for every isotopy class of contact structure we consider with $\mathbf{n} \cdot \nabla \times \mathbf{n} > 0$, there is a corresponding one with $\mathbf{n} \cdot \nabla \times \mathbf{n} < 0$. Henceforth we will consider only so-called 'positive' contact structures with $\mathbf{n} \cdot \nabla \times \mathbf{n} > 0$, but all our statements have their equivalents regarding negative contact structures.

While the distinction of handedness is trivial, what is surprising is that the theory of contact structures allows more subtle topological distinctions between cholesteric configurations. To understand this one needs to know the classification of isotopy classes of contact structures for a given manifold. This problem is in general unsolved though in many cases much is known. The principal distinction in this direction is the tight/overtwisted dichotomy. A contact structure is called overtwisted if one can find an embedded disk Σ such that the tangent vectors on each point of $\partial\Sigma$ are orthogonal to $\mathbf{n}$ and the normal to Σ coincides with $\mathbf{n}$ on $\partial\Sigma$. The condition of tight or overtwisted is preserved by isotopy and so can distinguish contact structures.

Mathematically this notion induces distinctions that are strictly finer than the homotopy classification of director field. One can convert any tight contact structure into an overtwisted one without changing its homotopy class as a 2-plane field [103, 135], through a process known as a Lutz twist. In fact, overtwisted contact structures have considerable topological freedom and in a seminal paper Eliashberg showed that the isotopy classes of overtwisted contact structures coincide with the homotopy classes of 2-plane fields [136]. In the language of liquid crystalline order this implies that the

topological classification of overtwisted cholesterics is the same as nematics. Tight contact structures are more elusive, and their classification is not yet fully understood mathematically, though many known results do correspond to experimentally relevant situations.

This perspective suggests an explanation for why chiral systems exhibit many soliton structures that are not found in regular nematics. If one has an overtwisted cholesteric, then it cannot relax to a helical state – which is shown below to be tight – without either passing through a region where it is not twisted or creating defects. Such an operation will be energetically costly, indeed a region of zero twist has a local free energy density cost which is bounded below by $K_2 q_0^2/2$. As such, solitons in cholesterics that correspond to overtwisted contact structures may well enjoy increased stability.

Amusingly, the standard examples of tight and overtwisted contact structures are very familiar to those who study cholesteric liquid crystals. The first is just the standard helical cholesteric phase, given in (4.1) The second is the 'double twist cylinder' texture, given by

$$\mathbf{n}_{ot} = \cos q_0 \rho \mathbf{e}_z - \sin q_0 \rho \mathbf{e}_\phi \tag{4.10}$$

where $\{\rho, \phi, z\}$ are cylindrical coordinates. Both (4.1) and (4.10) define contact structures, with $\mathbf{n} \cdot \nabla \times \mathbf{n} < 0$ (if $q_0 > 0$). The double twist cylinder is overtwisted, the disk defined by $z = 0$ and $\rho \leq \pi/q_0$ has a boundary curve whose tangent vector is orthogonal to $\mathbf{n}$. The standard helical cholesteric is tight, since there is an isotopy of contact structures given by

$$\mathbf{n}_t = \cos \phi_t \mathbf{e}_x + \sin \phi_t \mathbf{e}_y \tag{4.11}$$

with

$$\phi_t = t q_0 z - (1-t)\arctan z, \tag{4.12}$$

from the standard tight contact structure on $\mathbb{R}^3$ to the helical cholesteric. As

such, the standard cholesteric helical phase and the double twist cylinder are not isotopic as cholesterics, though they are as director fields.

While this example is a nice illustration of the distinctions induced by these considerations, it is only a toy set-up, the double twist cylinder is typically only used as a local model in the vicinity of the axis. Nevertheless it indicates that one might try to associate double twist cylinders, and hence umbilic lines, to measures of overtwistedness. This will be done in §4.8, where we will show that self-linking of umbilic lines in a cholesteric can relate to overtwistedness. Before this, however, we will go through an example of a physical situation where the notion of contact structures can help us understand chiral systems.

4.7.1 Solitons in a Cholesteric Background

As mentioned in the introduction, cholesteric liquid crystals support a large number of metastable soliton structures. A beautiful series of examples are given by Bouligand, who created a large number of different soliton structures in cholesterics against a helical background [45]. To construct a model for this situation we proceed as follows. We will assume that our soliton contains no disclinations lines, in fact we assume that $\mathbf{n}$ has no singularities, and that it is contained in a ball B such that $\mathbf{n}$ coincides with a standard helical phase on the complement of the interior of B.

We will first analyse this situation as a nematic. In this case we have to consider homotopy classes of maps $B \to \mathbb{RP}^2$ relative to the boundary. Restricted to ∂B we have a map $S^2 \to \mathbb{RP}^2$. This map must be null homotopic, since it extends to a non-singular map in the interior. The homotopy classes are therefore equivalent to maps $S^3 \to \mathbb{RP}^2$, which are classified by an integer, $h \in \mathbb{Z}$, the Hopf invariant.

Now we consider the case of contact structures. Our problem is isotopy classes of contact structures in a ball, relative to the boundary, where the contact structure on the boundary comes from the tight helical contact struc-

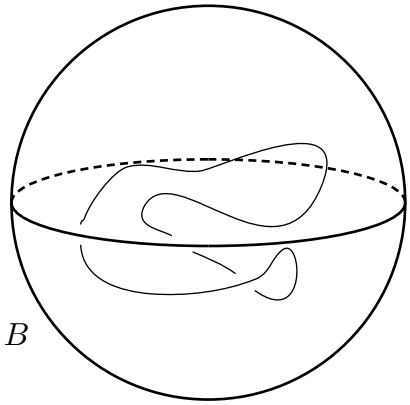

Figure 4.8: The setup for §4.7.1, outside of a ball B, the texture is the standard helical texture. Inside B is a non-singular soliton structure, S. The isotopy class of S relative to the boundary of B is given by the following information. If it is tight, then it is unique. If it is overtwisted then it is given by an integer, corresponding to the Hopf invariant.

ture. This problem has been solved, see [137], for example. The solution states that up to isotopy there is a unique tight positive contact structure which has $h = 0$, and a single overtwisted positive contact structure in every homotopy class of $\mathbf{n}$ as a director field. As such, we gain an extra topological distinction between configurations, the tight and overtwisted contact structures with $h = 0$, that does not exist in the nematic case. It is also interesting to note that all Hopf solitons are overtwisted.

The overtwisted $h = 0$ soliton would, therefore, be a cholesteric that was homotopic to the helical phase, but not isotopic as a contact structure. A transition to the helical phase would necessarily require passing through an energetically costly state where, in some portion of the material, $\mathbf{n}\cdot\nabla\times\mathbf{n} = 0$, and so may be suppressed.

4.8 Overtwistedness and Umbilic Lines

So far, our discussion of cholesterics has been split into two halves, the half concerned with contact topology and the half concerned with umbilic lines. The discussion of overtwisted contact structures suggests that one might find a connection between umbilics and overtwisted contact structures. Such

a connection does indeed exist, though we feel that what we present here represents only elementary aspects of a deeper theory.

Suppose one has a cholesteric with a transverse umbilic line. Recalling the definition in Chapter 3, these are umbilic lines whose tangent vector is always transverse to the 2-planes defined by $\mathbf{n}$. Amusingly such lines are intimately connected with the non-integrability of $\mathbf{n}$. More formally, in a simply connected domain transverse umbilics can only exist if $\mathbf{n} \cdot \nabla \times \mathbf{n} \neq 0$. If we are in such a domain and $\mathbf{n}$ defines a non-singular foliation then there is a function ϕ such that $\nabla\phi$ is parallel to $\mathbf{n}$. Then integrating along an umbilic loop we have

$$\int_U d\phi = 0 \tag{4.13}$$

and so $\nabla\phi$ must be orthogonal to the tangent vector at at least two points and the umbilic is not transverse. Hence transverse umbilics can only exist if $\mathbf{n} \cdot \nabla \times \mathbf{n} \neq 0$ somewhere in the material. Given such a transverse umbilic U, we defined a self-linking number which decomposes as

$$\mathrm{Sl}(U) = \overline{\mathrm{Sl}}(U) + \frac{1}{2}e(U). \tag{4.14}$$

In terms of the pitch axis, this can be thought of as the twisting of the pitch axis along a λ line. For us, the important component is $\overline{\mathrm{Sl}}(U)$. If $\mathbf{n}$ defines a (positive) contact structure, then a transverse U is a transverse knot in this structure. The definition of such a knot is simply a curve whose tangent vector is transverse to the contact structure. A theorem of Etnyre's states that, for such a knot U with Seifert surface Σ, if

$$\overline{\mathrm{Sl}}(U) > -\chi(\Sigma), \tag{4.15}$$

where $\chi(\Sigma)$ is the Euler characteristic, then the contact structure is overtwisted [138]. In particular, if U is an unknot, then its Seifert surface is a disk, which has $\chi = 1$ and so the existence of a transverse unknotted umbilic (λ

line), such as those observed in both torons and Hopf solitons discussed in Chapter 3, in a cholesteric implies that the cholesteric is overtwisted and as such cannot relax to a helical configuration without untwisting.

4.9 Floer Theories and Beyond

So far, throughout this entire thesis we have been primarily concerned with static configurations and have given only a cursory amount of attention towards dynamic configurations. Doing so reveals that the structure we have given so far is incomplete. Suppose one has a director field $\mathbf{n}_1$ in $\mathbb{R}^3$ with an initial set of defects $\mathcal{D}_1$ and then, after some time, the configuration changes to $\mathbf{n}_2$ with a new set of defects $\mathcal{D}_2$. To model this situation one can introduce a cobordism with the 4-manifold $M = \mathbb{R}^3 \times [0,1] - \mathcal{E}$, where one considers the fourth dimension as time and the set $\mathcal{E}$ is such that $\mathcal{E} \cap \mathbb{R}^3 \times \{0\} = \mathcal{D}_1$ and $\mathcal{E} \cap \mathbb{R}^3 \times \{1\} = \mathcal{D}_2$. M therefore represents the changing domain. Finally, one equips M with a director field $\mathbf{n}$, considered as a map $\mathbf{n} : M \to \mathbb{RP}^2$. Now, let $G(\mathcal{D}_1)$ denote the space of homotopy classes of textures with a given defect set. From Chapter 2 we know that this is equal to an abelian group $V(\mathcal{D}_1)$ modulo the equivalence relation $x \sim -x$. If we fix a lift to S^2 then we can, without ambiguity, consider both the beginning and final configurations as corresponding to elements in the groups $V(\mathcal{D}_1)$ and $V(\mathcal{D}_2)$. We would like to understand how one can go from an initial state to a final state. Ideally, there would be a map induced by the cobordism, that is $h_M : V(\mathcal{D}_1) \to V(\mathcal{D}_2)$. It is clear, through inspecting several examples, however, that in terms of the structures we have been considering, such a map cannot exist. However, there is a large class of theories associated to 3 manifolds, known under the umbrella term of Floer homology theories, which have precisely this property, they are functorial with respect to cobordisms [139]. Of particular interest are the class of such theories known as contact homology theories, such as embedded contact homology [140, 141] and symplectic field theory [142]. These theories are typically generated by closed orbits of the Reeb

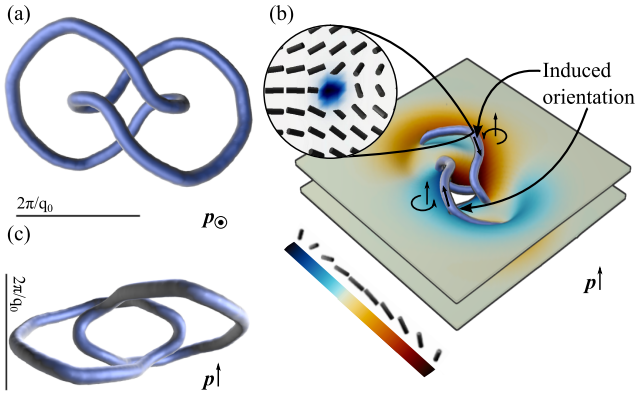

Figure 4.9: Stable Hopf link disclination embedded into a helical background. Note that the shape of the defect line is similar to that of a transverse knot in a contact structure [103]. It is hoped that such structures may be understood with a Floer theory.

vector field. In physical terms these are vortex loops, closed orbits of $\nabla \times \mathbf{n}$. It seems that a natural extension, therefore, of the perspective that we have developed is to construct a Floer theory of cholesterics, which is generated by either umbilic lines or vortex lines, and which is consequently functorial with respect to cobordisms, and thus changes in the defect topology. A further potential advantage of such a theory would be specific to cholesterics. Theories of contact homology are often sensitive to properties involving the tight/overtwisted dichotomy and, as such, one may be able to understand distinct tight cholesteric structures associated to defect lines and as a consequence the topology of various cholesteric solitons associated to knotted defects, such as those shown in Figure 4.9.

Chapter 5

Defects Induced by Non-Orientable Colloids

In modern experiments the most common way to manipulate and create defect-laden structures of liquid crystals on a fine scale is the use of colloidal particles. These micro- or nano-metre particles are dispersed into a liquid crystalline system with a particular material or coating inducing a particular alignment of the liquid crystal on the surface. These boundary conditions and the far field boundary conditions that are also controlled are often topologically incompatible leading to the creation of defects. A thorough review of these systems is available in [143].

Perhaps the most famous example of this is the Saturn's ring defect produced around a spherical colloid with homeotropic (normal) anchoring, illustrated in Figure 5.1. As we will discuss, in a system with a uniform far-field, the topology of a spherical colloid with homeotropic anchoring demands the creation of a defect. While this defect can be realised as a point defect in a dipolar configuration with the colloid [144], it may also be elongated to form a loop encircling the colloid [145]. This system and its extensions has produced many beautiful results, many of which inspired much of the work presented in this thesis.

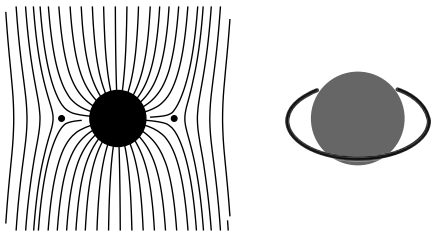

Figure 5.1: Saturn's ring defect line around a spherical colloid with homeotropic anchoring. The defect line has a $-1/2$ profile.

5.1 Colloids and the Topology of Surfaces

As mentioned, for a spherical colloid, the defect created can be either a point defect or a line defect. This suggests that the distinction between the line and the point defect is not a topological one but rather energetic[1] and so a discussion of the topological aspects of colloids is useful. From the point of view of the liquid crystal, colloids are determined entirely by their surface, as it is only the surface that comes into contact with the liquid crystal. As such, the topology of the defects created should be a direct consequence of the topology – as a surface – of the colloidal particle. Fortunately for us the topology of surfaces is a classical subject and so the analysis can be done with a minimum of effort.

A colloidal particle is always contained within a small region of space and we all assume that it is not particularly pathological, for example it has no fractal structure. Mathematically we will say that it is a compact surface. The classification theorem of surfaces [146] states that any compact surface can be classified up to homeomorphism by its genus, orientability and number of boundary components. The genus is equal to the number of holes or handlebodies possessed by a surface; for example, a torus has genus one and a sphere genus zero. Orientability implies a consistent choice of normal vector can be made on a surface. The one-sided Möbius strip is the classic non-orientable surface; any normal vector on the strip will be flipped by going

[1] We are not suggesting that a loop and a point are topologically equivalent!

around the strip once, forbidding a consistent choice of surface normal. Finally, the number of boundary components is simply the number of distinct connected components in the surface boundary, *e.g.* a disk has one boundary component and a torus has none.

While this is a complete topological classification of surfaces in an abstract setting, for applications they must also be embedded (no self-intersections) into ordinary three-dimensional space, $\mathbb{R}^3$. Different embeddings are interesting in their own right – the whole of knot theory concerns embeddings of a circle into $\mathbb{R}^3$ – but they do not affect the local class of the defect necessitated in the bulk, which we focus on first. Thus, with the classification of surfaces in mind it is natural to ask what topological implications each type of surface has for accompanying defects in the surrounding liquid crystal. The complete classification, summarised in Fig. 5.2, naturally separates into four classes of surfaces; orientable or non-orientable and closed or with boundary.

Closed, orientable surfaces are known to induce defects corresponding to the element $1-g = \chi/2$ of $\pi_2(\mathbb{RP}^2)$, where g is the genus of the surface and χ is the Euler characteristic [147, 148]. Briefly, this relation comes through computing the degree of the Gauss map of the surface. The Gauss map, $\mathcal{G}$, of a surface, X, is a map $\mathcal{G} : X \to S^2$ that sends every point of the surface to the direction of the surface normal at that point. For orientable surfaces with normal anchoring, the director can be given the orientation of the Gauss map, so that $\mathcal{G}$ describes precisely the molecular orientation at the surface. The degree of this map – the number of times every point on S^2 is visited, counted with sign – is a homotopy invariant [148] characterising the type of defect that the surface generates [147]. Although experimentally the same surface can produce seemingly different defects, they are always characterised by this same element of $\pi_2(\mathbb{RP}^2)$. As in our example, where spherical colloids can nucleate either a point defect [144] or disclination loop [145] but the loop can always be shrunk continuously into a point [149], so that it

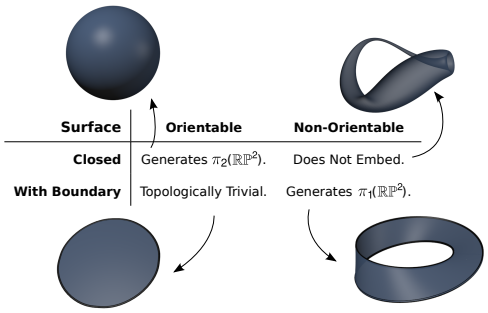

Figure 5.2: Topological characterisation of compact surfaces with homeotropic boundary conditions, embedded in a three-dimensional, nematic liquid crystal. Closed orientable surfaces generate elements of $\pi_2(\mathbb{RP}^2)$, equal to one minus the genus of the surface. Non-orientable surfaces with boundary generate the non-trivial element of $\pi_1(\mathbb{RP}^2)$, which forces the nucleation of disclination lines in the bulk.

is more properly classified by $\pi_2(\mathbb{RP}^2)$. More generally, orientable surfaces can never generate elements of $\pi_1(\mathbb{RP}^2)$, *i.e.* disclinations, as a topological requirement. Their orientability ensures that any disclination loops formed can always be removed in pairs or shrunk into points.

Closed, non-orientable surfaces cannot be embedded in $\mathbb{R}^3$ without self-intersection, meaning that a true representation of any of these (*e.g.* the real projective plane or the Klein bottle) in a liquid crystal is not possible. For this reason, we do not consider closed, non-orientable surfaces any further.

Orientable surfaces with boundaries have trivial topological implications for the surrounding liquid crystal. Their orientability, as in the closed case, forbids them from generating elements of $\pi_1(\mathbb{RP}^2)$ as a topological necessity. In addition, since they have a boundary, they cannot generate any elements of $\pi_2(\mathbb{RP}^2)$. We argue as follows. Closed, orientable surfaces separate space into an inside and an outside and they generate point defects in *both* regions. If one cuts a hole in the surface, creating a boundary component, then these defects can be combined to leave a defect-free texture. Cutting more holes in the surface will not change things as one could always make the texture on the new hole identical to the surface normal that was removed.

Non-orientable surfaces with boundary necessarily generate a non-trivial element of $\pi_1(\mathbb{RP}^2)$. A generalisation of the Gauss map to non-orientable

surfaces $\overline{\mathcal{G}} : X \to \mathbb{RP}^2$ assigns to every point of the surface the line element (point in $\mathbb{RP}^2$) corresponding to the direction of the (unoriented) surface normal[2]. Now consider the loop space of our surface, ΩX. Composition with the non-orientable Gauss map $\overline{\mathcal{G}}$ creates a set of representatives of $\pi_1(\mathbb{RP}^2)$. If X is non-orientable then there must be at least one map in this set which represents the non-trivial element (and generates a disclination). Suppose there was no such map, then every map in $\overline{\mathcal{G}}[\Omega X]$ could be lifted from $\mathbb{RP}^2$ to S^2 and we would have created an orientable Gauss map, $\mathcal{G}$, implying the surface is orientable, a contradiction. The disclinations created in this way *must* entangle the surface, since any disk spanning a non-orientable loop on the surface must be pierced by the defect.

5.2 Simulations of Non-Orientable Colloids

Non-orientability of the surface enforces the existence of a disclination loop but it leaves open the precise form of the defects and their equilibrium configuration. These are determined by energetics and by the nature of the embedding of the surface. While surfaces with boundary are unavoidably two-dimensional, experimentally realisable, but topologically equivalent, surfaces may be constructed by using thin material with homeotropic boundary conditions on the faces and planar anchoring on the thin edges, as shown schematically in Fig. 5.3. In this way a colloid with varying surface anchoring conditions can be made to faithfully represent a two-dimensional surface. Such boundary conditions are essential to mimic non-orientable surfaces and ensure the topological properties we describe – fully homeotropic boundary conditions simply replicate an orientable torus. Modern fabrication techniques allow for the manufacture of such exotic surfaces [150].

As the Möbius strip is the prototypical non-orientable surface – *all* non-

[2]It is more common, and more useful in general, to think of the non-orientable version of the Gauss map as a map to the Grassmannian $\mathrm{Gr}_2(\mathbb{R}^3)$ – see, *e.g.* J.W. Milnor, J.D. Stasheff *Characteristic Classes* (Princeton University Press, Princeton, 1974) – but since $\mathrm{Gr}_2(\mathbb{R}^3)$ is canonically homeomorphic to $\mathbb{RP}^2$ there is no loss in our discussion.

orientable surfaces contain the Möbius strip as a subset – it serves as an elementary guide to the behaviour of non-orientable surfaces in liquid crystals. A Möbius strip with homeotropic boundary conditions will generate a non-trivial element of $\pi_1(\mathbb{RP}^2)$ as one passes around the strip and hence must be threaded by a disclination loop of zero hedgehog charge, entangling the surface. The shape of disclination loops around colloidal particles is governed largely by the requirement to minimise the distortion energy of the surrounding director field. A simple heuristic for this can be constructed as follows. As one passes through a disclination line a rotation of approximately $\pi/2$ is induced in the director. This rotation mediates the transition from the surface normal orientation to that of the far-field and will best minimise the distortion in the director field when it is concentrated along those parts of the surface where the local anchoring and far-field directions are perpendicular. Since we consider colloids with homeotropic anchoring this simply gives the requirement that

$$\mathbf{S}_n \cdot \mathbf{n}_0 = 0, \tag{5.1}$$

along the disclination, where $\mathbf{S}_n$ is the surface normal and $\mathbf{n}_0$ is the far-field director. For a spherical particle in a uniform far-field, this predicts that the disclination will lie on a great circle in a plane perpendicular to this far-field direction, which is the observed position of Saturn ring defects [145]. Likewise the twisted shape of disclinations around spherical colloids in a cholesteric [132, 134] is correctly predicted by the same heuristic.

The preferred defect configuration for a Möbius strip can be found by numerical simulation using continuum Landau-de Gennes modelling (see Chapter 1). As shown in Fig. 5.3, the minimum energy configuration is a single disclination loop entangling the strip, in the location predicted by (5.1). Of course, the precise configuration depends on the strip's orientation relative to the far-field, but we have found that the orientation shown, with the strip's centreline in a plane perpendicular to the far-field orientation, has the lowest observed energy. The cross-section of the disclination loop shows a

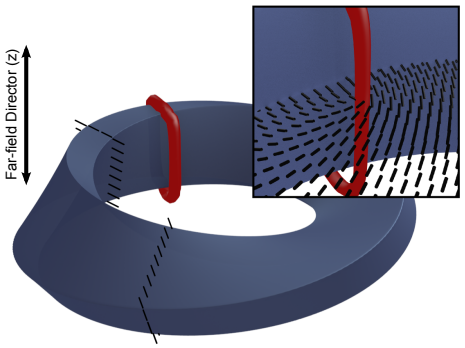

Figure 5.3: Simulation results of a Möbius strip with homeotropic boundary conditions on the flat faces, shown schematically in black along the strip. Note the planar anchoring on the short edge required to correctly represent a two-dimensional surface. The two-dimensional surface can then be thought of as living in the centre of the strip. The defect line (red) is clearly visible entangling the strip, as predicted by (5.1). The inset shows the local director profile near the defect, showing the +1/2 twist disclination on the inside of the strip; there is a corresponding -1/2 twist profile on the outside.

twisted $-1/2$ profile on the outside of the strip and a $+1/2$ twisted profile on the inside, as it has to in order to carry no hedgehog charge [151]. This hedgehog charge may be computed by several methods. The recently developed Pontryagin-Thom construction [9] and methods related to disclination profile switching [151] both assert that the charge of the disclination is zero, as required on topological grounds.

Perhaps the simplest generalisation of the Möbius strip topology is to vary its embedding in $\mathbb{R}^3$. Different embeddings can be obtained by changing the number, p, of half-twists that the strip contains. The 'canonical' Möbius strip has one half-twist ($p = 1$), but more generally if p is odd then the surface is still non-orientable and has the same topology as the Möbius strip. When p is even the surface is orientable and has the topology of an annulus. Nonetheless, the embeddings are distinct and carry their own topological embellishments. The boundary of a Möbius strip is a circle. For a single half-twist this is a simple unknot, but for p half-twists it is a $(p, 2)$ torus knot (p odd) or link (p even). To see this, note that the boundary of a p-twisted strip (p odd) lives on a torus whose major radius is that of the strip and whose minor radius is half the strip width. The curve the boundary draws on this torus goes round the meridional cycle p times – once for each half-twist – while

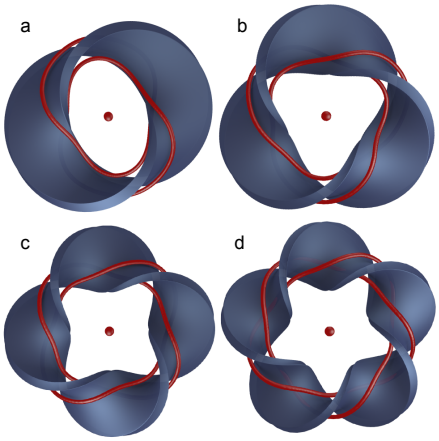

Figure 5.4: Knotted and linked disclinations in chiral nematics stabilised by the presence of twisted surfaces with homeotropic boundary conditions on the flat faces, and planar on the thin edges. They are torus knots and links of the form $(p, 2)$. Shown are: (a) $p = 2$ Hopf link, (b) $p = 3$ trefoil knot, (c) $p = 4$ Solomon's Seal and (d) $p = 5$ cinquefoil knot. The defects in the centre are hedgehogs, existing in pairs above and below the strip.

traversing the longitudinal cycle twice, which is the definition of a $(p, 2)$ torus knot. The story is the same for orientable strips with p even, except that there are two components to the boundary and they form a link.

Can this structure, coming from the nature of the embedding, be exploited to controllably produce knotted and linked disclination loops in liquid crystals? Disclination lines that follow the surface of such a multiply-twisted Möbius strip will have the same shape and properties as the colloid boundary, yielding precisely constructed knots and links. Here we show that such configurations can be stabilised in chiral nematics; examples for doubly, triply, quadruply and quintuply twisted strips are shown in Fig. 5.4. They produce the $p = 2$ Hopf link, the $p = 3$ trefoil knot, the $p = 4$ Solomon's Seal and the $p = 5$ cinquefoil knot, respectively. All these knots and links obey the topological requirements set out in the first section; the strips with an even number of twists are topologically trivial and the strip is entangled by an *even* number of disclinations, those with an odd number of twists are non-orientable and so enclose an *odd* number of disclinations.

The stablisation of these knotted structures is not just a question of topology, energetics also come into play. In this regard, the chirality (inverse pitch)

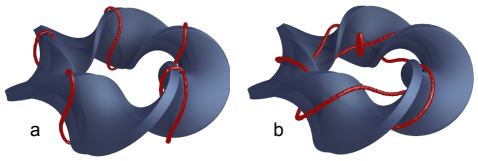

Figure 5.5: Comparison of configurations for a quintuply twisted strip. (a) Ground-state configuration consisting of 5 small disclinations loops at the locations predicted by (5.1). They have a slightly twisted profile, caused by both the twisting of the strip and the chiral nature of the system. (b) $(5,2)$ torus knot entangling the strip, with two hyperbolic hedgehogs nucleated above and below. The energy difference between these configurations is approximately 1.2%.

of the system has an important role in the stability of these configurations. Indeed it is generally true that chiral systems allow for more exotic structures [8, 134]. In the achiral nematic system, the knotted defects are unstable and the liquid crystal assumes a ground state configuration consisting of p small disclination loops entangling the strip along the contours where $\mathbf{S}_n \cdot \mathbf{n}_0 = 0$, as predicted by (5.1). A similar configuration, with slightly twisted loops (Fig. 5.5), is also the ground state in cholesterics – the knots are metastable – although the difference in energies is small (of order 1-2%) and decreases both with increasing chirality and knot complexity p. The behaviour with increasing p can be understood in terms of the total length of disclination line, which scales as p for the isolated loops and as $\sqrt{4+p^2}$ for the knots. If the chirality is increased such that the pitch becomes smaller than the width of the colloid then the disclinations develop twists analogous to those around spherical colloids [132, 134].

Like cholesterics, torus knots have a handedness – the $(p,2)$ and $(p,-2)$ knots are mirror pairs – and it is not surprising to find that the relative handedness influences the stability of the textures. The handedness of the knot is set by the shape of the colloid, and if this matches that of the cholesteric then knotted textures are stable, otherwise the system tries to expel the reverse twist in the configuration, resulting in an unstable knot.

The disclination lines themselves represent just a small portion of the entire system. Their knottedness imprints a complex orientational order on everything that is *not* the knot. Fig. 5.6a shows a slice through the director

field of a quintuply twisted Möbius strip in a cell with fixed normal boundary conditions. To match the boundary conditions of the cell, the knotted disclination is accompanied by two hyperbolic hedgehogs, expanded into small loops, above and below the strip. The disclination-colloid pair has a constant profile that simply rotates uniformly as one moves around the strip; qualitatively, this structure does not depend on p, the number of half-twists. The cross-section through the colloid has a profile reminiscent of a double twist cylinder [87], split apart by the colloid into two separate $+1/2$ twist disclinations.

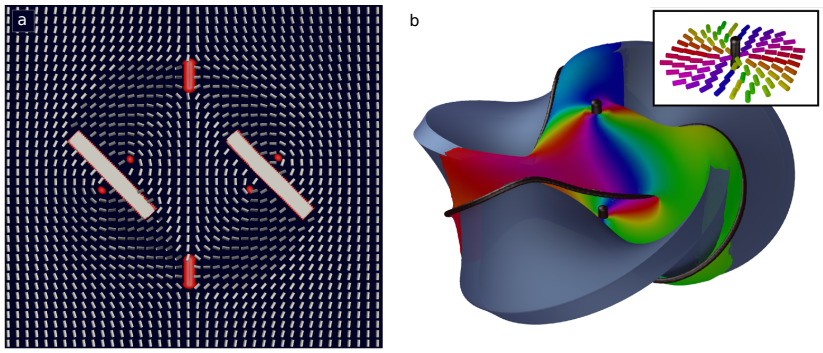

Figure 5.6: Field Structure. (a): Director field profile of a $(5,2)$ torus knot and the two accompanying hyperbolic hedgehogs, opened up into small rings, above and below the strip, with disclinations bound to the colloid's surface. The local disclination-colloid profile is largely constant up to a rotation as one moves around the strip. Though this profile is for a $p = 5$ configuration, qualitatively the director field does not change as one varies p. The far-field director is fixed to be vertical on the boundary of the cell. (b): Pontryagin-Thom surface [9] for the trefoil knot-colloid pair. The surface is constructed by considering all points where the director field is perpendicular to the far-field. The surface is then coloured with the remaining $\mathbb{RP}^1$ degree of freedom (as illustrated in the inset). The defects, disclination line and two accompanying hedgehogs, are shown in black. The colour winding around the hedgehogs establishes them as unit charge defects. The surface can be patched by removing the hedgehogs, and allowing the surface to pass through the colloid. One then obtains a Seifert surface for the knot, composed of two disks (top and bottom) connected by 3 (generally p) twisted bands. It is readily verified that this surface has genus 1 (generally $(p-1)/2$, for p odd), the genus of the trefoil knot. While there is also a colour winding around the disclination, this is a four-fold winding, giving the disclination even (equivalent to zero) hedgehog charge, as required.

Chapter 6

Constructing Knotted Textures with Milnor Fibrations

The knotted defects that we have studied in this thesis can be difficult to examine from a less abstract perspective, in determining their energetic properties or equilibrium shape for example, simply because it is difficult to write down an expression for a director field containing a knotted defect line, and even more difficult to write down an expression which minimises a particular energy functional. This chapter is concerned with giving a partial solution to this problem. We will show how to write down explicit expressions for director fields containing a variety of knotted and linked defect lines, and how these may be decorated with Skyrmion tubes in the manner considered in Chapter 2. The expressions we give are not minimisers of any particular energy functional and thus best serve as initial conditions for Landau-de Gennes simulations, indeed the knotted defect lines in the previous chapter were created in this way. The primary structure we exploit is that of Milnor fibrations [152]. These beautiful objects, at least the ones we're concerned with, are fibrations of S^3 associated to critical points of functions $\mathbb{C}^2 \to \mathbb{C}$ or $\mathbb{R}^4 \to \mathbb{C}$, though there is a far richer theory, the details of which can be found in the excellent books by Milnor [152] and Seade [153]. These structures have been used, in a very similar manner, by Mark Dennis [154] for the purpose of writing down knotted phase fields. Our use is similar, but the additional

richness of nematic order as opposed to a section of a trivial $U(1)$ bundle (a phase field) allows us more freedom. A brief summary of the structure is as

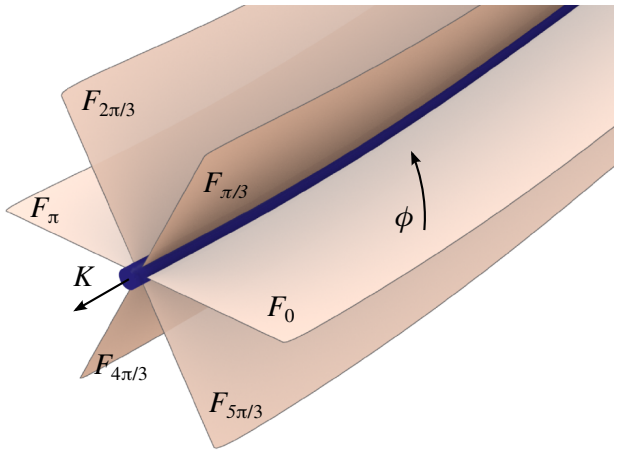

Figure 6.1: Milnor fibration of $S^3 - L$. The fibres, indexed by the phase ϕ, all join along the link L, which forms the binding of an open book decomposition of S^3.

follows, one takes a polynomial $f : \mathbb{C}^2 \to \mathbb{C}$ with an isolated critical point at the origin. Restrict this polynomial to a 3-sphere surrounding the critical point. Let $L = f^{-1}(0) \cap S^3$ be the (dimension one) intersection of the zero set of f with S^3, then the map

$$\phi : S^3 - L \to S^1 \tag{6.1}$$

$$x \mapsto \text{Arg}(f(x)). \tag{6.2}$$

defines a fibration of $S^3 - L$ over S^1 with fibre an orientable surface spanning L, as shown in Figure 6.1. The classic examples are given by the Brieskorn polynomials [155, 156]

$$f(z,w) = z^p + w^q, \tag{6.3}$$

with the neighbourhood S^3 chosen as the set $|z|^2 + |w|^2 = 1$. The zero set of f on S^3 is a (p,q) torus knot, has $d = \gcd(p,q)$ components and is given by the formula

$$L_j(t) = \left(r_1 e^{iqt}, r_2 e^{i(pt+2\pi j/d)}\right), \tag{6.4}$$

where $j \in \mathbb{Z}_d$ denotes the component of L and $r_1^{2p} + r_2^{2q} = 1$. The function

$\phi = \text{Arg}(f)$ then gives a fibration of the complement of the (p,q) torus knot. Note that if L has d components then one can write

$$f = \prod_{i \in \mathbb{Z}_d} f_i^{n_i}, \tag{6.5}$$

where each f_i is a polynomial whose zero set restricted to S^3 is L_i and n_i is an integer. For example, the $p = 2$, $q = 2$ Brieskorn polynomial for the Hopf link can be written

$$f_{2,2} = (z + iw)(z - iw). \tag{6.6}$$

To apply this to the construction of textures we use stereographic projection to turn ϕ into a function $\bar{\phi} : \mathbb{R}^3 - L \to S^1 = \phi \circ \pi^{-1}$ where $\pi^{-1} : \mathbb{R}^3 \to S^3$ is an inverse three-dimensional stereographic projection. At this point it is useful to make some choices. We will choose the point $(0,i) \in \mathbb{C}^2$ as the projection point for π and demand that $f = 1$ at $(0,i)$. With these choices we can write the Brieskorn polynomials as

$$f(z,w) = z^p + (-iw)^q. \tag{6.7}$$

With these conventions we are now studying the map $\bar{\phi} : \mathbb{R}^3 - L \to S^1$. Consider a loop γ_i going around the i^{th} component of L, then the degree of $\bar{\phi}$ restricted to γ_i is

$$\deg(\bar{\phi}|_{\gamma_i}) = n_i. \tag{6.8}$$

Assume that $|n_i| = 1$ for each component. We can guarantee this by ensuring that the multiplicity of each factor in (6.5) is 1, and in general the magnitude of n_i is equal to the multiplicity of the corresponding factor [153].

6.1 Constructing Knotted Textures

We can use these polynomials to construct knotted textures. Essentially the observation is that if $\text{Arg}(f)$ winds by 2π around L then $\text{Arg}(\sqrt{f})$ will wind by

π, and thus make L a nematic disclination. Formally we take a director field, considered as a map $\mathbf{n} : \mathbb{R}^3 - L \to \mathbb{RP}^2$, where L is a set of line defects. We assume that the director field is always orthogonal to some fixed direction $\mathbf{v}_0$, for examples we will choose $\mathbf{v}_0 = \mathbf{e_y}$ in the standard Cartesian basis. Then we can regard $\mathbf{n}$ as a map $\mathbf{n} : \mathbb{R}^3 - L \to \mathbb{RP}^1$. Passing to the double cover of the complement of L, $\widehat{\Sigma(L)}$ we can write $\mathbf{n}$ as an oriented map $\tilde{\mathbf{n}} : \widehat{\Sigma(L)} \to S^1$, equivariant with respect to the deck transformation that exchanges the two sheets of the cover (as discussed extensively earlier). Now if we take a new path γ_i going around L_i in the double cover (which can be thought of as going around L_i in $\mathbb{R}^3$ twice) then the fact that the lines L_i are line defects is given by the requirement that

$$\deg(\tilde{\mathbf{n}}|_{\gamma_i}) = 1. \tag{6.9}$$

So if we can find an equivariant map $\widehat{\Sigma}(L) \to S^1$ such that (6.9) is satisfied then we have constructed a texture with L as a defect set and with $\mathbf{n}$ always pointing orthogonal to $\mathbf{e}_y$. Such a function is supplied by $\mathrm{Arg}(f^{\frac{1}{2}})$.

So to summarise, let $\varphi = \mathrm{Arg}(f^{\frac{1}{2}})$. Then the director field

$$\mathbf{n} = \big(\cos(\varphi), 0, \sin(\varphi)\big) \tag{6.10}$$

contains a defect line L, defined by f. Of course $\mathbf{n}$ has discontinuities (with a branching given by an appropriate branching set as constructed in Chapter 2), but the associated Q tensor:

$$Q = \frac{s}{2}\left(\mathbf{n}\otimes\mathbf{n} - \frac{1}{3}\mathbb{I}\right), \tag{6.11}$$

is continuous and defines the appropriate uniaxial nematic texture. We note that by varying the choices made in defining Q (choice of projection point and plane in which to rotate $\mathbf{n}$, deforming the polynomial to $z^p + a(-iw)^q$ for $a \in \mathbb{C}$ for example), one can write down many different textures with the

same topology. The energetic properties of these configurations have not been explored though in a nematic they are guaranteed to be unstable by Derrick's theorem.

6.1.1 The Topology of the Texture

Constructing nematic textures in this way strongly constrains their topology. Because $\mathbf{n}$ is always pointing orthogonal to a particular direction, its topological class $[\mathbf{n}]$ in the group $H_1(\Sigma(L))$ must be of order two, that is $2[\mathbf{n}] \in H_1(\Sigma(L)) = 0$.

To show this, let ξ be the vector bundle of vectors orthogonal to $\tilde{\mathbf{n}}$ on the double cover of the link complement defined by the splitting, $T\widehat{\Sigma(L)} = L_{\tilde{\mathbf{n}}} \oplus \xi$. By construction our texture is locally of the form $\tilde{\mathbf{n}}(x) = (a(x), 0, b(x))$, and hence sections of ξ consist of vector fields that are locally of the form $\alpha(0,1,0) + \beta(-b(x), 0, a(x))$. The vector field $(0,1,0)$ is therefore a non-zero section of ξ (*i.e.* a non-zero vector field that is everywhere orthogonal to $\tilde{\mathbf{n}}$). As ξ admits two non-zero linearly independent sections it must be a trivial bundle, and hence have vanishing Euler class. As we know, the topological type of $\mathbf{n}$, up to sign ambiguity, is an element of the group $H_1(\Sigma(L))$. Then the Euler class of ξ is twice $[\tilde{\mathbf{n}}]$, but this must be zero, as we constructed a non-zero section. Hence

$$2[\mathbf{n}] \in H_1(\Sigma(L)) = 0. \tag{6.12}$$

which does not depend on the choice of orientation in the lift of $\mathbf{n}$ to the double cover.

One can also obtain insight using the Pontryagin-Thom construction. Take $\lim_{x\to\infty} \mathbf{n} = (0,0,1)$ as the chosen direction, then the PT surface will be regions where $\mathbf{n} = (1,0,0)$ and will be of one colour, and of course this is just a fibre of f.

6.2 The Hopf Link and Conjugate Polynomials

We will illustrate these ideas with our favourite example – the Hopf link. The Brieskorn polynomial is

$$f(z,w) = z^2 - w^2. \tag{6.13}$$

We use the stereographic projection

$$\pi^{-1}(x,y,z) = \frac{\big(2x + i2y, 2z + i(x^2+y^2+z^2-1)\big)}{1+x^2+y^2+z^2}. \tag{6.14}$$

The polynomial f, as a function of Cartesian coordinates (x,y,z), is then given as

$$f(x,y,z) = \left(1 + \frac{8(1+x^2) - 8(1+x^2+y^2+z^2)}{(1+x^2+y^2+z^2)^2}\right) + i4\left(\frac{2xy - z(x^2+y^2+z^2-1)}{(1+x^2+y^2+z^2)^2}\right). \tag{6.15}$$

Then the phase field $\varphi = \mathrm{Arg}(f^{\frac{1}{2}})$ takes the form

$$\varphi = \frac{1}{2}\arctan\left(\frac{\mathrm{Im}(f)}{\mathrm{Re}(f)}\right) \tag{6.16}$$

and one constructs the texture $\mathbf{n}$ as

$$\mathbf{n} = (\sin\varphi, 0, \cos\varphi). \tag{6.17}$$

The PT surface can be plotted as the intersection of the sets $\mathrm{Im}(f) = 0$ and $\mathrm{Re}(f) > 0$ and is shown in Figure 6.2.

In §6.1.1 we showed that textures generated in this manner are given by order two elements of $H_1(\Sigma(L))$. In the case of the Hopf link we know that $H_1(\Sigma(L)) = \mathbb{Z}_2$, both elements of which are of order two. Hence one might ask if we can create representatives of both textures with this method. The example illustrated above can be assigned a linking number invariant of $+1$ by considering the orientation on the boundary defined by the PT surface.

The corresponding -1 texture can be constructed by conjugating one of the component polynomials:

$$f_{-1} = (z+w)\overline{(z-w)} \tag{6.18}$$

which can be thought of as reversing the orientation of one of the link components. This procedure can be made more general, indeed each factor in the expression (6.5) may be conjugated to form a new fibration. Plots of the Milnor surfaces are shown in Figure 6.2. There is a slight subtlety, in particular one might like to ask which of the textures is $0 \in \mathbb{Z}_2$ and which of the textures is 1. The two textures can be related by a reflection, and so the choice of which texture corresponds to which element of $\mathbb{Z}_2$ is arbitrary. In fact, considerations of this type leads one to conjecture that for a given link, the order of the first homology of the branched double cover is bounded from below by $2^{|L|-1}$. We do not know the status of this conjecture in the mathematics literature.

6.3 Adding Skyrmions and Hedgehogs

By construction, the technique we have used so far gives textures which permit an everywhere orthogonal direction, the Euler class of the orthogonal 2-plane bundle must be of order 2. An alternative way of saying this is that one can construct a PT surface for these textures which can be of a single, solid colour, as shown in Figure 6.2. The next step is, of course, to construct textures for which the associated Euler class is not of order 2. To do this is simple, and requires but a small extension of our previous work.

The first step is to extend our formula (6.10) for $\mathbf{n}$ as follows

$$\mathbf{n} = \big(\sin\varphi\cos\chi, \sin\varphi\sin\chi, \cos\varphi\big) \tag{6.19}$$

for arbitrary maps $\varphi, \chi : \mathbb{R}^3 - L \to S^1$ this formula can give any texture. We have specified φ using the Milnor polynomials, so it remains to specify

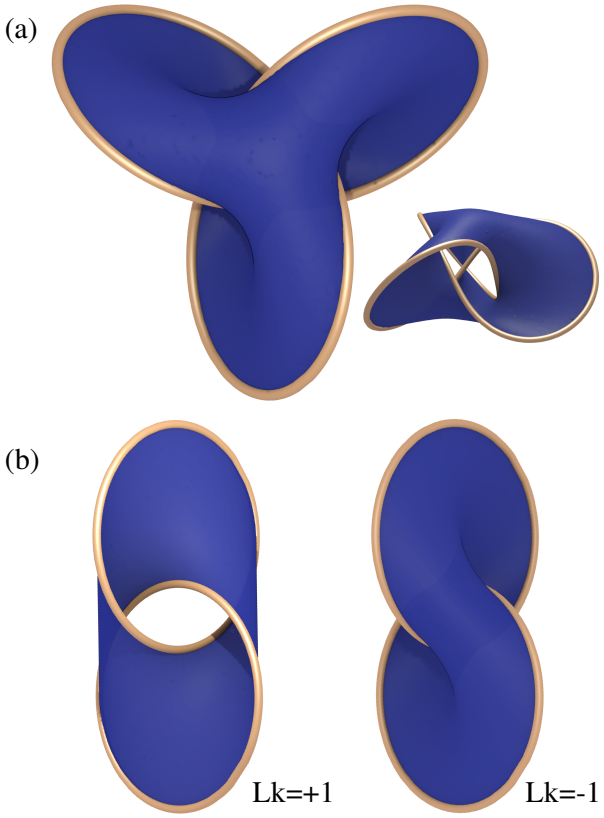

Figure 6.2: Pontryagin-Thom surfaces for a texture containing a knotted nematic defect line. (a) PT surface for a nematic containing a trefoil knot. (b) & (c) PT surfaces for nematic textures containing linked defects with linking numbers ± 1 respectively. These are generated using the equations (6.13) and (6.18). The linking number of ± 1 can be found by assigning orientations to the boundary that are induced by choosing an orientation of the surface. Note that choice of surface orientation changes the induced boundary orientations by a global sign, so that the overall linking number is the same.

χ. A natural choice is to make $\chi = \text{Arg}(h(x+iy,z))$, where $h(x+iy,z)$ is a smooth one-parameter family of meromorphic functions indexed by z (the Cartesian coordinate). While (6.19) contains singularities along the lines in $\mathbb{R}^3$ corresponding to the poles and zeros of h, they can be made removable by ensuring that the lines do not intersect the surface where $\varphi = \pi/2$. In fact, in this way, one can choose the surface $\varphi = \pi/2$ as a 'canonical' PT surface, $\Sigma_{\pi/2}$, and consider the poles and zeros of h as entangling it. A schematic of this situation is shown in Figure 6.3.

Once one makes this choice, it remains to identify the topological class to which it belongs. We need to do two things to achieve this, we first need to

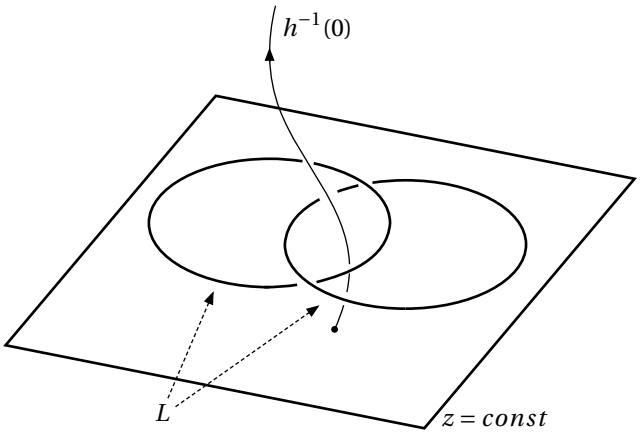

Figure 6.3: Extending the construction. The data from the Milnor polynomial is supplemented with a family of meromorphic functions h, which are indexed by z, the zeros of which entangle the link L. The homology class of the zeros and poles of h determine the topological class of the texture generated in this way.

remove the removable singularities from (6.19) and then identify the topology of the texture. As before we have the director $\mathbf{n}$ given by

$$\mathbf{n} = \big(\cos\varphi\cos\chi, \cos\varphi\sin\chi, \sin\varphi\big) \tag{6.20}$$

along with this there is the natural orthogonal direction given by

$$\mathbf{b} = (-\sin\chi, \cos\chi, 0). \tag{6.21}$$

Now $\mathbf{n}$ has singularities along the zeros and poles of h. We have promised they are removable, so we will remove them. Since h is a smooth 1-parameter family of meromorphic functions, its zeros and poles must intersect the $x-y$ planes transversely, except at a set of isolated points, where zeros and poles merge. If one assigns a line corresponding to a zero of h to be pointing along the positive z-axis direction, and poles to be pointing along the negative z-axis direction, then one obtains a set of cycles $\mathcal{C}$ in $S^3 - \Sigma_{\pi/2}$[1]; note that this is only possible because of the transverse intersection guaranteed by h. These cycles are precisely the locations of the singularities in $\mathbf{n}$.

[1] In principle, one obtains a singular set; arcs joined at nodes, but a perturbation of h removes these.

By construction, $\mathcal{C}$ does not intersect the surface $\Sigma_{\pi/2}$. Now consider a particular component $C_i \in \mathcal{C}$, φ restricted to C_i is a map[2] $S^1 \to \mathbb{RP}^1$. Because $\mathcal{C}$ does not intersect the surface $\Sigma_{\pi/2}$ the degree of the map $S^1 \to \mathbb{RP}^1$ must be zero, since it is not surjective. Take a neighbourhood $N(C_i)$, fix φ on $\partial N(C_i)$. Since φ is null-homotopic on $\partial N(C_i)$, one can perform a homotopy of φ in $N(C_i)$, such that $\varphi|_{C_i} = \pi/2$ (*i.e.* $\mathbf{n}$ is vertical). In doing so one has removed the singularities in $\mathbf{n}$, but $\mathbf{b}$ remains orthogonal.

The singularities in $\mathbf{b}$ are precisely the same as the original singularities in $\mathbf{n}$. Hence they are also the set of cycles $\mathcal{C}$. Passing to the cyclic double cover, this set $\mathcal{C}$ becomes an element (up to sign) $[\mathcal{C}] \in H_1(\Sigma(L))$, defined by the oriented cycles corresponding to the poles and zeros of h. The sign depends on the choice that zeros are oriented 'upwards' and poles oriented 'downwards', but there is a global sign ambiguity in the classification of nematic textures anyway, so it all comes out in the wash. Hence we have constructed a direction orthogonal to $\tilde{\mathbf{n}}$ whose singularities lie on $\mathcal{C}$. Since the Euler class is given by the Poincaré dual to zeros of a generic section, the Euler class of $\tilde{\mathbf{n}}$ is given by $PD([\mathcal{C}])$, which determines the topology of $\mathbf{n}$ up to elements of order 2 in $H_1(\Sigma(L))$. Aspects of order two textures can, as we have illustrated with the Hopf link, be explored by changing the orientations of the link components through partial conjugation of the appropriate Milnor polynomial, though we do not currently have a full theory for this.

Finally, we will briefly mention how one may add point defects to this system. The answer is predictably simple, one simply allows the zeros or poles of h to intersect the surface $\Sigma_{\pi/2}$.

6.3.1 Examples and practicalities

While conceptually the process outlined above is clear, actually choosing a family of meromorphic functions h can be difficult. The simplest choice is to set $h(x+iy,z) = h(x+iy)$, *i.e.* have no dependence on the z-direction.

[2] The target space is $\mathbb{RP}^1$ because we took the square root of ϕ.

In this case the lines corresponding to the poles and zeros of h will be vertical, and will meet 'at infinity' in $\mathbb{R}^3$. As such, this violates the assumption that $\lim_{|x|\to\infty} \mathbf{n} = \mathbf{n}_0$, and the knotted defect line will have an overall charge corresponding to the sum of the poles and zeros of h. Nevertheless, doing things in this way is by far the easiest, and a large gallery of examples are shown in Figure 6.4.

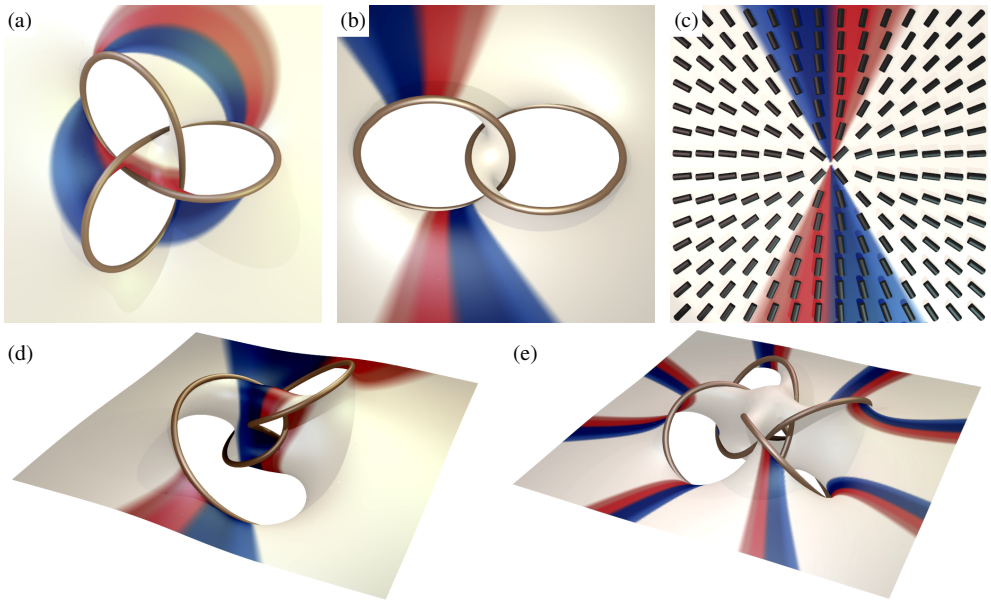

Figure 6.4: Gallery of knotted defect textures. The surfaces are where the director is horizontal, the colour is given by the horizontal orientation, and is indicated in (c). Note of particular interest the texture in (a), which has zero total hedgehog charge.

Bibliography

[1] P.G. de Gennes and J. Prost, *The Physics of Liquid Crystals*, 2nd Edition, (Oxford University Press, Oxford, 1993).

[2] P.M. Chaikin and T.C. Lubensky, *Principles of condensed matter physics* (Cambridge University Press, Cambridge, 1995).

[3] I.W. Stewart, *The Static and Dynamic Continuum Theory of Liquid Crystals: A Mathematical Introduction* (Taylor & Francis, London, 2004).

[4] R.B. Meyer, L. Liébert, L. Strzelecki and P. Keller, *Ferroelectric Liquid Crystals*, J. Phys. Lett, **36**, 69 (1975).

[5] U. Tkalec, M. Ravnik, S. Čopar, S. Žumer, and I. Muševič, *Reconfigurable Knots and Links in Chiral Nematic Colloids*, Science **333**, 62 (2011).

[6] A. Martinez, M. Ravnik, B. Lucero, R. Visvanathan, S. Žumer, and I.I. Smalyukh, *Mutually tangled colloidal knots and induced defect loops in nematic fields*, Nat. Mater. **13**, 258 (2014).

[7] Tasinkevych, M.G. Campbell and I.I. Smalyukh, *Splitting, linking, knotting, and solitonic escape of topological defects in nematic drops with handles*, Proc. Natl. Acad. Sci. USA **111**, 16268 (2014).

[8] I.I. Smalyukh, Y. Lansac, N.A. Clark, and R.P. Trivedi, *Three-dimensional structure and multistable optical switching of triple-twisted particle-like excitations in anisotropic fluids*, Nat. Mater. **9**, 139 (2010).

[9] B.G. Chen, P.J. Ackerman, G.P. Alexander, R.D. Kamien, and I.I. Smalyukh, *Generating the Hopf Fibration Experimentally in Nematic Liquid Crystals*, Phys. Rev. Lett. **110**, 237801 (2013).

[10] P.J. Ackerman, R.P. Trivedi, B. Senyuk, J. van de Lagemaat, and I.I. Smalyukh, *Two-dimensional skyrmions and other solitonic structures in confinement-frustrated chiral nematics*, Phys. Rev. E **90**, 012505 (2014).

[11] R.D. Kamien and J.V. Selinger. *Order and frustration in chiral liquid crystals*. J. Phys. Condens. Matter **13**, R1 (2001).

[12] O. Lavrentovitch and M. Kleman, *Cholesteric liquid crystals: defects and topology* in *Chirality in Liquid Crystals*, ed: H.S. Kitzerow and C. Bahr (Springer-Verlag, Berlin, 2001), 115.

[13] S. Chandrasekhar, *Liquid Crystals (2nd ed.)*. (Cambridge University Press, Cambridge, 1992).

[14] G.P. Alexander, *Liquid Crystalline Blue Phases and Swimmer Hydrodynamics* (DPhil thesis, University of Oxford, 2008).

[15] M. Ravnik and S. Žumer, *Nematic colloids entangled by topological defects*, Soft Matter **5**, 269 (2009).

[16] M. Ravnik and S. Žumer, *Landau-de Gennes modelling of nematic liquid crystal colloid*, Liq. Cryst. **36**, 1201 (2009).

[17] M. Ravnik and S. Žumer, *Nematic braids: 2D entangled nematic liquid crystal colloids*, Soft Matter **5**, 4520 (2009).

[18] I. Dierking, *Textures of Liquid Crystals* (Wiley-VCH, Weinheim, 2003).

[19] `https://commons.wikimedia.org/wiki/File:Nematische_Phase_Schlierentextur.jpg`

[20] B.G. Chen, Ph.D. thesis, University of Pennsylvania, 2012.

[21] G.P. Alexander, B.G. Chen, E.A. Matsumoto, and R.D. Kamien, *Colloquium: Disclination loops, point defects, and all that in nematic liquid crystals*, Rev. Mod. Phys. **84**, 497 (2012).

[22] P.E. Cladis and M. Kléman, *Non-singular disclinations of strength* $s = +1$ *in nematics*, J. Phys. (France) **33**, 591 (1972).

[23] R.B. Meyer, *On the existence of even indexed disclinations in nematic liquid crystals*, Philos. Mag. **27**, 405 (1973).

[24] C. Williams and Y. Bouligand, *Fils et disinclinaisons dans un nématique en tube capillaire*, J. Phys. (France) **35**, 589 (1974).

[25] P.S. Drzaic, *Liquid Crystal Dispersions* (World Scientific, Singapore, 1995).

[26] N.D. Mermin, *The topological theory of defects in ordered media*, Rev. Mod. Phys. **51**, 591 (1979).

[27] A. Hatcher, *Algebraic Topology* (Cambridge University Press, Cambridge, 2001).

[28] N.S. Manton and P.M. Sutcliffe, *Topological Solitons*, (Cambridge University Press, Cambridge, 2004).

[29] V. Poénaru and G. Toulouse, *The crossing of defects in ordered media and the topology of three-manifolds*, J. Physique **38**, 887 (1977).

[30] S. Čopar and S. Žumer, *Nematic braids: topological invariants and rewiring of disclinations*, Phys. Rev. Lett. **106**, 117801 (2011).

[31] M.I. Monastyrstky and V.S. Retakh, *Topology of linked defects in condensed matter*, Comm. Math. Phys. **103**, 445 (1986).

[32] K Jänich, *Topological properties of ordinary nematics in 3-space*, Acta. Appl. Math. **8**, 65 (1987).

[33] W.B.R. Lickorish, *An Introduction to Knot Theory*, (Springer-Verlag, New York, 1997).

[34] P. Olum, *Cocylce Formulas for Homotopy Classification; Maps into Projective and Lens Spaces*, Trans. Amer. Math. Soc. **103**, 30 (1962).

[35] J. Eells and L. Lemaire, *On the Construction of Harmonic and Holomorphic Maps between Surfaces*, Math. Ann. **252**, 27 (1980)

[36] J.F. Adams, *Maps from a Surface to the Projective Plane*, Bull. Lond. Math. Soc. **14**, 533 (1982).

[37] H. Hopf, *Die Klassen der Abbildungen der n-dimensionalen Polyeder auf die n-dimensionale Sphäre*, Comment. Math. Helv., **5**, (1932).

[38] L. Pontryagin, *A classification of continuous transformations of a complex into a sphere*, Dokl. Akad. Nauk SSSR **19**, 361 (1938).

[39] L. Pontryagin, *A classification of mappings of the three-dimensional complex into the two dimensional sphere*, Rec. Math. [Mat. Sbornik] N.S. **9**, 5, 331 (1941).

[40] R. Thom, *Quelques propriétés globales des variétés différentiables*, Comm. Math. Helv. **28**, 17 (1954).

[41] C.T.C Wall, *Surgery on Compact Manifolds, 2nd Edition* (ed. A.A. Ranicki), Mathematical Surveys and Monographs **69**, (American Mathematical Society, Providence) (1999).

[42] S. Bechtluft-Sachs and M. Hien, *The Global Defect Index*, Commun. Math. Phys. **202**, 403 (1998).

[43] D. Rolfsen, *Knots and Links*, (AMS Chelsea Publishing, Providence, 2003).

[44] J.W. Milnor and J.D. Stasheff, *Characteristic Classes*, (Princeton University Press, Princeton, 1974).

[45] Y. Bouligand, *Recherches sur les textures des états mésomorphes. 6 Dislocations coins et signification des cloisons de Grandjean-Cano dans les cholestériques*, J. Phys. (France) **35**, 959-981 (1974).

[46] Y. Bouligand, B. Derrida, V. Poénaru, Y. Pomeau, and G. Toulouse, *Distortions with double topological character: the case of cholesterics*, J. Phys. (France) **39**, 863 (1978).

[47] M. Kléman and J. Friedel, *Lignes de dislocation dans les cholestériques*, J. Phys. France Colloq. **30**, 43 (1969).

[48] I.I. Smalyukh and O.D. Lavrentovich, *Three-dimensional director structures of defects in Grandjean-Cano wedges of cholesteric liquid crystals studied by fluorescence confocal polarizing microscopy*, Phys. Rev. E **66**, 051703 (2002).

[49] N.D. Mermin and T.L. Ho, *Circulation and Angular Momentum in the A Phase of Superfluid Helium-3*, Phys. Rev. Lett. **36**, 594 (1976).

[50] G.E. Volovik and V.P. Mineev, *Vortices with free ends in superfluid He^3-A*, JETP Lett. **23**, 593-595 (1976). [Pis'ma Zh. Eksp. Teor. Fiz. **23**, 647 (1976).]

[51] P.W. Anderson and G. Toulouse, *Phase Slippage without Vortex Cores: Vortex Textures in Superfluid ^{3}He*, Phys. Rev. Lett. **38**, 508 (1977).

[52] P.M. Walmsley and A.I. Golov, *Chirality of Superfluid ^{3}He-A*, Phys. Rev. Lett. **109**, 215301 (2012).

[53] U.K. Rößler, A.N. Bogdanov, and C. Pfleiderer, *Spontaneous skyrmion ground states in magnetic metals*, Nature **442**, 797 (2006).

[54] S. Mühlbauer, B. Binz, F. Jonietz, C. Pfleiderer, A. Rosch, A. Neubauer, R. Georgii, and P. Böni, *Skyrmion Lattice in a Chiral Magnet*, Science **323**, 915 (2009).

[55] X.Z. Yu, Y. Onose, N. Kanazawa, J.H. Park, J.H. Han, Y. Matsui, N. Nagaosa, and Y. Tokura, *Real-space observation of a two-dimensional skyrmion crystal*, Nature **465**, 901 (2010).

[56] X. Yu, M. Mostovoy, Y. Tokunaga, W. Zhang, K. Kimoto, Y. Matsui, Y. Kaneko, N. Nagaosa, and Y. Tokura, *Magnetic stripes and skyrmions with helicity reversals*, Proc. Natl. Acad. Sci. USA **109**, 8856 (2012).

[57] P. Milde, D. Köhler, J. Seidel, L.M. Eng, A. Bauer, A. Chacon, J. Kindervater, S. Mühlbauer, C. Pfleiderer, S. Buhrandt, C. Schütte, and A. Rosch, *Unwinding of a Skyrmion Lattice by Magnetic Monopoles*, Science **340**, 1076 (2013).

[58] U. Al Khawaja and H. Stoof, *Skyrmions in a ferromagnetic Bose-Einstein condensate*, Nature **411**, 918 (2001).

[59] L.S. Leslie, A. Hansen, K.C. Wright, B.M. Deutsch, and N.P. Bigelow, *Creation and Detection of Skyrmions in a Bose-Einstein Condensate*, Phys. Rev. Lett. **103**, 250401 (2009).

[60] J.Y. Choi, W.J. Kwon, and Y.I. Shin, *Observation of topologically stable 2d Skyrmions in an antiferromagnetic spinor Bose-Einstein condensate*, Phys. Rev. Lett. **108**, 035301 (2012).

[61] J.Y. Choi, S. Kang, S.W. Seo, W.J. Kwon, and Y.I. Shin, *Observation of a Geometric Hall Effect in a Spinor Bose-Einstein Condensate with a Skyrmion Spin Texture*, Phys. Rev. Lett. **111**, 245301 (2013).

[62] M.J.H. Ku, W. Ji, B. Mukherjee, E. Guardado-Sanchez, L.W. Cheuk, T. Yefsah, and M. Zwierlein, *Motion of a Solitonic Vortex in the BEC-BCS Crossover*, Phys. Rev. Lett. **113**, 065301 (2014).

[63] S. Donadello, S. Serafini, M. Tylutki, L.P. Pitaevskii, F. Dalfovo, G. Lamporesi, and G. Ferrari, *Observation of Solitonic Vortices in Bose-Einstein Condensates*, Phys. Rev. Lett. **113**, 065302 (2014).

[64] J.F. Nye, *Lines of circular polarization in electromagnetic wave fields*, Proc. R. Soc. A **389**, 279 (1983).

[65] J.F. Nye and J.V. Hajnal, *The wave structure of monochromatic electromagnetic radiation*, Proc. R. Soc. A **409**, 21 (1987).

[66] J.V. Hajnal, *Singularities in the transverse fields of electromagnetic waves. I. Theory*, Proc. R. Soc. A **414**, 433 (1987).

[67] J.V. Hajnal, *Singularities in the transverse fields of electromagnetic waves. II. Observations on the electric field*, Proc. R. Soc. A **414**, 447 (1987).

[68] D. Hilbert and S. Cohn-Vossen, *Geometry and the Imagination*, (AMS Chelsea Publishing, New York, 1999).

[69] M.V. Berry and J.H. Hannay, *Umbilic points on Gaussian random surfaces*, J. Phys. A: Math. Gen. **10**, 1809 (1977).

[70] M.V. Berry and M.R. Dennis, *Polarization singularities in isotropic random waves*, Proc. R. Soc. A **456**, 2059 (2000).

[71] M.V. Berry and M.R. Dennis, *Polarization singularities in isotropic random vector waves*, Proc. R. Soc. A **457**, 141 (2001).

[72] M.R. Dennis, *Polarization singularities in paraxial vector fields: morphology and statistics*, Opt. Commun. **213**, 201 (2002).

[73] F. Flossmann, U.T. Schwarz, M. Maier, and M.R. Dennis, *Polarization singularities from unfolding an optical vortex through a birefringent crystal*, Phys. Rev. Lett. **95**, 253901 (2005).

[74] F. Flossmann, K. O'Holleran, M.R. Dennis, and M.J. Padgett, *Polarization singularities in 2D and 3D speckle fields*, Phys. Rev. Lett. **100**, 203902 (2008).

[75] V. Vitelli, B. Jain, and R.D. Kamien, *Topological defects in gravitational lensing shear fields*, J. Cosmol. Astropart. Phys. **09**, 034 (2009).

[76] T.H. Beuman, A.M. Turner, and V. Vitelli, *Stochastic geometry and topology of non-Gaussian fields*, Proc. Natl. Acad. Sci. USA **109**, 19943 (2012).

[77] T.H. Beuman, A.M. Turner, and V. Vitelli, *Critical and umbilical points of a non-Gaussian random field*, Phys. Rev. E **88**, 012115 (2013).

[78] I. Dzyaloshinsky, *A thermodynamic theory of "weak" ferromagnetism of antiferromagnetics*, J. Phys. Chem. Solids **4**, 241 (1958).

[79] T. Moriya, *Anisotropic superexchange interaction and weak ferromagnetism*, Phys. Rev. **120**, 91 (1960).

[80] E. Efrati and W.T.M. Irvine, *Orientation-Dependent Handedness and Chiral Design*, Phys. Rev. X **4**, 011003 (2014).

[81] A.S. Thorndike, C.R. Cooley, and J.F. Nye, *The structure and evolution of flow fields and other vector fields*, J. Phys. A: Math. Gen. **11**, 1455 (1978).

[82] S. Čopar, M.R. Dennis, R.D. Kamien, and S. Žumer, *Singular values, nematic disclinations, and emergent biaxiality*, Phys. Rev. E **87**, 050504(R) (2013).

[83] D.A. Beller, T. Machon, S. Čopar, D.M. Sussman, G.P. Alexander, R.D. Kamien, and R.A. Mosna, *Geometry of the Cholesteric Phase*, Phys. Rev. X **4**, 031050 (2014).

[84] R.A.P. Rogers, *Some Differential Properties of the Orthogonal Trajectories of a Congruence of Curves, with an Application to Curl and Divergence of Vectors*, Proc. R. Irish Soc. A **29**, 92 (1912).

[85] Yu. Aminov, *The Geometry of Vector Fields*, (Gordon and Breach Science Publishers, Amsterdam, 2000).

[86] S. Meiboom, J.P. Sethna, P.W. Anderson, and W.F. Brinkman, *Theory of the blue phase of cholesteric liquid crystals*, Phys. Rev. Lett. **46**, 1216 (1981).

[87] D.C. Wright and N.D. Mermin, *Crystalline liquids: the blue phases*, Rev. Mod. Phys. **61**, 385 (1989).

[88] A.A. Belavin and A.M. Polyakov, *Metastable states of two-dimensional isotropic ferromagnets*, JETP Lett. **22**, 245-247 (1975). [Pis'ma v. Zh. Eksp. Teor. Fiz. **22**, 503 (1975).]

[89] S. Banerjee, J. Rowland, O. Erten and M. Randeria, *Enhanced Stability of Skyrmions in Two-Dimensional Chiral Magnets with Rashba Spin-Orbit Coupling*

[90] R.B. Meyer, *Piezoelectric effects in liquid crystals*, Phys. Rev. Lett. **22**, 918 (1969).

[91] S. Armon, E. Efrati, R. Kupferman, and E. Sharon, *Geometry and Mechanics in the Opening of Chiral Seed Pods*, Science **333**, 1726 (2011).

[92] P.A.M. Dirac, *Quantised singularities in the electromagnetic field*, Proc. R. Soc. Lond. A **133**, 60 (1931).

[93] S.S. Chern, *A Simple Intrinsic Proof of the Gauss-Bonnet Formula for Closed Riemannian Manifolds*, Ann. Math. **45**, 747 (1944).

[94] S.S. Chern, *On the curvatura integra in a Riemannian manifold*, Ann. Math. **46**, 674 (1945).

[95] S.S. Chern, *Characteristic classes of Hermitian manifolds*, Ann. Math. **47**, 85 (1946).

[96] R. Bott and L.W. Tu, *Differential Forms in Algebraic Topology*, (Springer-Verlag, New York, 1982).

[97] S. Seki, X.Z. Yu, S. Ishiwata, and Y. Tokura, *Observation of skyrmions in a multferroic material*, Science **336**, 198 (2012).

[98] X.Z. Yu, N. Kanazawa, Y. Onose, K. Kimoto, W.Z. Zhang, S. Ishiwata, Y. Matsui, and Y. Tokura, *Near room-temperature formation of a skyrmion crystal in thin-films of helimagnet FeGe*, Nat. Mater. **10**, 106 (2011).

[99] A. Tonomura, X. Yu, K. Yanagisawa, T. Matsuda, Y. Onose, N. Kanazawa, H.S. Park, and Y. Tokura, *Real-Space Observation of Skyrmion Lattice in Helimagnet MnSi Thin Samples*, Nano Lett. **12**, 1673 (2012).

[100] N.S. Kiselev, A.N. Bogdanov, R. Schäfer, and U.K. Rößler, *Chiral skyrmions in thin magnetic films: new objects for magnetic storage technologies?*, J. Phys. D: Appl. Phys. **44**, 392001 (2011).

[101] R.D. Kamien, *Geometry of soft materials: a primer*, Rev. Mod. Phys. **74**, 953 (2002).

[102] M.V. Berry, *Index formulae for singular lines of polarization*, J. Opt. A **6**, 675 (2004).

[103] H. Geiges, *An Introduction to Contact Topology*, (Cambridge University Press, Cambridge, 2008).

[104] H.K. Moffatt, *The degree of knottedness of tangled vortex lines*, J. Fluid Mech. **35**, 117 (1969).

[105] H.K. Moffatt and R.L. Ricca, *Helicity and the Călugăreanu Invariant*, Proc. R. Soc. A **439**, 411 (1992).

[106] V.I. Arnold, *The Asymptotic Hopf Invariant and Its Applications*, Sel. Math. Sov. **5**, 327 (1986).

[107] E. Witten, *Quantum field theory and the Jones polynomial*, Commun. Math. Phys. **121**, 351 (1989).

[108] A.M. Polyakov, *One physical problem with possible mathematical significance*, J. Geom. Phys. **5**, 595 (1988).

[109] J. H. C. Whitehead, *An expression of Hopf's invariant as an integral*, Proc. Nat. Acad. Sci. USA **33**, 117 (1947).

[110] H. Grebel, R.M. Hornreich, and S. Shtrikman, *Landau theory of cholesteric blue phases*, Phys. Rev. A **28**, 1114-1138 (1983).

[111] P. Pieranski, P.E. Cladis, and R. Barbet-Massin, *Experimental evidence for a hexagonal Blue Phase*, J. Phys. France Lett. **46**, 973 (1985).

[112] P. Pieranski and P.E. Cladis, *Field-induced tetragonal blue phase (BP X)*, Phys. Rev. A **35**, 355 (1987).

[113] R.M. Hornreich and S. Shtrikman, *Field-induced hexagonal blue phases in positive and negative dielectric anisotropy systems: Phase diagrams and topological properties*, Phys. Rev. A **41**, 1978 (1990).

[114] J. Fukuda and S. Žumer, *Cholesteric blue phases: effect of strong confinement*, Liq. Cryst. **37**, 875 (2010).

[115] O. Henrich, K. Stratford, M.E. Cates, and D. Marenduzzo, *Structure of Blue Phase III of Cholesteric Liquid Crystals*, Phys. Rev. Lett. **106**, 107801 (2011).

[116] B Binz, A. Vishwanath, and V. Aji, *Theory of the Helical Spin Crystal: A Candidate for the Partially Ordered State of MnSi*, Phys. Rev. Lett. **96**, 207202 (2006).

[117] A. Hamann, D. Lamago, Th. Wolf, H. v Löhneysen, and D. Reznik, *Magnetic Blue Phase in the Chiral Itinerant Magnet MnSi,* Phys. Rev. Lett. **107**, 037207 (2011).

[118] A.O. Leonov, I.E. Dragunov, U.K. Rößler, and A.N. Bogdanov, *Theory of skyrmion states in liquid crystals*, Phys. Rev. E **90**, 042502 (2014).

[119] J.I. Fukuda and S. Žumer, *Quasi-two-dimensional Skyrmion lattices in a chiral nematic liquid crystal*, Nat. Commun. **2**, 246 (2010).

[120] R.M. Hornreich and S. Shtrikman, *Topological properties of cholesteric blue phases*, Phys. Rev. A **38**, 4843 (1988).

[121] M. Ravnik, G.P. Alexander, J.M. Yeomans, and S. Žumer, *Three-dimensional colloidal crystals in liquid crystalline blue phases*, Proc. Natl. Acad. Sci. USA **108**, 5188 (2011).

[122] Y. Bouligand. *Recherches sur les textures des états mésomorphes-2. – Les champs polygonaux dans les cholestériques.* Journal de Physique **33**, 715 (1972).

[123] Y. Bouligand. *Recherches sur les textures des états mésomorphes. 3. Les plages à éventails dans les cholestériques.* Journal de Physique **34**, 603 (1973).

[124] G.E. Volovik and V.P. Mineev, *Investigations of singularities in superluid He^3 in liquid crystals by the homotopic topology methods.* Zh. Eksp. Teor. Fiz. **72**, 2256 (1977).

[125] F. Grandjean, C.R. Hebd. Seances Acad. Sci. **172**, 71 (1921).

[126] R. Cano, Bull. Soc. Fr. Mineral. Cristallogr. **90**, 333 (1967).

[127] R. Cano, Bull. Soc. Fr. Mineral. Cristallogr. **91**. 20 (1968).

[128] D. Seč, T. Porenta, M. Ravnik and S. Žumer, *Geometrical frustration of chiral ordering in cholesteric droplets*, Soft Matter **8**, 11982 (2012).

[129] P. J. Ackerman, R. P. Trivedi, B. Senyuk, J. van de Lagemaat, and I. I. Smalyukh *Two-dimensional skyrmions and other solitonic structures in confinement-frustrated chiral nematics*, Phys. Rev. E **90**, 012505 (2014).

[130] B.G. Chen, G.P. Alexander and R.D. Kamien, *Symmetry breaking in smectics and surface models of their singularities*, Proc. Natl. Acad. Sci. USA **106**, 15577 (2009).

[131] V. Poénaru, *Some aspects of the theory of defects of ordered media and gauge fields related to foliations*, Commun. Math. Phys. **80**, 127 (1981).

[132] J.S. Lintuvuori, D. Marenduzzo, K. Stratford and M.E. Cates, *Colloids in liquid crystals: a lattice Boltzmann study.* J. Mater. Chem. **20**, 10547 (2010).

[133] J.S. Lintuvuori, K. Stratford, M.E. Cates, D. Marenduzzo, *Colloids in cholesterics: size-dependent defects and non-Stokesian microrheology*, Phys. Rev. Lett. **105**, 178302 (2010).

[134] V.S.R. Jampani, M. Škarabot, M. Ravnik, S. Čopar, S. Žumer, and I. Muševič *Colloidal entanglement in highly twisted chiral nematic colloids: twisted loops, Hopf links, and trefoil knots*, Phys. Rev. E **84**, 031703 (2011).

[135] J. Martinet, *Formes de contact sur les variétés de dimension 3*, in Proceedings of the Liverpool Singularities Symposium II, Lecture Notes in Math. 209, (Springer-Verlag, Berlin, 1971).

[136] Y. Eliashberg, *Classification of overtwisted contact structures on 3-manifolds*, Invent. Math. **98**, 623 (1989).

[137] Y. Eliashberg, *Contact Manifolds Twenty Years Since J. Martinet's Work*, Ann. Inst. Fourier (Grenoble) **42**, 165 (1992).

[138] J.B. Etnyre, *On knots in overtwisted contact structures*, ArXiv:1012.3745 (2012).

[139] P. Kronheimer and T. Mrowka, *Monopoles and Three-Manifolds*, (Cambridge University Press, Cambridge, 2007).

[140] M. Hutchings and M. Sullivan, *Rounding corners of polygons and embedded contact homology*, Geometry and Topology **10**, 169 (2006).

[141] M. Hutchings and C.H. Taubes, *Gluing pseudoholomorphic curves along branched covered cylinders I*, J. Symplect. Geom. **5**, 43 (2007).

[142] Y. Eliashberg, A. Givental and H. Hofer, *Introduction to Symplectic Field Theory*, ArXiv:math/0010059 (2000).

[143] R.D. Kamien, *Colloidal Inclusions in Liquid Crystals*, Lecture Notes, ArXiv:1506.06815 (2015).

[144] P. Poulin, H. Stark, T.C. Lubensky, D.A. Weitz, *Novel colloidal interactions in anisotropic fluids*, Science **275**, 1770 (1997).

[145] E.M.Terentjev, *Disclination loops, standing alone and around solid particles, in nematic liquid crystals*, Phys. Rev. E **51**,1330 (1995).

[146] S.K. Donaldson, *Riemann Surfaces*, (Oxford University Press, Oxford, 2011).

[147] B. Senyuk, Q. Liu, S. He, R.D. Kamien, R.B. Kusner, T.C. Lubenskuy and I.I. Smalyukh, *Topological colloids*, Nature **493**, 200 (2013).

[148] J.W. Milnor, *Topology from the Differential Viewpoint*, (Princeton University Press, Princeton, 1965).

[149] H. Stark, *Physics of colloidal dispersions in nematic liquid crystals*, Phys. Rep. **351**, 387 (2001).

[150] I. Muševič, private communication.

[151] S. Čopar, PhD Thesis, University of Ljubljana (2012).

[152] J. Milnor, *Singular Points of Complex Hypersurfaces*, (Princeton University Press, Princeton NJ, 1968).

[153] J. Seade, *On the Topology of Isolated Singularities in Analytic Spaces*, (Birkháuser Verlag, Basel, 2006).

[154] M.R. Dennis, R.P. King, B. Jack, K. O'Holleran, and M.J. Padgett, *Isolated optical vortex knots*, Nat. Phys. **6**, 118-121 (2010).

[155] F. Pham, *Formules de Picard-Lefschetz généralisées et ramification des intégrales*, Bull. Soc. Math. France **93**, 333 (1965).

[156] E. Brieskorn, *Beispiele zur Differentialtopologie von Singularitäten*, Invent. Math. **2**, 1 (1966).